UNIVERSITEIT VAN PRETORIA
UNIVERSITY OF PRETORIA
YUNIBESITHI YA PRETORIA

Temporal Gap Detection in Electric Hearing: Modeling and Experiments

by

Tiaan Andries Geldenhuys

Submitted as partial fulfillment of the requirements for the degree
Master of Engineering (Bio-Engineering)
in the
Faculty of Engineering, Built Environment and Information Technology
University of Pretoria
Pretoria, South Africa

December 2007

UNIVERSITEIT VAN PRETORIA
UNIVERSITY OF PRETORIA
YUNIBESITHI YA PRETORIA

Temporal Gap Detection in Electric Hearing: Modeling and Experiments

by

Tiaan Andries Geldenhuys

Advisor	:	Prof. Johan J. Hanekom
Department	:	Electrical, Electronic and Computer Engineering
Degree	:	Master of Engineering (Bio-Engineering)

Summary

To advance the understanding of electric hearing, from both a theoretical and practical perspective, the present study employs an engineering approach to examine whether a fundamental stochastic link exists between neural stimulation and perception. Through the use of custom-developed psychophysics software, temporal gap-detection experiments were carried out and compared with simulation results of a theoretical model. The results are informative, and the suggested modeling principles may be a step forward to a clearer understanding of how the hearing system perceives temporal stimuli.

To enable the implementation of psycho-electric experiments involving cochlear implants, a software framework was developed for Matlab version 6.5, called the Psychoacoustics Toolbox, which can present stimuli either acoustically or (for interfacing with cochlear implants) using Cochlear Ltd. hardware. This toolbox facilitates easy setup of experiments based on extensible markup language (XML) templates, and allows for both adaptive-staircase procedures and presentation of a fixed set of stimuli to a participant. Multi-track

interleaving of stimuli is also supported, as put forward by Jesteadt (1980), to allow for capturing of subjective responses (such as loudness perception).

As part of this research, experiments were performed with three subjects, with a total of four cochlear implants. For the temporal gap-detection experiments, the rate of electrical stimulation varied over a range from 100 to 2700 pulses per second; both periodic stimulus sequences and stimuli reflecting a dead-time-modified Poisson process were used. Also, three spatially distinct stimulation sites were used with each implant to allow comparison among basal, central and apical cochlear responses.

A biologically plausible psychophysical model (in contrast with a phenomenological one) was developed for predicting temporal gap-detection thresholds in electric hearing. The model was applied to both periodic and Poisson stimuli, but can easily be used with other kinds of stimuli. For comparison with experimental results, model predictions were made over the same range of stimulus rates. As a starting point, the model takes the neural stimuli, runs them through a neural filter, and then draws statistical interspike-interval (ISI) distribution data from the generated spikes. From the ISI statistics, psychometric curves can be calculated using the principles of Green and Swets (1966), from which predictions can be made for threshold measurements based on the percentage-correct mark for the specific experimental setup.

With a model in place, simulations were executed to compare the model results with experimental measurements. In addition to the simulations, mathematical equations for the periodic types of stimuli were derived, given that numerical calculations could be made with higher computational efficiency for this kind of stimulus. These equations allowed for an investigation into the implications of varying the values of different neuron-model parameters. Clear similarities were found between the shapes of gap-threshold curves for experimental and modeled data, and qualitative links have been identified between model parameters and features recognized in threshold curves. For periodic stimuli, quantitative predictions of gap thresholds are close to experimental ones, although measured values cover a larger range. The results of experimental measurements using Poisson stimuli are generally somewhat larger than model predictions, although the shapes of the curves show resemblance. A possible explanation is that participants may find decision tasks involving Poisson stimuli, as opposed to periodic stimuli, confusing.

Overall, model predictions and experimental results show close correspondence, suggesting

that the principles underlying the model are fundamentally correct.

KEYWORDS

Electric hearing, neural hazard function, temporal gap detection, cochlear implant, pulse train, periodic stimulus, Poisson stimulus, psychometric function, stochastic neural model, refractory function, psychophysics software.

PACS numbers: 43.66.Mk, 43.64.Me, 43.66.Ba, 43.66.Ts

TEMPORALE GAPINGSDETEKSIE IN ELEKTRIESE GEHOOR: MODELLERING EN EKSPERIMENTE

deur

Tiaan Andries Geldenhuys

Raadgewer	:	Prof. Johan J. Hanekom
Departement	:	Elektriese, Elektroniese en Rekenaar-Ingenieurswese
Graad	:	Magister in Ingenieurswese (Bio-Ingenieurswese)

OPSOMMING

Ten einde ’n beter begrip van elektriese gehoor te bewerkstellig, vanuit sowel ’n teoretiese as ’n praktiese perspektief, volg die huidige studie ’n ingenieursbenadering om vas te stel of daar moontlik ’n fundamentele stogastiese verband tussen neurale stimulasie en persepsie bestaan. Deur die gebruik van pasgemaakte psigofisiese sagteware is temporale gapingsdeteksie-eksperimente uitgevoer en vergelyk met simulasieresultate van ’n teoretiese model. Die resultate is insiggewend en die voorgestelde modelleringsbeginsels mag ’n stap vorentoe wees vir ’n duideliker begrip van hoe die gehoorstelsel temporale stimuli waarneem.

Om die implementering van psigo-elektriese eksperimente met betrekking tot kogleêre inplantings moontlik te maak, is ’n sagteware-raamwerk ontwikkel vir weergawe 6.5 van MATLAB, naamlik die PSYCHOACOUSTICS TOOLBOX, wat stimuli òf akoesties òf (vir die raakvlak na kogleêre inplantings) met hardeware van Cochlear Bpk. kan aanbied. Hierdie gereedskapskis fasiliteer maklike opstelling van eksperimente gegrond op uitbreibare-opmaaktaal-

profielvorms (XML-profielvorms[1]) en maak sowel trapsgewyse aanpassingsprosedures as aanbieding van ’n vaste stel stimuli aan ’n deelnemer moontlik. Multibaandeurvlegting van stimuli word ook ondersteun, soos voorgestel deur Jesteadt (1980), om die vaslegging van subjektiewe response (soos luidheidspersepsie) moontlik te maak.

As deel van hierdie navorsing is ekperimente uitgevoer met drie proefpersone, vir ’n totaal van vier kogleêre inplantings. Vir die temporale gapingsdeteksie-ekperimente is die tempo van stimulasie gevarieer oor ’n reeks vanaf 100 tot 2700 pulse per sekonde; beide periodiese stimulusreekse en prikkelings wat ’n dooie-tyd-gewysigde Poisson-proses reflekteer, is gebruik. Daarbenewens is drie ruimtelik verskillende stimulasieplekke op elke inplanting gebruik ter vergelyking van basale, sentrale en apeksale kogleêre reaksies.

’n Biologies aanneemlike psigofisiese model (in teenstelling met ’n fenomenologiese een) is ontwikkel vir die voorspelling van temporale gapingsdeteksiedrumpels in elektriese gehoor. Die model is toegepas op beide periodiese en Poisson-stimuli, maar kan ook maklik gebruik word met ander soorte stimuli. In vergelyking met eksperimentele resultate is modelvoorspellings gemaak oor dieselfde reeks stimulustempo’s. As vertrekpunt gebruik die model die neurale stimuli, voer hulle deur ’n neurale filter en onttrek dan statistiese inter-impuls-interval-verspreidingsdata (ISI-verspreidingsdata[2]) van die opgewekte neurale pulse. Psigometriese kurwes kan vanaf die inter-impuls-intervalstatistiek bereken word deur gebruik te maak van die beginsels van Green en Swets (1966). Hieruit kan voorspellings gemaak word oor die drumpelmetings gebaseer op die persentasie-korrekte punt vir die spesifieke opstelling van eksperiment.

Met hierdie model wat ontwikkel is, is simulasies uitgevoer om die modelresultate te vergelyk met eksperimentele metings. Bykomend tot die simulasies is wiskundige vergelykings vir die periodiese stimuli ook afgelei, aangesien numeriese berekeninge met beter rekeningseffektiwiteit vir hierdie tipe stimulus gemaak kon word. Hierdie vergelykings het dit moontlik gemaak om die implikasies van variëring van waardes vir verskillende neuronmodelparameters te ondersoek. Duidelike ooreenkomste tussen die vorms van gapingsdrumpelkurwes van eksperimentele en gemodelleerde data is gevind, en kwalitatiewe verbintenisse tussen modelparameters en kenmerke in drumpelkurwes is geïdentifiseer. Kwantitatiewe voorspellings van gapingsdrumpels vir periodiese stimuli stem hoofsaaklik ooreen met eksperimentele waardes, alhoewel gemete waardes ’n groter bereik dek. Die

[1] Engels: “extensible markup language”, afgekort as “XML”.
[2] Engels: “interspike interval”, afgekort as “ISI”.

resultate van eksperimentele mates vir Poisson-stimuli is oor die algemeen ietwat groter as modelvoorspellings, alhoewel die fatsoene van die krommes ooreenkoms vertoon. 'n Moontlike verklaring hiervoor is dat deelnemers die besluitnemingstaak met betrekking tot Poisson-stimuli, in teenstelling met periodiese stimuli, verwarrend mag vind.

Oorhoofs toon die modelvoorspellings en eksperimentele resultate sterk ooreenstemming, wat daarop dui dat die onderliggende beginsels van die model fundamenteel korrek is.

SLEUTELWOORDE

Elektriese gehoor, neurale gevaarfunksie, temporale gapingsdeteksie, kogleêre inplanting, puls-trein, periodiese stimulus, Poisson-stimulus, psigometriese funksie, stogastiese neurale model, refraktêre funksie, psigofisiese sagteware.

PACS nommers: 43.66.Mk, 43.64.Me, 43.66.Ba, 43.66.Ts

List of Abbreviations

2AFC	two-alternative forced choice
ANSI	American National Standards Institute
API	application programming interface
ARP	absolute refractory period
BP	bipolar (stimulation mode; see Clark et al. (1997, fig. 9-3) for an illustration)
CCW	COM callable wrapper
CDF	cumulative distribution function
CDFC	complementary CDF (a.k.a. survivor function)
CF	characteristic frequency
CHF	cumulative hazard function
CI	cochlear implant
CL	current level (clinical electrical-current units)
COM	component object model
CPS	clinical programming system
CRLB	Cramer-Rao lower bound
DHF	discrete hazard function
DHFC	complementary discrete hazard function
DLL	dynamic link library
DOM	document object model
DTD	document type definition
FDA	Food and Drug Administration
GUI	graphical user interface
HRF	hazard rate function
ICE	intracochlear electrode
ISI	interspike interval
JND	just-noticeable difference

MP	monopolar (stimulation mode; see Clark et al. (1997, fig. 9-4) for an illustration)
NIC	Nucleus implant communicator
NMT	Nucleus MATLAB Toolbox
OOP	object-oriented programming
PACS	physics and astronomy classification scheme
PDF	probability density function
PC	personal computer
PMF	probability mass function
pps	pulses per second
PPS	portable programming system
RF	radio frequency
RRP	relative refractory period
RV	random variable
SPL	sound pressure level
USB	universal serial bus
XML	extensible markup language

Table of Contents

CHAPTER 1

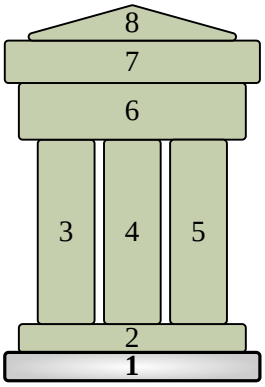

INTRODUCTION

This first chapter provides an introduction to the document, which constitutes the formal record of the research work performed as part of the present study. The initial sections place the study in an academic context and are followed by an overview of subsequent chapters.

1.1 BACKGROUND: UNDERSTANDING ELECTRIC HEARING

The field of bio-engineering is an application of engineering tools and principles to solve problems in the biological and medical (i.e., biomedical) sciences. In this field of study, the physical and natural sciences — here including physics and chemistry as well as biology — are considered from an engineering perspective[1] with regard to their applications in the field of medicine. The invention of hearing implants provides an excellent example of how

[1] An *engineering perspective* here embraces both theories and practices of systems design based on mathematical frameworks.

the marshaling of knowledge from various disciplines (including, in this case, electronics, neurophysiology and biochemistry) has led to the development of a medical prosthesis. Despite the notable success of this prosthetic device, which has been implanted in thousands of hearing-impaired subjects, much remains to be learned about the underlying processes involved in the perception of electric hearing. A more comprehensive understanding of these processes may clear the path to further advances in the field.

The precise nature of the mechanisms involved in hearing perception is still a topic of debate. However, one general conclusion (as cited by Zeng (2002),[2] among others) is that temporal (rate) and place information constitute two components of auditory perception experienced as a result of cochlear stimulation (both acoustic and electric). With the aid of experiments, strong arguments can be (and have been) made for the encoding of pitch using either of these mechanisms, which seems to indicate that these two spatiotemporal components do intermingle. In the context of normal hearing through acoustical stimulation, these arguments merit particular attention when considering the physiological properties[3] of the basilar membrane. The result, for traditional acoustical research, is that the individual contribution made by each of the components toward the complete auditory experience becomes obscured. Fortunately, cochlear implants provide a unique avenue for research on this topic, because they allow temporal and place information to be manipulated independently from each other. Thus, one can follow this route to probe the underlying mechanisms of hearing.

Though providing new perspectives for hearing research, electrical stimulation brings its own complications. Neural spikes elicited by electrical stimulation are highly synchronized to the time instants when individual electrical pulses are presented. This results in very regular intervals between spikes evoked by constant-rate electrical pulse-trains presented at a single stimulus site[4]. Such predictable behavior is not observed in normal hearing, where internal neural noise promotes more stochastic firing patterns. Spikes from electrical stimulation not only synchronize to *stimulus instants* for individual neurons, but (owing to relatively wide electrical *current spread*) large numbers of neurons in the vicinity of a *stimulus channel* (i.e., electrode pair) also fire synchronously. The perceptual implications of these synchronous

[2]The introduction of this article provides a concise summary of this longstanding debate, substantiated by various references.

[3]Models of the physical processes involved (for example, basilar membrane motion and cochlear fluid mechanics) can be found in literature such as Allen and Sondhi (1979).

[4]The *stimulus site*, i.e., the combination of electrode (active and return) locations used for electrical stimulation, is also referred to as a *stimulus channel*.

firing patterns (relating to the aforementioned temporal and spatial aspects of stimuli) are not yet fully understood.

1.2 RESEARCH QUESTION

The principal intent of the study presented in this document is to further the understanding of the way in which cochlear-implant users perceive temporal noise in the pulse trains that are used as stimuli for electric hearing.

In this context, *temporal noise* refers to the changes in the normal temporal placement of stimulation pulses, including their addition, removal or displacement. Using this guideline for the interpretation of temporal noise, the synchronous firing patterns of electrically stimulated neurons also constitute temporal noise. While in normal hearing the neurons would fire more chaotically, in electric hearing these apparently random firing patterns are substituted by (i.e., temporally altered into) highly synchronized patterns. From this perspective the lack of more natural firing patterns can be interpreted as some form of noise. Realizing this, the principal focus thus involves making progress in understanding the implications of the strong synchronization of action potentials[5] and stimulation pulses present in electric hearing.

One objective of advancing researchers' understanding of temporal noise perception is to improve the prosthetic devices implanted in the profoundly deaf. In terms of electric hearing, the auditory path holistically consists of the bio-engineered equipment (e.g., the speech processor and implanted electrodes) and the biophysical part that is interpreted by the brain. Over the latter, one has relatively little direct control. However, the former can be manipulated to a large extent, which gives one a means to indirectly influence the latter. Once the electrodes have been implanted, the speech processor is the component that one has most control over. Improvements in prosthetic hearing devices can, therefore, relatively easily focus on sharpening the algorithmic strategies used to manipulate the perceptions evoked by these devices. Currently there is no clear direction for how improvements should proceed in this area to create the next generation of these devices. The way forward may become clearer if one can find a mathematical connection between stimuli and observable perception, which would allow one to better predict perception when one knows what stimulus is applied. This

[5]The term *action potential* refers to a sudden change of electrical potential across a neural membrane; it is generally synonymous with a neural spike or the firing of a neuron, but may also include sub-threshold electrical changes that do not propagate along an axon.

could lead to better control over perception.

To this end, unless one can say with almost 100% statistical certainty what both the physical and perceptual effects of each and every stimulus pulse in a stimulation sequence are going to be, one is not in control of the process. In effect, if one does not understand the process completely to the point where mathematical models give rise to statistical predictions with great certainty, one leaves some aspects of the experience of electric hearing to chance. Ideally one would want to formulate custom statistical models on an individual basis, and make predictions and optimize using such personalized models. With this as an ideal, it may be interpreted that the present state of electric hearing is one in which much is still left to chance, despite some breakthroughs that have already been made in this field. With tailored mathematical models, it should be possible to dramatically improve implementations of stimulation strategies, as well as the customization of implanted devices, to optimize the certainty that stimulation pulses would in fact result in desired action potentials. Understanding the implications of temporal placement of stimulus pulses and noise introduced by misplacement and other alterations, such as the effective removal of a stimulus pulse because it evokes no perceivable action potentials, are important steps on the road to further improvements in electric hearing. Finding such a mathematical link in one type of experiment, one could hypothesize that similar relationships exist in other areas of hearing research, which could build the foundation for the formulation of mathematical models of hearing perception.

Having identified a focus area for the research to be embarked upon, it is now possible to formalize this goal into a specific primary research question:

> What can be inferred from the temporal aspects of highly synchronized neural firing patterns that will advance the understanding of electric hearing?

To highlight the specific intentions behind this comprehensive question, it would make sense to qualify this through a set of modest questions, which could more reasonably be investigated and provide guidelines for exploration. To this end, the following sub-questions are formulated:

1. When considering temporal aspects of pulse trains in electric hearing, what is the relationship between stimulus and perception?

2. Is it possible to formulate this relationship through mathematical means?

3. If a mathematical formulation is possible, do mathematical predictions agree with experimental measurements?

1.3 APPROACH

In previous psychophysical studies, temporal gap detection has been identified as a successful measure for probing temporal resolution. Gap detection (which is a psychoacoustic measurement used to probe psychological properties of the auditory system) is temporal by nature, making it a useful tool for investigating the effects of different temporal patterns. To address the research questions formulated above, it was decided to approach this topic using temporal gap-detection measurements. For example, to investigate the relationship between stimulus and perception, one can examine the possibility of a link between the mathematical uncertainty of the stimuli on the edges of the gap in pulse trains and the variance in the smallest gap that can be perceived by listeners. Such an approach would make sense in the light of the pathbreaking work of Siebert (1970), which seems to suggest that one can equate the smallest perceivable psychophysical effects (i.e., *just-noticeable differences*, or JNDs) to the statistical standard-deviation of those stimuli that evoke the measured response. This approach is, therefore, based on the hypothesis that there is a direct relationship between pulse positioning (stimulus) and the gap threshold that can be psychoacoustically (perceptually) measured.

As is the case for many engineering approaches, a thorough understanding of a specific problem involves modeling of the system. Simulations based on an accurate model can quickly lead to insights that would take much longer to discover through conventional methods. To test the predictions of those simulations, key findings can then be checked by experiment in a much more focused approach. This was the approach taken in the present study: one in which both predictions through modeling and measurements through experiments were used in an attempt to understand the implications of the temporal patterns discussed earlier.

Regarding the stimulus sequences to be used to measure gap-detection thresholds, one may consider constant-rate pulse trains. It is possible (at least conceptually) to mimic more spontaneous activity by replacing the constant-rate stimulation with a pulse train incorporating more randomness, one in which the average pulse rate remains the same as

for the original pulse train. (For the moment, some considerations will be left aside that may require further attention before one can make a blind substitution, such as whether the electrical stimulations would cause neurons to exhibit complete entrainment[6] that could influence perceived loudness.) This substitution does not eliminate the synchronization between firing instants of the neural population in the vicinity of the stimulation channel, but does influence the otherwise synchronized effect observed at a single stimulus site. It is for this reason that the perceptual influences of such modified pulse-trains are investigated through psychoacoustic experiments in this study. The approach is then to choose two very distinct styles of temporal stimulation trains that can clearly discriminate between degrees of synchronization. To this end, the first kind of stimulation sequence chosen is that of periodic trains similar to those used in most present hearing implant stimulation strategies. In contrast to this highly synchronous (periodic) stimulation sequence, the other type of stimulus sequence is one that mimics the Poisson statistics of natural neural firing patterns. Both of these kinds of sequences are then presented at a wide range of (average) stimulation rates to investigate the influence of rate on the measured gap thresholds reflecting the temporal resolution of electric hearing.

1.3.1 Modeling of Temporal Gap Detection

The modeling of temporal gap detection lends itself to a deep understanding of the theoretical aspects involved in the psychophysical process of electric hearing. In this regard, the approach was to base the model on a biologically plausible mechanism and to use equally appropriate parameter values. In the model, the physical part of the electric hearing system is, at its core, the refractory behavior of biological neurons being stimulated. The psychological part of the system is approached in a way that is conceptually similar to that employed by Green and Swets (1966) using signal detection theory, but fewer assumptions are made about statistical properties of the neural signals (rather, statistics are determined either through calculation or simulation). In a psychophysical sense, overall, the model focuses on the effects of neural refractoriness on the statistics of interspike intervals and consequently on the detection of temporal gaps.

The model that was developed permits computer simulations of experimental results. Simulated and experimental results can then be compared when interpreting the findings of the study.

[6] In the case of 100% entrainment, each and every stimulus pulse generates a spike.

1.3.2 Psychophysical Experiments

Psychoacoustic, or rather psycho-electric, experiments needed to be performed with cochlear-implant subjects,[7] gathering practical measurement data that can be verified alongside predicted results from simulations. To enable execution of these psychoacoustic experiments, a software package, called the PSYCHOACOUSTICS TOOLBOX, was written in MATLAB (Magrab et al. 2000).

The results of the experimental and modeling research, using gap detection to probe this temporal domain, led to some interesting insights into the ways in which cochlear-implant users perceive temporal noise. For example, for experiments involving periodic stimuli, what appears to be a direct link was identified between one of the model parameters and the stimulation rate at which gap-threshold minima are measured.

1.4 OBJECTIVES

With the research questions in mind, the following key milestone objectives were defined.

1. Custom software was to be developed, in MATLAB, that can be used to perform psychophysical experiments, such as those envisioned for the present gap-detection study. This MATLAB toolbox was required to integrate with the *Nucleus Implant Communicator* (NIC) library provided by Cochlear Ltd., which enables hardware interfacing between a computer and implant devices manufactured by the company (e.g., the Nucleus CI-22 and CI-24 models used by subjects available for this study).

2. Another objective was to perform psycho-electric gap-detection experiments with cochlear implant users, using the custom software, to investigate the implications of the highly synchronized temporal nature of neural firing patterns for electric hearing.

3. A model had to be designed and built that could be used to predict the outcomes of the measured results from experiments. The model needed to be based on biologically plausible mechanisms.

[7] The research protocol has been approved by the Faculty of Health Sciences Research Ethics Committee, University of Pretoria (Protocol No. 183/2002).

4. Furthermore, a deeper understanding had to be gained of the way in which cochlear-implant users perceive temporal noise in electric hearing, using insights illuminated by the combination of modeling and experimental results.

1.5 CONTRIBUTION

As discussed in the preceding sections, a principal theme that underlies the present study is the desire to find an entry point to a suitable theoretical grasp of the relationship between stimulus and perception in electric hearing. This approach is one that should naturally flow from an engineering perspective, which in this case has been applied to gap detection. It is postulated that if a mathematically sound link is found in one type of psychophysical experiment, the concept should be more widely applicable to other areas of perception. Through the present study, such an entry point may have been found, as should become clear through the remainder of this document. The relationship identified between stimulus and perception for gap detection in electric hearing is seen as the primary contribution made by this study, and should be viewed as the starting point of further research flowing from these concepts.

1.6 DOCUMENT OUTLINE

An overview of the remaining chapters is provided next. Refer to fig. 1.1 for a structural framework of how the chapters conceptually fit together to form the document. A smaller version of the edifice depicted in this figure is displayed at the beginning of chapters.

Chapter 2 identifies and discusses the literature on the topics relevant to this document. Topics include gap detection, neural modeling, psychophysics and general aspects of cochlear implants. Since the recovery behavior of neurons forms the basis of the model developed in a later chapter, this topic is also discussed. A background is also given on the sometimes overlooked procedures that have been used in the kinds of experiments found in this study.

In **Chapter 3** the discussion focuses on the development of the software package, the PSYCHOACOUSTICS TOOLBOX, that was used to perform the actual experiments for this study. Hardware interfaces are also discussed. As experiments are configured through a specially

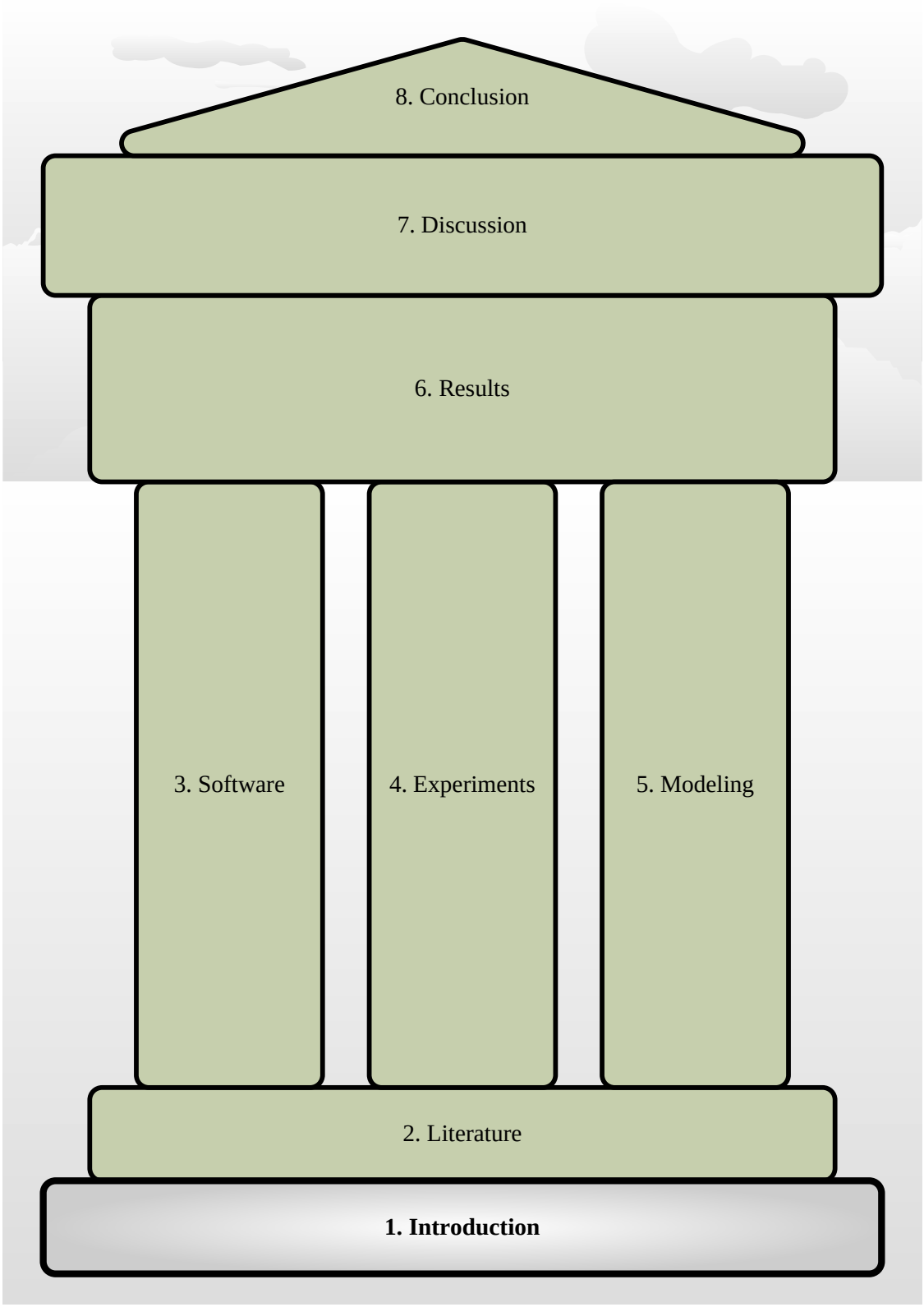

Figure 1.1: This edifice depicts a conceptual framework of how the chapters in this document fit together.

designed markup language, this core aspect of the toolset is explored.[8]

In **Chapter 4** the experiments themselves are addressed. The use of duration-discrimination experiments as a forerunner to the main gap-detection experiments is discussed. The issue of mode of stimulation, monopolar versus bipolar, is highlighted. The issue of constant-current versus equal-loudness stimulation, another primary concern[9] in the design of the gap-detection experiments, is also addressed.

Using the tools that are typically associated with engineering, **Chapter 5** develops the theoretical model for psychophysical gap-detection predictions. This model is based on neurophysiological properties of the nervous system and uses statistics of the time intervals between neural spikes to predict the psychological perceptions that can be measured through experiments (i.e., psychometric functions). A theoretical background of this model is sketched using mathematics as a solid foundation. One of the more intriguing and easily overlooked aspects of point-process statistics is also discussed, namely length-biased sampling.

The results of both the modeling and the experiments are presented in **Chapter 6**. As a reference, the duration-discrimination results are presented. The outcomes of the investigation into the monopolar versus bipolar stimulation modes and constant-current versus equal-loudness stimulation issues are documented. These are followed by the results from the gap-detection experiments for both the periodic and dead-time-modified Poisson stimuli at various rates of stimulation. The data resulting from the gap-detection model are also presented, those of the simulations as well as the mathematical calculations for the case of periodic stimuli.

Chapter 7 discusses the results highlighted above — those of the experiments and simulations. The discussion examines discoveries related to the classification of gap-detection-threshold versus stimulation-rate curves and their psychophysical origins. Mathematical formulations of the boundary that separates curve types, as they pertain to results obtained through experiments, are also given. The striking similarities between these curves and

[8] For the non-periodic stimulation sequences a Poisson generator was constructed. Although the Poisson generator is also implemented as part of the PSYCHOACOUSTICS TOOLBOX, in view of its different nature (i.e., being less software-related and more mathematical), some aspects of the design and implementation of this generator are addressed separately in appendix C.

[9] This issue becomes important when comparing the results of experiments with those of simulations (see § 4.5.2 for the detailed argument).

those resulting from data found in other literature are also discussed, including previous results from Busby and Clark (1999) that might have incorrectly suggested that gap-detection thresholds remain constant irrespective of stimulation rate.

The document concludes with **Chapter 8**, which examines lessons learned. Suggestions are also offered for future research directions.

In summary, the present chapter provided an introduction to this document and an outline of chapters to follow. An overview of literature is provided next, which places the present study in the context of existing research performed on relevant topics.

CHAPTER 2

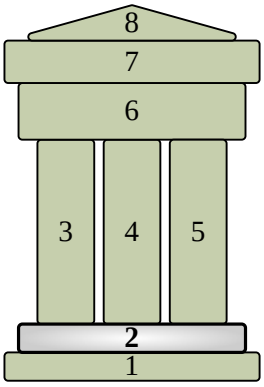

OVERVIEW OF LITERATURE

This chapter provides an overview of literature that is relevant to the present study. Rather than attempting to discuss all references in this chapter, additional literature is cited contextually throughout the remainder of the document. For this chapter, a number of high-level subject areas have been identified to provide a coarse structure for the presentation of the information.

2.1 COCHLEAR IMPLANTS

The history of electric hearing can be traced back to Alessandro Volta (better known for the electric battery), who, around the year 1790, applied electricity to his own ears and reported the resulting perception of sound (Niparko and Wilson 2000). By the time of Hill (1936), research into the conditions for electrical excitation of neurons was making good progress, and understanding of the electric nature of neurons reached a pivot point when Hodgkin and

Huxley (1952) published their quantitative description of membrane current based on ionic gating mechanisms. The first cochlear implantation of an electrical device was reported by Djourno and Eyries early in 1957 (Djourno et al. 1957, Mudry 2007). This pioneering work led to progressive development over subsequent decades, eventually being driven more by commercial interest. In 1984 the United States *Food and Drug Administration* (FDA) approved the first cochlear implant for use in deaf adults, which was a 3M/House device, and the Nucleus device was approved a year later (Blume 1997). (For a good basic introduction to cochlear implant technology, including discussions of the 3M/House and Nucleus devices and the speech-processing strategies that drive these implants, refer to Clark (1996) and Loizou (1998, 1999).) Today, research continues in an effort to improve cochlear implants and speech-processing strategies, while an ultimate understanding of hearing and its relation to electrical stimulation is still being pursued.

Stimulation by cochlear implants typically results in a high level of synchrony of neural firing patterns, a factor believed likely to hinder speech recognition (Collins et al. 2000). This synchronization effect was also noted in § 1.1. Recently, numerous studies designed to promote the more natural stochastic firing behavior of auditory neurons have been performed with cochlear implants. Examples include the deliberate incorporation of noise (Morse and Evans 1996, 1999, Morse and Meyer 2000, Morse et al. 2007) and the use of high-rate pulse trains (Rubinstein et al. 1999, Litvak et al. 2003, Hong and Rubinstein 2003). A more detailed summary can be found in Collins et al. (2000), in which the authors also present theoretical results from a model simulating the response of neurons to electrical pulse trains, as well as psychophysical data suggesting a link between internal stochastic resonance and improved speech-recognition performance. In addition, experimental data on the use of high-rate desynchronizing pulse-trains in animal subjects have been documented by Litvak et al. (2001). Thus, considering spike synchrony and suggested improvements, it appears that a better understanding of the temporal aspects of neural stimulation may lead to fruitful discoveries. To this end, the first of the three secondary research questions identified in § 1.2 deals with the temporal features of pulse trains in electric hearing.

Discharge patterns in the auditory nerve fiber can be influenced by electrical stimulation waveform parameters, some of which are temporal in nature, and descriptions of these are readily available. A series of articles by Shepherd and Javel (Shepherd and Javel 1997, 1999, Javel and Shepherd 2000) serves as a good reference on this topic, and for the present study the third in the series, dealing with place (i.e., tonotopical) and rate aspects, is of particular interest.

When the normal-hearing cochlea encodes acoustic features (such as frequency) and the auditory systems of the brain decode the neural activity to give perceptions of hearing (such as pitch), the peripheral auditory system appears to have both place and rate mechanisms available to do so (Zeng 2002). The independence of these mechanisms was investigated by McKay et al. (2000) with cochlear implant participants. In the study's conclusion, the usefulness of high-rate temporal cues for prosthesis users was questioned. This longstanding debate about the use of rate and place information by the brain may benefit from different approaches to the problem. When cochlear implants are employed in hearing research, rate and place information can be presented independently — a technique that would be difficult (if not impossible) to use with acoustic stimulation. The use of cochlear implants in research makes the relationship between stimulus and perception more accessible to investigation. This further relates to the specific secondary research question of the present study, mentioned above, concerning temporal aspects of stimuli.

2.2 TEMPORAL GAP DETECTION

A study by Hanekom and Shannon (1998) illustrates how gap-detection experiments (that are structurally temporal in nature) can be used as a measure of current spread (which is fundamentally a spatial property, from a quasi-static-electromagnetic-field-theory perspective). Thus, gap-detection threshold measurements can also be used as a very powerful tool to probe the mysteries of the spatiotemporal properties of auditory information coding mechanisms.

Shannon (1989) inferred, based on his experimental results, that the enhanced neural synchrony of cochlear stimulation is not of great importance in the detection of gaps. However, the neural synchrony does allow one to predict with greater certainty when neurons will fire in response to stimuli, and this provides an opportunity to investigate with more confidence the relation between stimulus and perception. From this standpoint, temporal gap detection does appear to be an attractive instrument for the present research objectives, as results may not be tainted by enhanced neural synchrony, such that conclusions about any link that is found are likely to be applicable not only to electric hearing, but also to auditory perception in general.

An abundance of literature can be found with results on gap-detection threshold measurements, in which various parameters have been varied for both electric and acoustic hearing. Much less common, however, is literature regarding gap detection for pulsatile stimuli that

have been varied over a range of stimulation rates in a within-channel setup. References that are most relevant to the gap-detection experiments envisaged for the present research include Busby and Clark (1999), van Wieringen and Wouters (1999), Dobie and Dillier (1985), Preece and Tyler (1989) and Chatterjee et al. (1998) (discussed below). Even within this body of literature, the range of rates and resolution of measurements are not as extensive as one would have hoped for, and the present research is aimed at filling this gap in the knowledge base.

Experimental results involving 15 subjects with cochlear implants (all Cochlear devices) are documented by Busby and Clark (1999), who used pulsatile stimuli over a range of frequencies that included 200, 500 and 1000 pulses per second (pps). Gap thresholds varied over a wide range from about 1 ms to 60 ms. The authors concluded that pulse rate essentially has no effect on gap thresholds. But the resolution of step-sizes used for the adaptive procedure was always an integer pulse interval, which could have masked the fine structure of threshold measurements, especially for small measurements. The present study incorporates non-integer steps for a finer gap resolution.

Four cochlear implantees with Laura devices were studied by van Wieringen and Wouters (1999). Within-channel measurements were performed at two different rates, namely 400 and 1250 pps, and all within-channel gaps (including those for low rates) were in a threshold range from 1 ms to just over 8 ms. The authors also reported a tendency observed in three of the subjects, in which longer gaps were measured at lower stimulation rates, but suggested that it may have been a result of the speech-processing strategies used by the individuals. The within-channel measurements also contain data of three to five different stimulation sites per subject for a specific experiment setup, which would be useful for comparison with the present study.

The experiments by Dobie and Dillier (1985) include gap-detection results for two subjects using pulsatile electrical stimuli. Applicable measurements were performed for about four to five different stimulation rates per subject in the range of 80 pps to 1000 pps. As noted by van Wieringen and Wouters (1999), the results of Dobie and Dillier do show a general tendency of increasing thresholds for lower pulse rates.

Sinusoidal stimuli were investigated with two cochlear implant subjects by Preece and Tyler (1989, figures 3 and 4) for basal and apical electrodes, using a wide range of stimulation frequencies measured at octave rates from 125 Hz to 4000 Hz. The stimulus level was

also varied, and the authors reported no difference in threshold for high stimulus levels, though differences were observed for low stimulus levels (or loudness). The results for high stimulus levels, which should correspond with the comfortably loud stimuli used in the present study, are not particularly useful from a comparison perspective, because of the compressed resolutions of the figures displaying the specific results. (The graphs might have been more useful if a logarithmic scale were used.)

Chatterjee et al. (1998) also present some interesting gap-detection results for cochlear implant participants, although most of the results are for dissimilar markers surrounding the gap. However, three data points can be extracted for each of three subjects from their fig. 3, which would then result in three same-rate marker curves with data points at 125, 500 and 1000 pps. This same figure also holds some promising ideas for further research involving this study's model, which will be discussed in more detail in § 8.2.

As mentioned in § 1.3, the present research would not only use experimental means but also employ a modeling approach to the identified problem. Hardly any literature could be found that deals specifically with gap-detection modeling for electric hearing, but in Hanekom (2001, pp. 84–85) the author identifies requirements for such a model. The focus there is on a general model that also incorporates gap-detection results for dissimilar markers surrounding the gap, while the intention with the present study is to focus exclusively on markers that are the same on both sides of the gap, which deserve further investigation. However, the aspect of biological (i.e., physical) plausibility is taken seriously, and the model developed for the present study also places high value on being psychologically plausible. Thus, psychophysical plausibly as a whole is accommodated. The model developed here ignores stimulus sensitivity in this study, but such a requirement can easily be incorporated into future investigations, in a manner similar to the handling of stimulus intensity by Xu and Collins (2003, 2007).[1]

2.3 PSYCHOPHYSICS

This study will use psychophysical techniques to relate electrophysical stimulation quantitatively to auditory perception. For the sake of efficiency, staircase procedures are often preferred as the method of psychophysical experimentation, and this is also the case in the present study. Levitt (1971) described efficient methods for measuring perceptions for

[1] Xu and Collins used the auditory nerve model of Bruce, White, Irlicht, O'Leary, Dynes, Javel and Clark (1999) and Bruce, Irlicht, White, O'Leary, Dynes, Javel and Clark (1999).

which correct presentation intervals can categorically and objectively be determined (e.g., the longer temporal duration of otherwise identical stimuli). These transformed up-down procedures are widely used (Zeng et al. 2005, Hong and Rubinstein 2006, Moore et al. 2006, van Wieringen et al. 2006, Pretorius and Hanekom 2006, Dingemanse et al. 2006). However, for the procedures to work properly as an alternative to conventional methods, a simple *psychometric function* (Klein 2001), i.e., a monotonically non-increasing or non-decreasing one, needs to govern the parameter to be measured (at least over the range of observations), and compliance with this requirement may not always be known beforehand.

Psychometric functions do not appear to be available in literature for gap detection involving pulsatile stimuli in electric hearing. The present study takes a theoretical approach in an attempt to fill this void by means of calculations. However, as a reference, some gap-detection psychometric functions have been measured for sinusoidal and noisy stimuli (Irwin and Kemp 1976, Shailer and Moore 1987, Green and Forrest 1989, Moore et al. 1989, He et al. 1999, Florentine et al. 1999). In general, psychometric curves are sigmoidal functions, and the monotonic requirement will be assumed to be met or to be an omissible issue for the present experimental measurements.

For subjective measurements, where the "correct" presentation interval cannot be determined objectively (e.g., a loudness comparison of different kinds of stimuli), an adaptive procedure was developed by Jesteadt (1980) that is an expansion of standard staircase procedures in which multiple tracks of measurement are randomly interleaved. For example, one track could measure a response that resembles a slightly greater perception, and another track could measure a slightly lesser perception. By averaging the resulting track measurements, it is then possible to estimate the point of equal subjective perception. This procedure has gained much popularity over the last decade (Collins et al. 1997, Chatterjee et al. 1998, Zeng et al. 1998, Florentine et al. 1998, Donaldson et al. 2005).

Green and Swets (1966) approached psychophysics from the perspective of signal detection theory, presenting a well-founded mathematical way of thinking about sensory psychology and its measurements. For the present study, the author's bias toward this approach finds an application in chapter 5, in which the modeling aspects of gap detection are discussed. Alternative theoretical mechanisms also exist for the formulation of decision criteria, for example, the Cramer-Rao Lower Bound (CRLB) or Neyman-Pearson objective.

Through analytical modeling, Siebert (1970) evaluated frequency discrimination of the

human ear, similar to what Colburn (1973) later described in more detail. However, Siebert calculated the Cramer-Rao inequality (also known as the CRLB) for frequency discrimination. He argued that the variance (σ^2) in a frequency estimate must place a limit on the discrimination performance and, therefore, set the JND in frequency equal to the standard deviation (σ) of the best frequency estimate.[2] Although this JND-versus-standard-deviation technique can be applied quantitatively, and the concept behind it appears to be quite unique, it is perhaps best used as a guideline in the context of higher-level approaches. Nevertheless, it can be applied numerically to problems in which the signal-detection route would better be avoided, for whatever reason. The combination of Siebert's principle and the CRLB has intuitively been applied to modeling of gap detection for acoustic hearing in Hanekom (2001, chapter 3) where, in particular, the question of the accuracy of detecting the change-point in a Poisson process was addressed. This work complements the procedures of change-point detection, which are typically the focus of others (e.g., West and Ogden 1997, Jansen 2007).

The Neyman-Pearson theorem (Neyman and Pearson 1933, Kay 1998) can also be used to formulate decision criteria quantitatively, as was done in Hanekom (2001, chapter 4) for modeling of gap detection in electric hearing. In Green and Swets (1966, pp. 23–25), the authors showed that the Neyman-Pearson criterion is equivalent to a decision rule based on the likelihood-ratio[3] criterion. However, Solomon (1975) noted that, when dealing with such equivalencies, one must be on guard against unwarranted assumptions.

It is difficult to conceive that much psychophysical research would be performed today without the aid of computers, especially experiments that are based on adaptive methods, which would be very labor intensive without automated procedures. The development or use of software to perform the experiments is almost a given. Although this aspect of modern experimentation does not appear to be documented very extensively in literature, some research platforms have been discussed. Of particular interest to the present study is software that can facilitate psychophysical experiments involving Cochlear Nucleus hardware. A custom interface was developed by Shannon et al. (1990) that can communicate with that brand of implant hardware for experimental purposes. The interface is not officially endorsed by Cochlear and, considering the typically short lifetime of software, is probably already

[2] Further details on calculating parameters of Siebert's equation from practical measurement data can be found in the (theoretical) examples given in Snyder (1975), as indexed under the subject of "auditory electrophysiology". Additional information on Siebert's equation is apparently also available in Siebert (1968).

[3] The *likelihood ratio* refers to the so-called β parameter, which is also explained in Hartmann (2000) as "the criterion chosen by the subject".

out of date. However, Cochlear does make software and hardware available to appropriate parties for clinical and research purposes, and derived software platforms can utilize these available programming interfaces. An excellent example of such a research platform is APEX, an acronym for Application for Psycho-Electric eXperiments, which was developed at the Catholic University of Leuven in Belgium (Geurts and Wouters 2000, Laneau et al. 2005). For the present research, the requirements specified a total software solution that integrates seamlessly with MATLAB, and a research framework, called the PSYCHOACOUSTICS TOOLBOX, was developed based on the Nucleus programming interface supplied by Cochlear.

2.4 AUDITORY NEURAL BEHAVIOR

The evolution of a neural action potential is often described as an all-or-none event (e.g., McCulloch and Pitts 1943, Rieke et al. 1999), such that the instant of its occurrence carries most weight. Furthermore, the waveforms of spikes (especially the ones that successfully propagate along axons) are all nearly identical (Adrian 1926, Han et al. 2002). As a result, firing patterns are often described mathematically as point processes (Perkel et al. 1967). In passing, it is of interest to note that alternative, more complex, views of neurons as chemical symbolic messengers are also still researched (Rocha 1997). That debate is best left to others, given that the present study will focus primarily on the temporal aspects of neural activity (i.e., the inter-event intervals). In this context, the exact nature of messages (be they simple electrical ones or more complex chemical ones) is less important than the time at which the message is sent (i.e., when the spike event happens).

Under conditions of spontaneous activity, the firing of neurons is sometimes described as a Poisson point process (Molnar and Pfeiffer 1968, Turcott et al. 1994). As noted by Perkel et al. (1967) and Teich and Khanna (1985), however, this is not always the most appropriate description. Other types of renewal point-processes, or even descriptions based on chaos theory (Richardson et al. 1998, So et al. 1998), may sometimes be more suitable for different activity conditions or nerves. Doob (1948) also uses probability theory to inform its general renewal process perspective, which forms a conceptual basis for the probabilistic-hazard-function approach taken for the present modeling work.

Following a spike (i.e., suprathreshold depolarization), there is some period afterwards in which the neuron is unlikely to respond to any additional electrical stimulation. From a bioelectrical perspective (Plonsey and Barr 2000), this is the interval in which (primarily) the sodium and potassium ionic imbalances are restored and, consequently, the neural membrane

is repolarized. The refractory period of the hazard function for an auditory nerve is typically split into a shorter *absolute refractory period* (ARP) with almost zero firing probability immediately after the spike, followed by a longer *relative refractory period* (RRP) of increasing hazard probability. With theoretical predictions, Johnson and Swami (1983) showed that the effects of the ARP give rise to more distortion of the neural information signal than those of the RRP.

Extensive experimental studies have been performed to investigate neural recovery behavior. Resulting timing information about the refractory parameters of auditory nerves can be found in Gaumond et al. (1982) and Prijs et al. (1993). Gaumond et al. built primarily on the conditional spike-discharge probability concepts introduced by Gray (1967) for the cat cochlear nerve fiber, and extended this into comprehensive spike-discharge models that use Markov-chain theory. This framework was then applied to experimental measurements obtained for cat cochlear nerve fibers, and the trends were thoroughly discussed for different groups of nerve responses identified within experimental results. Prijs et al. studied recovery data of the guinea pig's cochlear nerve under conditions of spontaneous activity; one of the main differences in that study's results is that the average value of the exponential time-constant, $\tau = 1.6$ ms, is less than half the value required for the longer recovery period found by Gaumond et al. and Gray. Furthermore, the rate constant, a, averaged to 110 Hz for the Prijs et al. results, which may be on the low side, although one should take into account that this number was for spontaneous activity, not in response to stimulation. At least the magnitude of the absolute refractory period, t_0, is comparable between cat and guinea pig data. Thus, there appear to be potentially substantial differences between some auditory neural parameters even when comparing mammalian species.

The present body of literature describes various models that have been developed in attempts to explain the different aspects of the perception of hearing. In Herz et al. (2006), the authors provide a very accessible overview of the modeling of single neurons at different complexity levels. In Eliasmith and Anderson (2003), the authors provide an extensive framework for modeling neurobiological systems at various levels of detail. Numerous biologically plausible models of electrical nerve stimulation have been developed and researched by Rattay, which include models for general neural behavior but also ones applicable specifically to auditory neurons (to name a few, Rattay 1986, 1988, 1989, 1990, 1998, 1999, 2000). Work by Bruce, Irlicht, White, O'Leary, Dynes, Javel and Clark (1999) provides a MATLAB model for analyzing the auditory nerve's response to constant-rate pulse trains. Bruce also used this model for work on his Ph.D. thesis (Bruce 1997), in which

it is mentioned that the model can be used to investigate how the pitch percept that is related to stimulation rate may arise. More recently, Macherey et al. (2007) developed a phenomenological model, which was used to predict and compare data relating to loudness perception and threshold current-levels of cochlear implantees.

According to the *lower envelope principle* (see Barlow 1995, Parker and Newsome 1998), psychophysical threshold detection may be governed by individual neurons. The idea behind this principle is that the brain should be able to identify and use the best neural information that describes an aspect (e.g., the spiking data representing the lowest gap threshold) to be measured psychophysically. In combination with the knowledge about synchronous firing of neurons for electric hearing, it would then seem plausible that a relatively simple mechanism should govern temporal gap detection when stimuli are presented through a cochlear implant, especially for the case of within-channel gap detection. The hypothesis for the present research is that temporal spiking intervals are what best describe the lower envelope for gap detection. For a single stimulation site, it should be possible to describe the collective neuronal activity in much the same way one would describe the behavior of a single electrically stimulated neuron. The standpoint taken in this document is that neural recovery (i.e., refractory) behavior provides an effective mechanism for describing firing patterns that result from electric stimuli. As substantiating evidence, such conditional probabilities (e.g., Gray 1967) have previously been applied successfully to neural models where the firing probabilities form an integral part of a Markov chain (Meyn and Tweedie 1993, Gallager 1996) representing the temporal progression of periodic neural stimuli; see Xu and Collins (2004) for an example of such a model. From a stochastic perspective, the influence of refractory behavior on spiking probabilities can be described as a statistical hazard function, which can be evaluated at the temporal instants of stimuli.

This chapter discussed some literature relevant to the present study and provided a baseline of references for the experimental, modeling and software-development work documented in subsequent chapters. Additional citations augment this baseline throughout the remainder of the document from within contexts where the supplementary references can more suitably be discussed.

CHAPTER 3

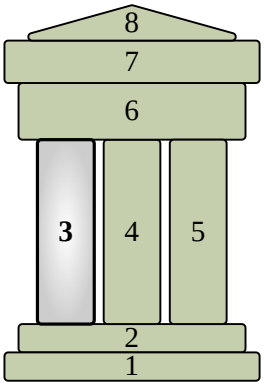

DEVELOPMENT FRAMEWORK FOR EXPERIMENTS

In order to perform psychophysical experiments, a framework was developed for collecting data from subjects and performing postprocessing of the captured results. To be used for cochlear research, hardware equipment, accompanied by some software *application programming interfaces* (APIs) and a few utilities, was made available by the supplier, Cochlear, as discussed in § 3.1. To allow for easier maintenance, the MATLAB product was selected as the programming environment for nearly all of the newly developed software, given that knowledge about this product is readily available in the bio-engineering research group where this study was performed. Not limited to acoustical experiments (despite its name), the PSYCHOACOUSTICS TOOLBOX was developed as a full-fledged MATLAB toolbox, which is discussed in § 3.2.

3.1 TECHNOLOGY BY COCHLEAR

An overview of terminology relating to a wide range of hardware and software components provided by Cochlear is provided in appendix E. The current section will deal more specifically with the portions of the technology used in this study.

The stimulus pulse from a Nucleus implant is a biphasic charge-balanced electrical wave, as shown in fig. 3.1 and detailed in Clark et al. (1997, fig. 9-6). For each stimulus pulse, the parameters that can be controlled directly are the *phase-width* duration applied to both stimulation phases of the pulse, the magnitude of the electrical *current* (i.e., *amplitude* of both phases) and the *phase-gap* duration between the two stimulation phases. Physically, the amplitude parameter specifies an electrical-current value, but such values are provided to the implant as integers that represent *clinical-level* values; the conversion between these values is documented in appendix F. Another parameter that can be controlled indirectly is the total *period* between one pulse and the next pulse, which is typically measured as the duration between the initial onsets of a chronological pair of stimulus pulses. The temporal segment of electrical activity during this complete waveform *period* is sometimes also referred to as the activity during a stimulus *frame*, and the inactive period between the termination of the second phase of one pulse and the onset of the initial phase of the next pulse is referred to as the *frame gap*. The ordered combination of a number of frames is referred to as a stimulus *sequence*. It is worth noting that the waveform shown in fig. 3.1 represents the electrical activity of one stimulus electrode only (in this case, the *active* electrode, as is typically shown) and that a matching waveform with reverse polarity exists for *bipolar* (BP) stimulation (as applied to the *reference* electrode). For stimulation in a multipolar mode, the reversed reference electrical activity could also be shared among a number of reference electrodes.

Cochlear provides a number of hardware devices. The equipment that was used in the present work is presented next; familiarity with Cochlear terminology, of which an overview can be found in appendix E, is assumed. So as not to interfere with the normal operation of the speech processors owned by the individual implant subjects who took part in the experiments, a separate SPrint speech processor was used to connect with the implants using the magnetically coupled transcutaneous *radio frequency* (RF) interface. For the hardware programming interface between the computer and the speech processor, either the *clinical programming system* (CPS) or *portable programming system* (PPS) was used — the former mostly for experiments performed in the university laboratories, and the latter for all visits

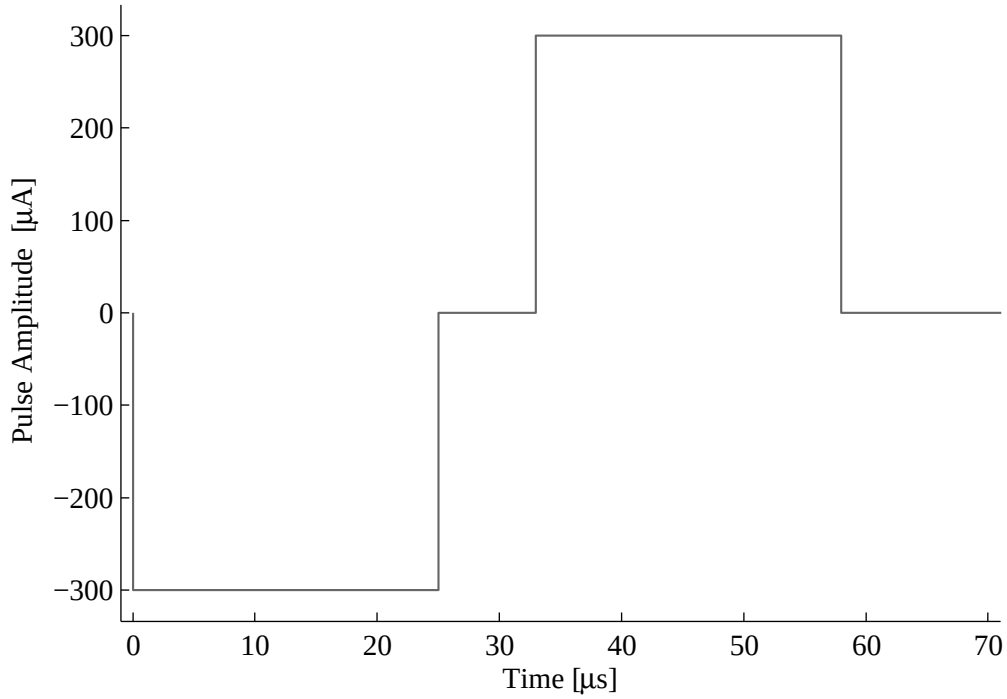

Figure 3.1: An example of the electrical-current waveform of a Nucleus implant is shown, as it would be measured for a single pulse on the active electrode. This is the temporal microstructure of each stimulus pulse. In this example, the phase-width was 25 μs for each phase of the charge-balanced biphasic pulse, with a phase-gap of 8 μs between the two phases and a typical current amplitude of 300 μA.

to the sites of subjects who could not travel to the research center. Whenever the CPS device was used, it was connected to the *personal computer* (PC) through the IF5 card (plugged into an ISA slot on the PC motherboard). The PPS device was connected either directly to a standard RS-232 serial port (whenever a PC was used to run experiments), or indirectly via a *universal serial bus* (USB) to RS-232 connector (when using the laptop computer). The CPS was also used in combination with the Cochlear RxFrames utility to record stimulation sequences via the PCI box for validation during the testing phases of newly developed software. In the latter scenario, to ensure independent operation of the generation and recording phases of stimulation, the PPS was typically employed through the laptop to generate the stimuli, while the CPS (with PCI) was used to record the stimuli. Further analysis of the recorded signal could then be performed with the custom-developed MATLAB toolbox.

When working with software that interacts with the cochlear implant, the numbering of electrodes (or channels) is of importance. Lower-level software, such as RxFrames and the encoding of the RF signal, tends to number electrodes starting from 0, which is assigned to the most apical electrode, where neuronal *characteristic frequencies* (CFs) tend to be low. On the other hand, higher-level software, such as the Nucleus MATLAB Toolbox (NMT), tends to number "channels" starting from 1, which is assigned to the most basal channel, where CFs tend to be high. Note that channels do logically correspond with a group (e.g., a pair) of electrodes, and the characteristics of the selected group depend on the mode of stimulation (e.g., bipolar). For *monopolar* (MP) stimulation there is a one-to-one correlation between an electrode and a channel. Also, for bipolar stimulation the more apical electrode is typically considered the return electrode of a channel (e.g., when referring to channel 2 in BP+1 mode, the return electrode would be number 4).

3.2 PSYCHOACOUSTICS TOOLBOX FOR MATLAB

The custom PSYCHOACOUSTICS TOOLBOX software was developed for the MATLAB 6.5 platform. To allow for easier integration with other systems and applications, a custom XML[1] format was also developed to represent various components of the PSYCHOACOUSTICS TOOLBOX, including configuration data for experiments and output data gathered from experiments. Cochlear provides the NIC software library[2] to specific researchers and investigators through

[1] For an introduction to *extensible markup language* (XML), see Marchal (2001) or Young (2001).

[2] Cochlear NIC 1.0 is essentially a *dynamic link library* (DLL) that provides a programming interface to Nucleus implant hardware. The software library can be accessed from various

a research agreement; for the present study, the library was available for use as the underlying interface mechanism for cochlear hardware. To allow the NIC interface to be used from within MATLAB, a *component object model* (COM) programming interface[3] was developed for the NIC API — in fact, the COM interface was implemented as a *COM callable wrapper* (CCW)[4] for the Microsoft .NET Framework[5] (version 1.1). The NICnet library also allows for an optional client-server setup (using .NET Remoting[6]), which may be desirable given the nature of some experiments. Cochlear's IF5 card technology, which is compatible with the Cochlear NIC API, is based on the obsolescent ISA standard. An older PC might be needed, then, because of its ISA slots. The older machine, however, is unlikely to have the computational processing power necessary to run the experiments' complex algorithms in MATLAB. The solution is to run the PSYCHOACOUSTICS TOOLBOX on a newer, more powerful machine, and the NIC-API-controlled hardware on an aging laggard equipped with ISA slots.

When performing psychoacoustic experiments, some tasks can become quite tedious for subjects when input to the computer needs to be performed with a mouse that requires the subject to aim at a specific user-interface control and then click on it. This is especially true of forced-choice tasks where successive trials are spaced just seconds apart. Therefore, a need was identified to allow subjects to operate alternative input devices when using the PSYCHOACOUSTICS TOOLBOX software, such as *game controllers* with physical buttons that would eliminate the need for graphical-user-interface input. To this end, the toolbox also depends on the Microsoft Managed DirectX library (Miller 2003),[7] which it uses to communicate with hardware input devices such as those shown in fig. 3.2.

programming languages; its use in the C language is detailed in Irwin (about 2002*a*). More general technical concepts related to NIC programming are discussed in Irwin (about 2002*b*). For additional information on DLL programming, refer to Richter (1996), Rector and Newcomer (1997) and Hart (2004).

[3]The Microsoft COM programming mechanism is an industry standard for providing software interfaces. Software developed with a COM interface is generally compatible with MATLAB, such that it can be accessed from within its programming environment. For details on COM programming, see Box (1997), Rogerson (1997).

[4]This CCW, named NICnet, also allows the NIC API to be used from within .NET applications without having to use COM directly. For details on CCW programming, see Nathan (2002).

[5]For more information about the Microsoft .NET Framework, with examples provided in the C# programming language, refer to Troelsen (2001), Richter (2002).

[6]Refer to Rammer and Szpuszta (2005) for details on Microsoft .NET Remoting technology.

[7]The Microsoft Managed DirectX library must be installed before proceeding with installation of the PSYCHOACOUSTICS TOOLBOX software.

Figure 3.2: Some hardware input devices are shown that are compatible with DirectX and could be used with the PSYCHOACOUSTICS TOOLBOX to capture responses during experiments.

3.2.1 Installation

The installation procedure for the PSYCHOACOUSTICS TOOLBOX is mostly an automated one. Installing the toolbox is simply a matter of ensuring that the prerequisite software has been installed, copying a single folder containing all the PSYCHOACOUSTICS TOOLBOX software to the machine, and then running the `ToolboxInstall` function from within MATLAB to perform the rest of the installation automatically.

The following prerequisite software must be installed on a Microsoft Windows operating system[8] before installing the PSYCHOACOUSTICS TOOLBOX software:

- Cochlear NIC API (including the NICstream component that ships with it),[9]
- MathWorks MATLAB 6.x, ideally version 6.5 (release 13),

[8]The experiments for the present study were executed primarily on machines with Windows 2000 SP4 and Windows XP SP2, while the server component of NICnet remoting sessions was also used on a Windows 98 machine.

[9]Although it is the NIC API that provides the main interface to the cochlear hardware for the NICnet module of the PSYCHOACOUSTICS TOOLBOX, the MATLAB installer of the PSYCHOACOUSTICS TOOLBOX also verifies that the NICstream ActiveX component is properly installed. This ensures that all NMT functions are available in MATLAB, since NMT needs the NICstream component to function completely.

- Microsoft XML Parser (MSXML) 3.0 with latest service pack (SP7 at the time of writing),
- Microsoft DirectX 9.0c with Managed DirectX, and
- Microsoft .NET Framework 1.1.

All required components are detected by the PSYCHOACOUSTICS TOOLBOX installer, and a descriptive error message is displayed during installation if any of these components are not installed. Additional spreadsheet functions become available though the PSYCHOACOUSTICS TOOLBOX when the optional Microsoft Office Web Components (OWC) are installed.

The directory containing the PSYCHOACOUSTICS TOOLBOX software must be copied to the machine where MATLAB will run, in a location chosen by the user.[10] Once the prerequisite software is installed, one can launch MATLAB and complete the installation procedure as described below.

From the MATLAB prompt, navigate to the `Matlab` folder (found within the PSYCHOACOUSTICS TOOLBOX folder that was copied to the PC), e.g.:

`cd c:\PsychoacousticsToolbox\Matlab` [Enter].

Type the command:

`ToolboxInstall` [Enter].

The automated installation procedure will continue. Messages displayed during installation will indicate any failure condition or successful completion.

3.2.2 XML Data Representation

The XML representation of PSYCHOACOUSTICS TOOLBOX data benefits from built-in features of the XML specification itself. The custom XML format was designed with human readability in mind (as opposed to computational efficiency), as the intent was to allow for easy manual editing. This allows the format to be used for configuration data (e.g., constructing new experiments from similar existing experiments or templates), and also allows output data from experiments to be read by humans in a text-based format. Therefore, the structure of this custom XML format follows a few basic patterns that are relatively easy to remember,

[10] The PSYCHOACOUSTICS TOOLBOX will subsequently load and execute from this folder even after the installation has been completed.

which are described next.

In many other specific XML formats, the names of elements play an important role, as the name usually determines which attributes may be specified for that named element and dictates how the element should be interpreted. This allows for *document type definition* (DTD) data to be specified, which makes it easier for computers to validate the correct formatting of the specific XML document. However, a different approach was taken with the design of the XML format for the PSYCHOACOUSTICS TOOLBOX, which results in a more compact and readable format. The XML elements themselves are treated in a more generic way, and the attributes assigned to an element dictate much of the element's interpretation. As a result, the names of elements can be more descriptive and logically tend to correspond with property names of objects, while the attributes of an element dictate how the inner content of that element (such as contained text) must be interpreted. There are two primary generic attributes that dictate a PSYCHOACOUSTICS TOOLBOX XML element's interpretation, namely the `type` and `trans` attributes. The `type` attribute specifies the raw data-type of the inner content of the element as it needs to be deserialized from the element's child node(s). The `trans` attribute specifies a transformation (if needed) to be performed on the extracted raw data. The combination of the two attributes allows for a very powerful data serialization mechanism.

The `type` attribute represents the fundamental data-type of the variable represented by the XML element's content. Some of the more common values of the `type` attribute are `string`, `bool`, `cell`, `code`, `double`, `function` and `struct`, as illustrated in fig. 3.3.

```
<TypeAttributeExample type="cell">
  <item type="string">XYZ</item>
  <item type="double">3.14159</item>
  <item type="struct">
    <SomeFlag type="bool">true</SomeFlag>
    <SomeFunction type="function">cos</SomeFunction>
  </item>
  <item type="code"><![CDATA[
    if (getat(clock, 6) < 30), eps, else pi, end
  ]]></item>
</TypeAttributeExample>
```

Figure 3.3: XML elements can specify a `type` attribute, which is recognized by the PSYCHOACOUSTICS TOOLBOX and defines the fundamental data-type of an XML element's content.

The XML code of this figure also demonstrates how larger structures of XML elements are

handled in such a way that leaf elements are processed first and then combined progressively with parent elements in the XML data tree, such that for the previous example the resulting data output would be a single cell array consisting of data items of different types. Further note in this example how the content of the `code` typed element is used in conjunction with the standard XML `CDATA` section sequences, allowing for cleaner code containment, since characters such as the left angle bracket (i.e., the less-than sign) do not need to be XML-escaped. There are numerous other `type` values, including some that represent the graphical objects of MATLAB. For example, the `grobfigure` and `grobmenu` values represent a figure and a menu object, respectively. Various XML examples of different data types and varying degrees of complexity can be found in the `Matlab\Example` directory of the PSYCHOACOUSTICS TOOLBOX. However, the `type` attribute is an optional attribute; when the `type` attribute is not specified, the default value of the attribute is determined using the algorithm depicted in the flow diagram of fig. 3.4. This algorithm was engineered in such a way that one generally would not need to specify the `type` attribute explicitly; the type of data would (as in the previous type-attribute example) default to the "obvious" type. To elaborate, within the context of the previous example XML code, if no `type` is specified and an element's context is `XYZ`, the data will be interpreted as a string, while an element content value of `3.14159` will, by default, represent a floating-point number, and an element with sub-elements specifies a data structure by default.

The `trans` attribute specifies an optional transformation to be executed after deserialization of the XML content into the raw-data format. A special case for using this attribute is to convert raw `struct` data into a cell-array by specifying the value `cell` for the `trans` attribute, which allows for a more verbose syntax of defining cell-arrays that are more descriptive and easier to read, as shown in fig. 3.5. Also note that specifying `cell` for the `trans` attribute would (by default) result in a cell-array with a single column, while specifying this instead as the `type` attribute value produces (by default) a single-row cell-array. More often, though, the `trans` attribute would specify the name of a MATLAB class (in terms of *object-oriented programming*, i.e., OOP) or ActiveX component, of which an instance needs to be constructed from the raw data, or the name of a function that needs to be called with the raw data as parameter. This last usage is illustrated in fig. 3.6, in which the parsed result would be a random number from 1 to 10, generated by passing the text content as a string to the `eval` function. When the `trans` attribute is the name of a class, the raw data could be a string value if it is supported as a parameter to the constructor of that class, as shown in fig. 3.7, where a symbolic expression (i.e., a `sym` object) is constructed from the text string content. (The parameter could also be any other data type supported

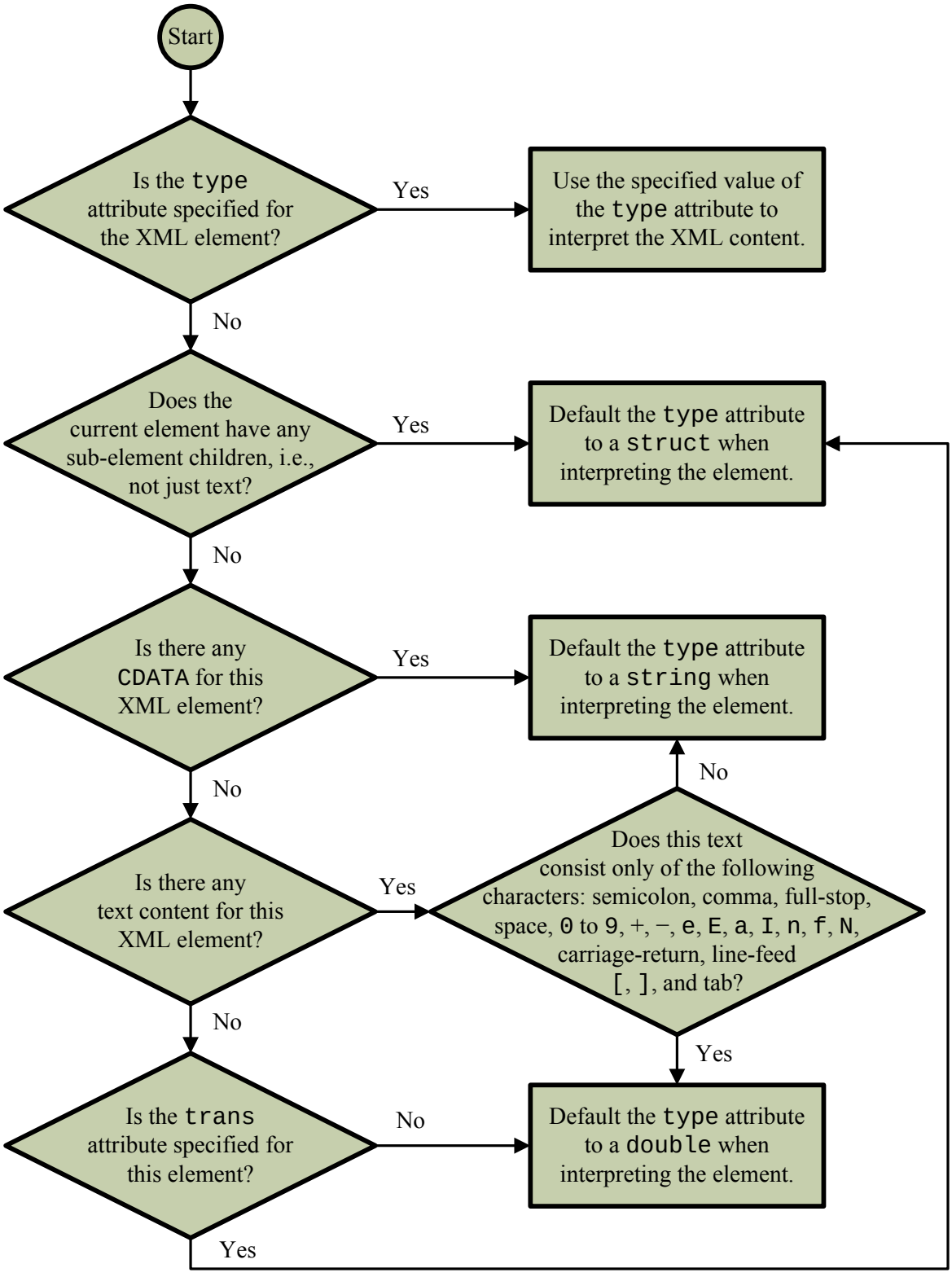

Figure 3.4: Depicted in this flow diagram is the algorithm used to determine the data type when a PSYCHOACOUSTICS TOOLBOX XML element needs to be deserialized into a MATLAB variable representation. Since the `type` attribute is optional (to allow for more readable XML), a well-defined algorithm is needed to determine the default value of this attribute when it is omitted.

by an object's constructor.) However, a more common way of specifying a class name for the transformation is to do so in combination with raw `struct` data, as shown in fig. 3.8 (where the `type` attribute of the outer XML element would default to `struct`, since it contains child nodes that are XML elements). When the XML text of this example is converted into a MATLAB variable, it results in the creation of a `timer` object in which properties that correspond with the names of the sub-elements are assigned the (deserialized) value for each matching property. For example, the `Tag` property is assigned the string value `CustomTimer`, while the object's `StartDelay` property is set to a 0.5 double-precision floating-point value. For ActiveX components (i.e., integration with Microsoft's

```
<CellTransformationExample type="struct" trans="cell">
  <FirstRow>A string value</FirstRow>
  <DoubleNumberInLastRow>123.456789</DoubleNumberInLastRow>
</CellTransformationExample>
```

Figure 3.5: A specific case is shown for transforming a data structure into a cell array using the `trans` attribute, such that descriptive names can be used for XML sub-elements instead of the standard `item` name (as used in fig. 3.3).

```
<data trans="eval">1 + floor(rand * 10)</data>
```

Figure 3.6: An XML example is shown, in which the transformation attribute specifies a MATLAB function (named `eval`, in this case). The XML element's contained text is passed as a parameter to the function, which in turn evaluates the text string and returns a random number for the final value of the XML element.

```
<data trans="sym">x + 3</data>
```

Figure 3.7: This example shows how the name of an object constructor can be specified with the `trans` attribute. Here, the XML element's contained text is passed as a string to the constructor of MATLAB's standard `sym` object (which will create a symbolic object).

COM technology), a component is constructed in an almost identical way, with sub-elements used to specify values for the properties of the COM object. For example, a Microsoft XML Parser COM object can be constructed by specifying `COM.Microsoft.XMLDOM` for the `trans` attribute's value, along with appropriate sub-elements such as `async` and `preserveWhiteSpace`.

The `size` attribute is another generic XML attribute of interest, although it might not be

```
<TimerObjectConstructedFromStructData trans="timer">
  <Tag>CustomTimer</Tag>
  <Name>Timer123</Name>
  <BusyMode>drop</BusyMode>
  <ExecutionMode>fixedRate</ExecutionMode>
  <StartDelay>0.5</StartDelay>
  <Period>1.5</Period>
</TimerObjectConstructedFromStructData>
```

Figure 3.8: The XML example shown here illustrates the transformation of a data structure into an object (in this case, a `timer` object), in which sub-elements of the root node map to properties of the MATLAB object.

used very often. This attribute is used in the context of arrays to specify the dimensions of the XML element's contained array data, as shown in fig. 3.9 for a 2×3 cell array.

```
<SizeAttributeExample type="cell" size="2␣3">
  <item>Data for row 1, column 1</item>
  <item>Data for row 2, column 1</item>
  <item>Data for row 1, column 2</item>
  <item>Data for row 2, column 2</item>
  <item>Data for row 1, column 3</item>
  <item>Data for row 2, column 3</item>
</SizeAttributeExample>
```

Figure 3.9: This XML code illustrates the use of the `size` attribute to specify array dimensions.

For the conversion of different data representations between XML and various other formats, such as the native MATLAB variable representation, numerous utility functions were developed as part of the PSYCHOACOUSTICS TOOLBOX software. The possibilities of these conversions are summarized in fig. 3.10 in a graph format similar to a state diagram, which shows the different data representations and the functions to be used for the various conversions. Specific functions can also operate in a number of different conversion roles (i.e., in programming jargon, the functions are overloaded). More details about the parameters to be used for the different conversions can be obtained using the standard MATLAB `help` and `doc` features for each function. An illustration of the usage of some of the conversion functions can be found in the transcript of an interactive MATLAB session shown in fig. 3.11.

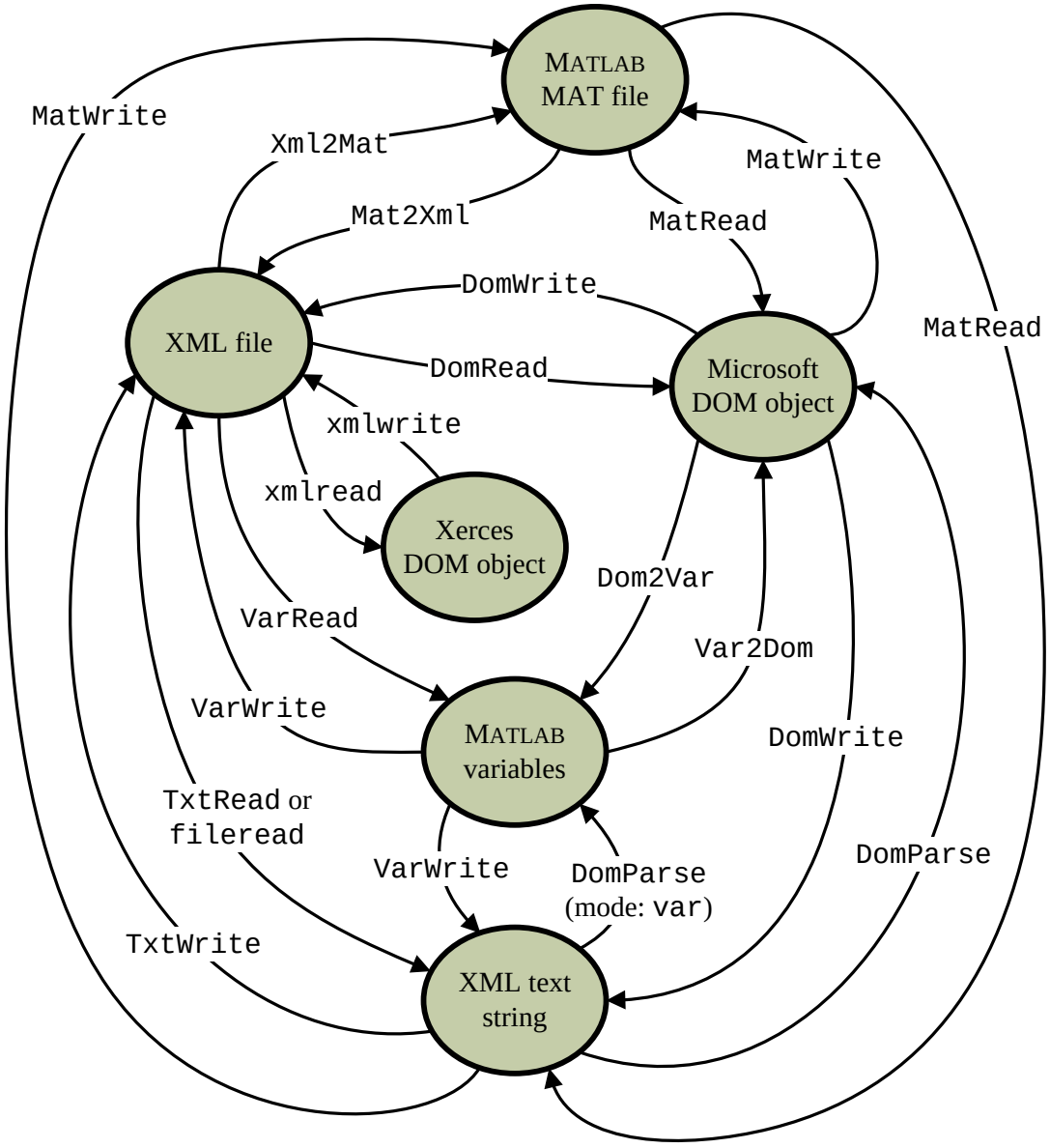

Figure 3.10: The functions to be used for conversion of XML data in the PSYCHOACOUSTICS TOOLBOX are illustrated. Arrows represent the functions, while the filled areas represent the various types of data representation. For example, to write the value of a MATLAB variable out as an XML string to the console, the `VarWrite` function can be used. Also note that data can be represented in memory as *document object model* (DOM) objects for programmatic navigation between XML nodes. Further details on using the functions can be found in their respective built-in help documentation using the standard MATLAB `help` and `doc` facilities. Of the functions depicted, the three all-lowercase ones are built-in MATLAB functions, while the rest are part of the PSYCHOACOUSTICS TOOLBOX.

```
>> % Initialize an array variable
>> x = [1, 2, 3; 4, 5, 6];
>> % Convert the variable to an XML string
>> s = VarWrite(x)

s =

<x>1 2 3;4 5 6</x>


>> % Convert the XML string to a variable
>> x = DomParse(s, 'var')

x =

     1     2     3
     4     5     6

>>
```

Figure 3.11: Interactions with a MATLAB session are shown, illustrating how the `VarWrite` and `DomParse` functions of the PSYCHOACOUSTICS TOOLBOX can be used to convert data between XML and MATLAB variable formats.

3.2.3 Experiment Templates and Logical Flow

The PSYCHOACOUSTICS TOOLBOX has a number of templates available for implementing experiments, which can be used as the basis for developing specific new experiments. The structure of the experiments can broadly be classified into two categories, namely those experiments that consist of a predefined set of stimuli and those that dynamically determine which set of stimuli needs to be presented to the subject taking part in the experiment. The former category of experiments works well for cases in which the subject needs to make judgements about a fixed number of stimuli, while the latter category typically makes use of a well-defined adaptive procedure to determine the sequence and number of stimuli to be presented. The PSYCHOACOUSTICS TOOLBOX implements these two categories of experiments in the `ConstantStimuliExperiment` and `ForcedChoiceExperiment` classes, respectively. In addition, when it comes to adaptive procedures, there are two general types of experiments that can be implemented: those in which responses collected by the subject can objectively be judged as correct or incorrect (such as which interval contains a stimulus of longer duration), and those in which the correctness of the response is subjective and depends on the subject's own perception (such as loudness comparisons between different

cochlear electrodes). The combination of these options makes for three basic formats of experiments:

- constant stimuli experiments,
- adaptive procedure experiments with objective answers, and
- adaptive procedure experiments with subjective answers.

All these types of experiments are catered for by the PSYCHOACOUSTICS TOOLBOX, and different templates are available to develop any such experiment. Along with other examples of experiments based on templates that can be found in the `Matlab\Example` directory of the PSYCHOACOUSTICS TOOLBOX, the following template files are of interest as a baseline for these three formats of experiments:

`DemoExperimentConstantStimuli.xml` demonstrates a multitask experiment consisting of a constant set of stimuli;

`DemoExperimentObjective2AFC.xml` implements an experiment with objectively correct or incorrect answers, using a standard "2-down 1-up" *two-alternative forced choice* (2AFC) procedure; and

`DemoExperimentSubjective2AFC.xml` shows an experiment with subjectively correct or incorrect answers, using the 2-track interleaved 2AFC procedure of Jesteadt (1980) with a "2-up 1-down mostly-softer" and "2-down 1-up mostly-louder" track.

To contrast the usage of a computer's standard sound hardware as a stimulus mechanism with the Cochlear hardware, the following two template files are illustrative. Each example implements an adaptive-procedure experiment with subjective answers, using the random-interleaved-track procedure of Jesteadt (1980):

`DemoExperimentPoissonRatePitch.xml` matches the pitch of a Poisson process[11] with that of an isochronous stimulus using the computer's standard sound hardware, and

[11] Refer to appendix C for a description of how the Poisson-process generator was implemented in the PSYCHOACOUSTICS TOOLBOX.

`DemoExperimentImplantLoudness.xml` implements a loudness-balancing experiment of stimuli with different phase widths using a cochlear implant through the NICnet interface.

The basic structure for the chronological execution of any experiment that is based on the templates implemented within the PSYCHOACOUSTICS TOOLBOX is shown in fig. 3.12. The

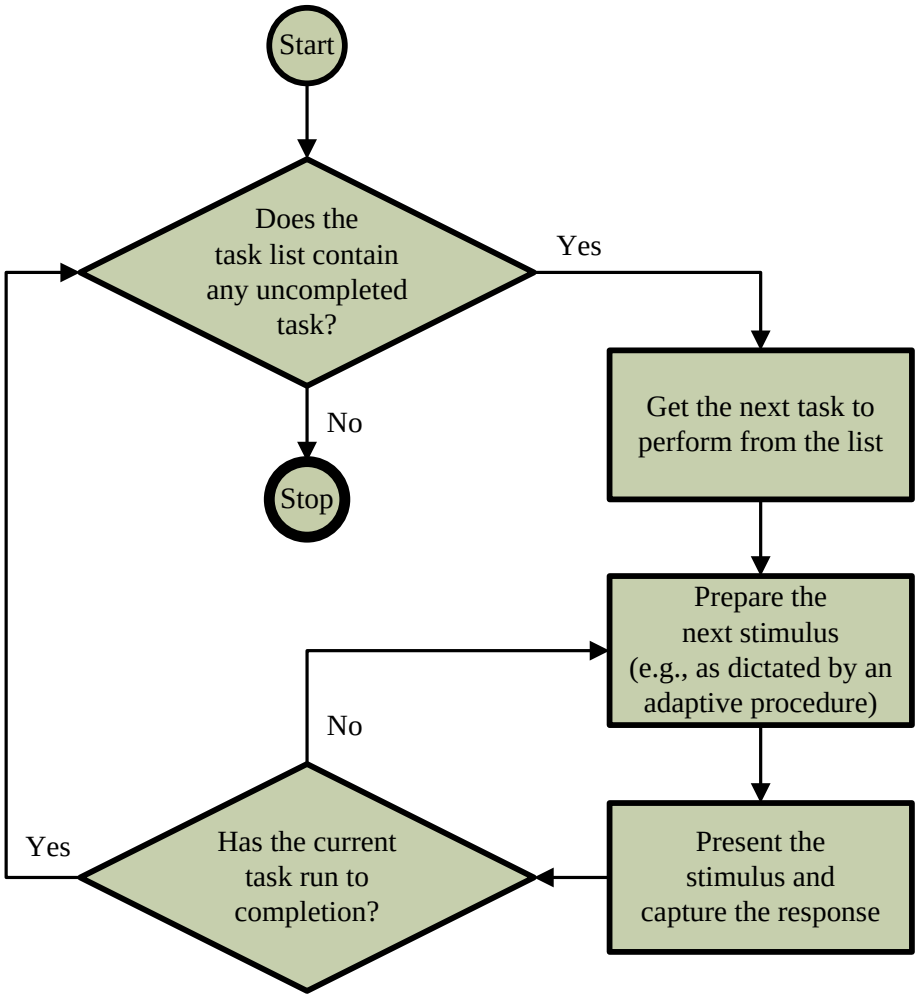

Figure 3.12: The basic chronological structure of each PSYCHOACOUSTICS TOOLBOX experiment is depicted in this flow diagram.

specifics of each of these activities could differ for the various experiments. For example, some experiments may consist only of a single task, while others may contain a whole list of tasks. The procedure for dynamically determining the parameters and generating sequential stimuli may be different, and the hardware mechanism used to present a stimulus may be different. However, the essential sequential flow of activities during any experiment remains the same. With an understanding of the usage of XML templates in the PSYCHOACOUSTICS TOOLBOX and the aspects that may differ between them, it is possible to proceed with the

construction of specific experiments for research purposes.

3.2.4 Example Experiment

To illustrate the usage of the PSYCHOACOUSTICS TOOLBOX, a complete example is included and discussed in this section. The example implements a psycho-electric gap-detection experiment consisting of three tasks (one task for three stimulation sites, using different electrical current levels). For illustrative purposes, the example is of an intermediate complexity level and avoids some of the more advanced features that are typically found in real experiments, which may include complex task lists, multi-track procedures, temporal roving, validation of trial values (i.e., bounding), automation of batches of experiments (using the `RunExperimentList` function) and management of results databases.

The example code that implements the experiment consists of a single XML file, called `ExampleGapDetection.xml`, but is presented as three separate code figures (because of its length). The main structure of the XML document is listed in fig. 3.13, which includes all the XML nodes that constitute the experiment; however, the bulk of the MATLAB callback function (which presents the trial stimulus to the participant) has been omitted from the figure. The latter is listed in figures 3.14 and 3.15.

The root XML element of the example represents a `ForcedChoiceExperiment` object, which implements the chronological experiment structure depicted in fig. 3.12. One may start the experiment by typing the commands in fig. 3.16 at the MATLAB prompt. The example experiment's task list consists of three tasks, each represented by a matrix row of the `FullTaskList` element (see fig. 3.13). Upon creation, the experiment object will start to process the task list, running an adaptive-staircase procedure for each of the specified tasks until all tasks have completed. As each task is executed, the experiment object's `Tasks.CurrentTask` property contains the present task being executed.[12] The primary callback function (by convention named `PresentTrialStimulus`) represents the code logic for the second block shown in fig. 3.12, in which the stimulus sequence is prepared for a specific trial. As the function completes, it initiates asynchronous presentation of the sequence, and control returns to the experiment object that coordinates the signaling lights displayed on the GUI to indicate signal intervals as they are presented asynchronously (for an illustration of the animation, refer to fig. 4.4). User feedback is collected, and the procedure

[12] Refer to fig. 3.14 for the `CurrentTask` code, and see the block at the top of fig. 3.12 for the control logic.

```
<!-- Specify the experiment setup: 2AFC, 3-down 1-up -->
<ExampleGapDetection trans="ForcedChoiceExperiment">
  <ChoiceCount>2</ChoiceCount>
  <AdaptiveProcedure trans="AdaptiveStaircaseProcedure">
    <RuleName>3-down 1-up</RuleName>
  </AdaptiveProcedure>
  <!-- Name of the file in which results would be saved -->
  <OutputFilename>ExampleGapDetection.mat</OutputFilename>
  <!-- A description of the task to display on the GUI -->
  <TaskDescription>Pick the interval...</TaskDescription>
  <GUI>
    <DialogTitle>Gap-Detection Example</DialogTitle>
  </GUI>
  <!-- List of values to be varied for different tasks -->
  <Tasks trans="TaskListManager">
    <!-- e.g., 3 tasks: channel vs. current-level values -->
    <FullTaskList>4,193; 12,186; 20,179</FullTaskList>
  </Tasks>
  <!-- Start value for gap duration, e.g., 0.020 seconds -->
  <StimulusStartValue>0.020</StimulusStartValue>
  <!-- Specify the code that would present each trial -->
  <StimulusCallback type="code"><![CDATA[
function [SigDurations,LogData] = PresentTrialStimulus(this)
    % [Function code omitted for clarity; see next figure]
  ]]></StimulusCallback>
</ExampleGapDetection>
```

Figure 3.13: An XML example is shown for an electro-acoustic gap-detection experiment, as it can be constructed using the PSYCHOACOUSTICS TOOLBOX. The embedded MATLAB code that constructs and presents the stimuli has been omitted for the sake of clarity, but can be found in figures 3.14–3.15. The experiment is set up with a 2AFC 3-down 1-up adaptive-staircase procedure and contains three tasks to be completed by the participant. Each staircase starts with a gap duration of 20 ms. The *graphical user interface* (GUI) presented with an experiment is configurable, and, in this example, a task description is specified (the short text contained by the `TaskDescription` element), along with a title for the dialog window. Although not demonstrated here, the output filename (specified through the `OutputFilename` attribute) can incorporate a time-stamping mechanism for real experiments.

```
<!-- [XML code continues above; see previous listing] -->
  <!-- Specify the code that would present each trial -->
  <StimulusCallback type="code"><![CDATA[
function [SigDurations,LogData] = PresentTrialStimulus(this)
% Specify the values to be used for the present task
Task = this.Tasks.CurrentTask;  % One task from FullTaskList
StimCH = Task(1);     % Retrieve the present channel number
StimCL = Task(2);     % Retrieve the present current level
StimMode = 'MP1+2';   % Stimulation mode; reference electrode
StimRate = 900;       % Hz, i.e., pulses per second
PhaseWidth = 25;      % Stimulus phase-width, in microseconds
PhaseGap = 8;         % Stimulus phase-gap, in microseconds
T_on = 0.400;         % Interval time-durations, in seconds
T_off = 0.200;        % Duration between intervals (seconds)
T_dead = 250e-6;      % Dead-time period, in seconds
% Obtain the adapting gap-duration for the present trial
T_gap = this.AdaptiveProcedure.CurrentTrialValue;  % seconds
% Construct the stimulus sequence for present trial values
t_ini = GeneratePoissonInstants(...  % Instants without gap
          T_on, (1 / StimRate), T_dead, '-tolerance=0.3%');
T_ini = [diff(t_ini(:)); (1 / StimRate)];  % as periods [s]
t_mod = t_ini;  idx = find(t_ini >= (T_on / 2));
t_mod(idx) = t_mod(idx) + T_gap;  % Instants with the gap
T_mod = [diff(t_mod(:)); (1 / StimRate)];  % as periods [s]
T_on = t_ini(end);  % Actual on-time duration of interval
Seq_ini = NICnetFormatSequence(struct( ...
    'T',  1e6 * T_ini, ...      % Frame period [microseconds]
    'PW', PhaseWidth, ...       % Phase width [microseconds]
    'PG', PhaseGap, ...         % Phase gap [microseconds]
    'CL', StimCL, ...           % Stimulus current-level
    'E',  StimCH, ...           % Active electrode
    'R',  StimMode));           % Reference electrode
Seq_mod = NICnetFormatSequence(struct( ...
    'T',  1e6 * T_mod, 'PW', PhaseWidth, 'PG', PhaseGap, ...
    'CL', StimCL,      'E',  StimCH,     'R',  StimMode));
% [Function code continues below; see next figure]
```

Figure 3.14: This listing contains primarily the first part of the MATLAB function that has been omitted from fig. 3.13. The function's purpose is to build and present the entire stimulation sequence for a single trial, which, in this example, consists of two 400 ms signal intervals (one containing an additional temporal gap) with a 200 ms silence period between the two intervals. The macrostructure of the sequence is similar to that of fig. 4.3, which shows periodic signals, but in the present case a Poisson sequence is generated. The second part of the MATLAB function is listed in fig. 3.15.

```
% [Function code continues above; see previous figure]
Seq_off = NICnetFormatSequence(struct(   ...
    'T',  repmat([1e6 / StimRate],       ...
            round(StimRate * T_off), 1), ...  % "Off" period
    'PW', PhaseWidth,  'PG', PhaseGap,   ...
    'CL', 0,           'E',  StimCH,     'R',  StimMode));
TrialInterval=this.AdaptiveProcedure.CurrentDesiredResponse;
if (TrialInterval == 1)
  Sequence = NICnetAppendSequence(Seq_mod, ...
             NICnetAppendSequence(Seq_off, Seq_ini));
else
  Sequence = NICnetAppendSequence(Seq_ini, ...
             NICnetAppendSequence(Seq_off, Seq_mod));
end
% Use NICnet (custom CCW for NIC 1) to stream the sequence
Success = NICnetStreamSequence(Sequence, ...
            struct('compression', 'run_length'));
if (~Success)
  SigDurations = [];   % Indicate stimulus failure
else
  % Specify signaling time-periods of intervals (lights)
  SigDurations = [(T_on+T_gap/2), T_off, (T_on+T_gap/2)];
end
LogData = struct([]);  % Don't write anything to the log
  % Close the outer XML nodes
  ]]></StimulusCallback>
</ExampleGapDetection>
```

Figure 3.15: The listing presented here is a continuation of the code from fig. 3.14, which specifies the MATLAB code for the stimulation function that is part of the example XML file shown in fig. 3.13. The code determines which interval should contain the gap, concatenates the segments of the stimulation intervals and then initiates the asynchronous streaming of the stimulation sequence to the hardware (using the `NICnetStreamSequence` function). If this succeeds, the code specifies the durations for which the signaling lights should be animated, and then returns control to the calling `ForcedChoiceExperiment` object.

```
experiment = VarRead('ExampleGapDetection.xml');
experiment = create(experiment);
```

Figure 3.16: The MATLAB commands shown here illustrate how one can start the example experiment. It is assumed that the code for the example, listed in figures 3.13–3.15, is stored in a file named "`ExampleGapDetection.xml`". The first command deserializes the XML file into in-memory MATLAB data (see `VarRead` in fig. 3.10), with the root of the data tree being a `ForcedChoiceExperiment` object. The second command creates the GUI and starts running the experiment, which prompts the user to indicate readiness for stimulation.

continues as dictated by the configured `AdaptiveProcedure` element (which, in the case of this example, is an `AdaptiveStaircaseProcedure` object with a "3-down 1-up" rule). If required, the adaptive procedure will adjust the trial value, and the experiment object will again loop though stimulation callback logic (refer to the smaller control loop in the bottom-right corner of fig. 3.12). As soon as the adaptive procedure determines that the staircase has executed to completion (which is exposed through a boolean property called `DoneState`, e.g., on the `AdaptiveStaircaseProcedure` object), the experiment object saves its present state to the output file (specified though the XML element that represents the `OutputFilename` property). The state of the experiment that is persisted to the file system will contain the feedback received from the user and turnaround trial values that can be processed for analysis when results need to be consolidated.[13] The experiment object would then move to the next task in the list as it cycles though the outer control path depicted in fig. 3.12.

The code snippet in fig. 3.17 illustrates how the output file, which is generated by the example experiment object, can be processed at a later stage. The output of the commands at the MATLAB prompt would display the estimates of the gap thresholds for the three tasks. To calculate the estimates, the default averaging algorithm of turnarounds for a single-track experiment will be used, which is the same as discussed in § 4.4.[14]

```
output = struct2cell(load('ExampleGapDetection.mat'));
GapThreshold = output{1}.AdaptiveProcedure.BlockValueEstimate
GapThreshold = output{2}.AdaptiveProcedure.BlockValueEstimate
GapThreshold = output{3}.AdaptiveProcedure.BlockValueEstimate
```

Figure 3.17: The measured values of the three gap-detection thresholds, which are recorded as part of the output from the example experiment, can be retrieved as shown in the MATLAB code.

In addition, it is often useful to know the statistical standard-deviation of the estimates measured through an experiment's adaptive procedure (as shown in the data tables of appendix D). The code snippet in fig. 3.18 shows how the turnaround data that are used to calculate a staircase estimate can be obtained and used in further calculations.

[13] For performance reasons, the PSYCHOACOUSTICS TOOLBOX stores output files in the standard MATLAB format (i.e., in "`.mat`" files). However, the data may be converted to XML format, which can more easily be inspected visually (see fig. 3.10 for conversion options).

[14] More advanced functions for collecting, storing and retrieving task data are available through the PSYCHOACOUSTICS TOOLBOX's `DataBagProcessorCore` object.

```
output = struct2cell(load('ExampleGapDetection.mat'));
experiment = output{1};
[GapThreshold, TurnaroundData] = ...
  getBlockValueEstimate(experiment.AdaptiveProcedure)
StandardDeviationOfGapThreshold = std(TurnaroundData)
```

Figure 3.18: The MATLAB code shown here illustrates how the standard deviation can be calculated for the turnaround points of a completed adaptive-staircase experiment.

This chapter provided an overview of the PSYCHOACOUSTICS TOOLBOX, the software package developed as part of the present study. A complete description of the software is beyond the scope of this document, but the interested reader is encouraged to explore the examples (with comments) and MATLAB help documentation that are included with the software. The software provides a framework for developing psychophysical experiments, and has been employed for the construction of the present electro-acoustic experiments that focus primarily on the measurement of gap-detection thresholds. The research experiments are documented in the next chapter.

CHAPTER 4

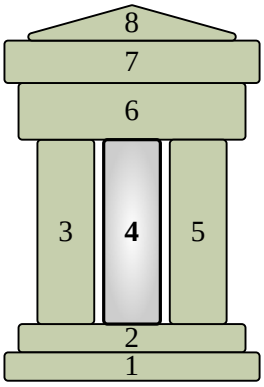

METHODS FOR PSYCHOPHYSICAL EXPERIMENTS

After the preceding discussion of the software that was developed, the PSYCHOACOUSTICS TOOLBOX, which enables the execution of psychophysical experiments, the focus now turns to the experiments themselves. These include gap-detection experiments that were part of the initial pilot studies performed with one of the subjects, initial duration-discrimination experiments conducted with three subjects, as well as the primary gap-detection experiments that were repeated numerous times with various parameters on three subjects (with four implants in total, since one subject has an implant in each ear). The use of loudness-balancing experiments in preparation for the primary gap-detection experiments is also addressed.

4.1 TIMING OF PULSES

Two different types of stimulus sequences used in the psychophysical experiments will be encountered frequently throughout this chapter. These sequences are referred to as either

periodic stimuli or *dead-time-modified Poisson* stimuli (or *Poisson* for short). The names refer to the temporal positioning of the individual stimulus pulses, which can be observed from the differences in fig. 4.1. The *periodic* stimuli are positioned, as one would expect, at regular intervals. The *Poisson* sequences refer to the positioning of pulses defined by a Poisson point-process, and more specifically to processes that are always homogeneous; in short, this means that the average rate of stimulation remains constant. The "dead-time-modified" part simply means that there is a short period after the occurrence of a pulse during which the following pulse has no chance of being present.[1] This serves primarily two purposes:

- since the equipment that was available to be used for cochlear stimulation in the present research cannot stimulate on two channels concurrently (a condition, born out of concern for biological safety,[2] that allows one to calculate safe stimulus levels more easily), this offers a mathematically elegant means to take these hardware limitations into account, and

- it provides a mechanism to establish an upper limit on the instantaneous stimulation rate of a single stimulation site, which (to stay clear of irreversible Faradaic reactions[3]) may also be a concern for biological safety.

The durations between successive stimulation pulses can be expressed in mathematical terms using a statistical *cumulative distribution function* (CDF). (The mathematical notation and definition of the CDF is properly formulated in appendix A and used more extensively in chapter 5, in which statistical nomenclature is formally introduced, but a basic understanding of this general probability concept would suffice for the present discussion.) The CDF for the durations between consecutive stimulation pulses of the generic dead-time-modified Poisson-process, where these durations are represented by τ, can be specified as follows:[4]

$$cdf(\tau) = \begin{cases} 0 & \forall \quad \tau < \tau_d \\ 1 - \mathrm{e}^{-(\tau-\tau_d)/(\tau_\lambda-\tau_d)} & \forall \quad \tau \geq \tau_d \end{cases} \tag{4.1}$$

[1] Note that the dead time that is discussed here refers to that of the stimuli themselves (i.e., the presented electrical input's stimulus-on duration), and this should not be confused with the "dead time" or "paralysis" of the neurons shortly after being stimulated (i.e., the response of the nerves to the presented stimuli), which is also referred to as the refractive period of the neuron.

[2] For example, safety issues of electrical stimulation have been documented by Shannon (1992).

[3] See Merrill et al. (2005) for more on Faradaic reactions in the context of stimulation safety.

[4] This equation also corresponds with the point-process generator-function from eq. C.2, with identical variable interpretation.

$$= \theta(\tau - \tau_d) \cdot \left\{1 - \mathrm{e}^{-(\tau-\tau_d)/(\tau_\lambda-\tau_d)}\right\} . \tag{4.2}$$

Variables τ_d and τ_λ represent the dead-time period and average period (i.e., statistically expected period, or the reciprocal of the mean rate) of the point process, respectively. The reduced form shown in eq. 4.2 makes use of $\theta(\tau - \tau_d)$ to represent the Heaviside function (i.e., unit step function) displaced by the dead-time duration.

For the actual experiments, the dead-time parameter was chosen as $\tau_d = 250\,\mu$s, consequently limiting the maximum instantaneous stimulation rate to $\lambda_d = 4\,$kHz (which is below the maximum reported rate used by other experimenters, where the upper limit per channel is usually below the 5000–6500 pps range). For examples of high channel rates used by others for experimental purposes, see Rubinstein et al. (1999) and Büchner et al. (2004). Also note that, although the Clarion CII device is capable of delivering up to 373000 pps in total, software limits the maximum non-simultaneous update rate to 6500 biphasic pulses per second (Frijns et al. 2002) to mimic the Clarion CI, an older device. Furthermore, in recent clinical studies on Nucleus hardware (Plant et al. 2007, Balkany et al. 2007) where high total stimulation rates were used, the reported maximum rate per channel was typically well below 5000 pps. In addition to using the dead-time parameter, selected realizations of the Poisson process (i.e., those with short-term statistics sufficiently close to the long-term statistics) were used; see p. 161 for details about the tolerance criterion.

4.2 EXPERIMENT SUBJECTS

Details of the three cochlear implant users (with four implants in total) who participated in psycho-electric experiments for this study are shown in table 4.1. All subjects were female adults, aged between 37 and 55, and had had at least one implant for four years or more at the time of this study. The primary implant type used with each subject was a Cochlear Nucleus CI-24 device, and additional sets of experiments were performed with subject S3a using her CI-22 implant. The CI-24 devices were all implanted in the right ear, while the CI-22 was implanted in the left. Note that the processor and strategy data shown in the table are for normal operation by the subjects and are listed for informational purposes only. Their processors were not used for experiments — instead, a dedicated SPrint speech processor was used for all experiments, and the PSYCHOACOUSTICS TOOLBOX constructed all stimulation sequences without the use of any map strategy.

Table 4.1: This table shows details of cochlear implant users who participated in the study. The information includes the age of the subjects (in *years*) at the time when each performed the majority of their gap-detection experiments, the cause of deafness (etiology), duration since onset of complete deafness (T_{deaf}, in *years*), duration since implant activation ($T_{implant}$, in *years*), type of Nucleus *cochlear implant* (CI), the external speech processor and its normal map's strategy.

	Subject S3a	Subject S3b	Subject S5	Subject S10
Age [*years*]	55.3	55.1	37.2	51.4
Etiology	congenital progressive	congenital progressive	congenital progressive	unknown
T_{deaf} [*years*]	approx. 10	approx. 10	5.5	approx. 1.5
$T_{implant}$ [*years*]	9.0	0.5	5.0	4.0
CI type	CI-22	CI-24	CI-24	CI-24
Processor	ESPrit 22	ESPrit 3G	ESPrit 3G	ESPrit 3G
Strategy	SPEAK	ACE	ACE	ACE

4.3 LOUDNESS BALANCING

In preparation for the primary experiments that were performed, electrical-current values had to be determined for stimulation sequences. For some cases of gap-detection experiments, where it would be clearly indicated, quoted currents used for stimuli have been balanced for loudness.

For the loudness-balancing steps, the 2AFC two-track (consisting of one "1-up 2-down" and one "2-up 1-down" track), randomly interleaved adaptive procedure described by Jesteadt (1980) was used to measure the currents. This procedure is ideal for subjective percepts such as loudness, and proved to be very useful in the present study. It is interesting to note that this adaptive procedure has gone unnoticed for so long after it was published, but it is encouraging to see that the procedure has gained much in popularity in recent years and has been put to good use, especially by the psychoacoustics research community. This procedure does deserve more recognition and should be considered seriously by all researchers investigating subjective perceptions. To make this procedure more easily accessible, the random interleaving of multiple adaptive-staircase tracks has been added as a standard feature to the PSYCHOACOUSTICS TOOLBOX.

Each sequential run was terminated after both tracks had undergone ten reversals. The step-factor values were progressively decreased as the number of reversals increased, for each track, in the same way as for the duration-discrimination experiments discussed in § 4.4, but, in addition, a maximum change of seven *current levels* (CLs) was imposed to avoid

sudden over-stimulation. To obtain a single loudness-balanced current-level estimate for an experiment run, the last six reversals of each track were averaged and, subsequently, the two-track estimates were averaged (resulting in an effective average of 12 turnarounds in total).

The experiments in which loudness balancing is applicable for the present study always involve subject S3b, and the participant was asked to "pick the louder of the two sounds". The signaling intervals that were to be balanced were always 350 ms in duration, and the silence interval between signaling intervals was typically 300 ms (in a few cases, however, the inter-interval duration was set to 250 ms or 500 ms, as appropriate values were initially still being evaluated). The details of specific loudness-balancing measures are addressed later in this chapter, including discussion of why loudness balancing was intentionally omitted for certain experiments (refer to § 4.5.2 in particular).

4.4 DURATION-DISCRIMINATION EXPERIMENTS

One of the more challenging aspects of psychophysical research is design of the actual experiments, and more specifically the need to eliminate any cues that might influence desired measurements. The primary experiments of this study revolved around temporal-gap percepts. Consequently, one needs to critically examine all temporal aspects of the stimulation sequence that might have undesirable effects on the measurements, not to mention other aspects that are themselves influenced by temporal aspects.[5]

Temporal roving is a mechanism that is sometimes used in an attempt to prevent a subject from listening to the total duration of a stimulus or to a loudness cue that might be linked to the duration. In trying to suppress one particular cue, however, the experimenter might unintentionally introduce another. For example, by adding extra signal time to the non-gap interval to compensate for its length (as is done with roving), one might introduce a loudness cue, since the total amount of signal energy present in one interval will then be higher than in the other (similar to Plomp and Bouman 1959). Measuring gap thresholds without using roving duration would be preferable, but only if the outcome of the measurements would not be affected in any meaningful way. To determine the point at which duration cues start to play a role, it was decided to conduct a set of pilot experiments that would investigate duration discrimination. This could give a preliminary indication of an upper limit for stimulation

[5] An example of the latter is perceptual loudness that can vary based on the stimulation's total duration (especially for shorter durations) even when the level of stimulation remains constant.

duration when performing further gap-detection experiments, a limit below which one might not need to use a roving mechanism.

A stimulation rate that was roughly in the center of the total range that would be used for gap-detection experiments was chosen for these pilots, namely 900 Hz.[6] Furthermore, a central stimulation site was used, with an electrical current that was comfortably loud and remained constant across all the periodic and dead-time-modified Poisson stimulus types for a particular subject. A two-interval, 3-down 1-up, adaptive staircase procedure was used,[7] with the reference interval always being 400 ms long and a 400 ms silence between the two intervals. The stimulation mode was always MP1+2,[8] and the phase-width was 25 μs for each phase of the charge-balanced biphasic stimulus pulses, with a phase-gap of 8 μs between the two phases. The start value for duration differences of all staircase procedures was a clearly distinguishable 200 ms, resulting in an initial total duration of 600 ms for the longer of the two stimulation intervals. To formulate the decision task, participants were asked to "pick the interval with the longer sound". Examples of the stimulation sequences are shown in fig. 4.1. The staircase sequence was considered to be stabilized and terminated after 15 reversals, and the estimated measurement for each run was calculated as an average of the last 10 reversals (i.e., an equal number of tops and bottoms). The step-factor values decreased progressively during the course of a sequential run — starting at 20% for the first four reversals, set to 5% for the next three reversals, and remaining constant at 2% thereafter. The results of the duration-discrimination experiments can be found in § 6.1.

4.5 GAP-DETECTION EXPERIMENTS

The most in-depth experiments performed as part of this study involve within-channel gap detection in electric hearing, similar to the example shown in fig. 4.3. Since temporal noise was of prime importance for this investigation, stimulation sequences needed to be used that would differ in the amount of noise that is part of their temporal properties. For a reference

[6] Although the stimulation rate for the actual duration-discrimination experiments was 900 Hz, for illustration purposes a rate of only 200 Hz was used in figures 4.1 and 4.2, accentuating the finer structure of the stimulation sequences (by providing more visual space between successive pulses).

[7] Refer to § 4.5 for an explanation of why this specific adaptive rule was preferred.

[8] The Cochlear CI-24 device has two extracochlear electrodes that can serve as reference electrodes for monopolar stimulation: a separate ball electrode (electrode number 1, which is used as the reference path for stimulation mode MP1) and a plate electrode mounted on the casing of the internal receiver (electrode number 2, which is used as the reference path for stimulation mode MP2). For stimulation mode MP1+2, both extracochlear electrodes are simultaneously enabled for the electrical reference path.

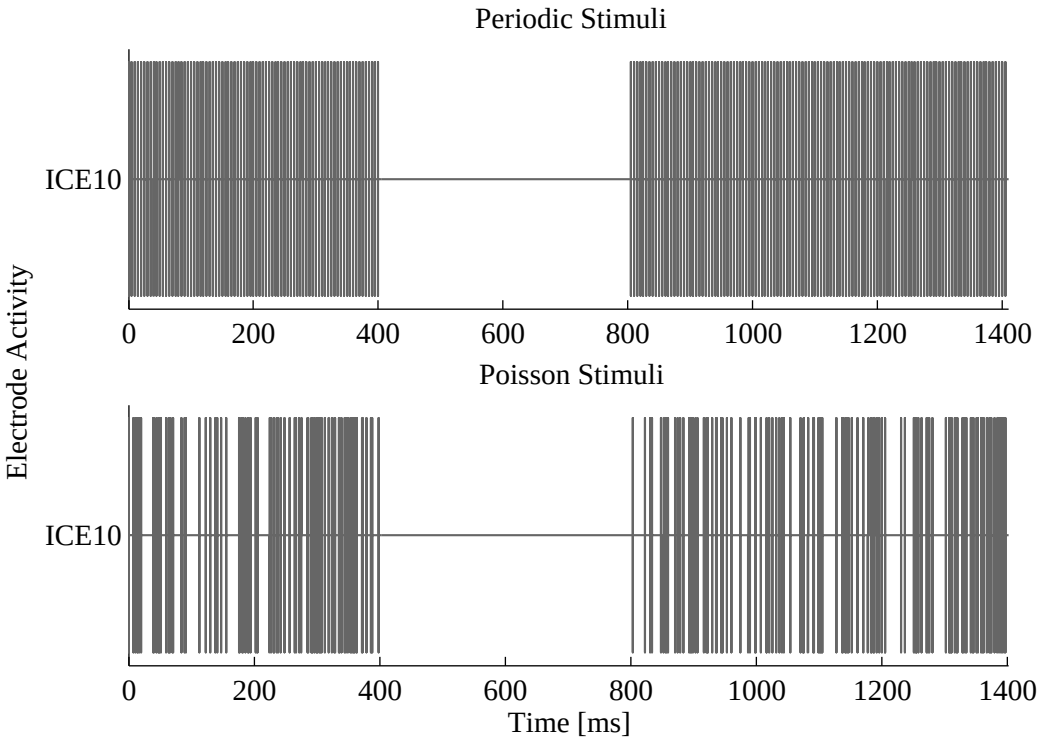

Figure 4.1: Example stimulation sequences similar to those used for duration-discrimination experiments are shown. Both periodic and dead-time-modified Poisson sequences were presented in different experiments, shown here as electrical activity on the tenth intracochlear electrode (ICE10). This depicts the temporal macrostructure of these stimulation sequences, each containing two intervals, with the second intervals in the example being the longer ones (by 200 ms). The average rate of the Poisson stimuli is approximately equal to the rate of the periodic stimuli. The substructure of the two types of stimulation sequences is explored further in fig. 4.2.

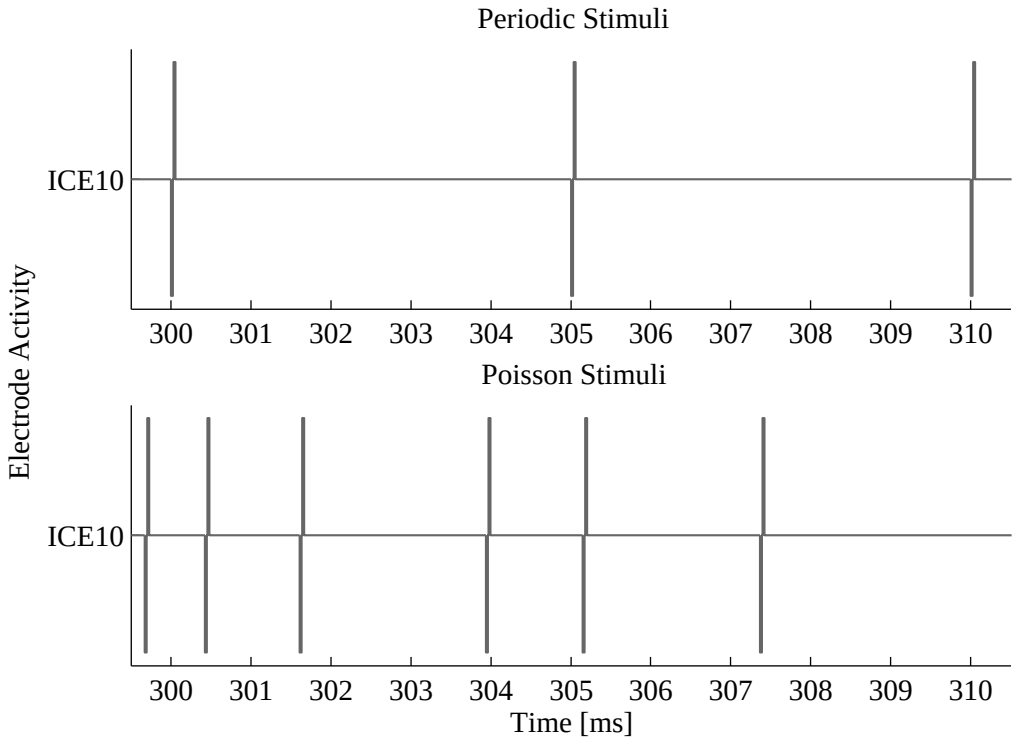

Figure 4.2: This figure shows a close-up of a small region of fig. 4.1, emphasizing the substructure of the two types of stimulation sequences. The interval chosen for this figure highlights the irregularity of the Poisson stimuli and is one in which the instantaneous stimulation rate of the Poisson process is much higher than its average rate, the latter being approximately the same for the Poisson and periodic sequences (as is more clearly evident from fig. 4.1). The details of each stimulus pulse shown in this diagram are identical to the microstructure shown in fig. 3.1.

stimulation sequence that is least noisy, the periodic sequence of pulses can be identified as the most regular temporal structure. Poisson processes exhibit the property that the events belonging to the process are scattered with uniform randomness across all possible time instants in a given observation window, and for that reason may be interpreted as the noisiest sequences — as Johnson (1996) nicely put it: "in point process theory, the Poisson process is akin to white Gaussian noise in random process theory". However, for reasons noted at the beginning of this chapter, a dead-time-modified version of the Poisson process was used instead to represent the high-noise type of stimulation for comparison purposes.

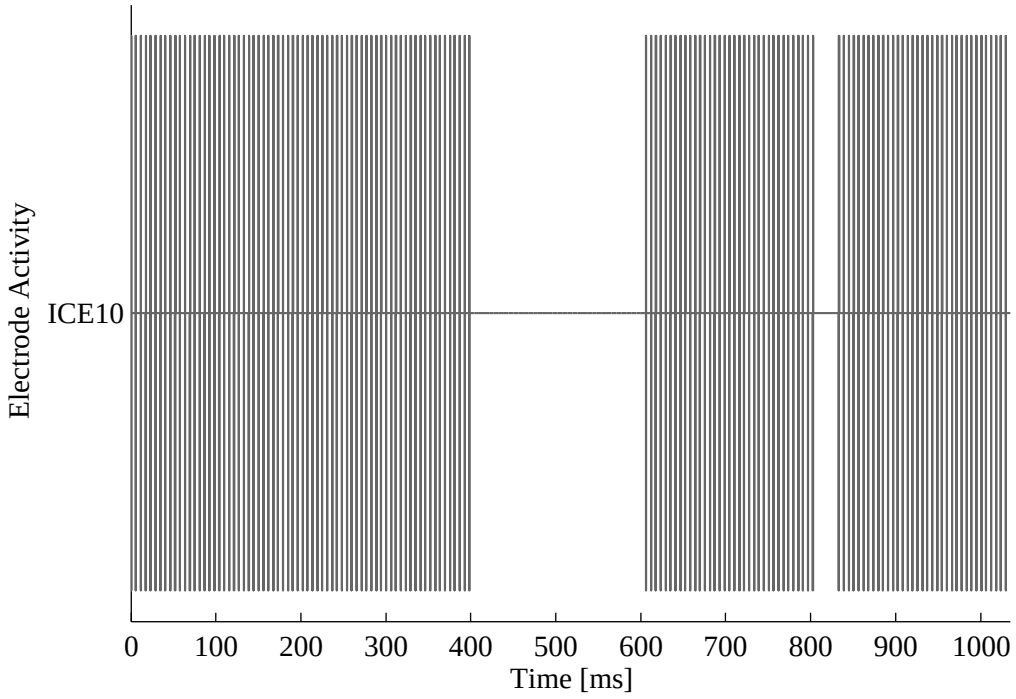

Figure 4.3: The basic macrostructure of a stimulation sequence used for the two-interval gap-detection tasks is shown. In this case a periodic sequence is used, and the second interval contains a 25 ms gap. For simplicity, the activity on the reference electrode is not shown.

Although the Poisson process has very random temporal events, its application in electric hearing as a replacement for acoustical noise is not a perfect substitute — though it may be the best one can do. This is particularly true for single-channel stimulation in which all pulses are presented at the same spatial position within the cochlea. Owing to the cochlea's tonotopic property, the temporally noisy stimulation would still have a narrow-band perceptual frequency spectrum.[9] To make the Poisson process sound more like

[9] Another interesting experimental observation related to homogeneous Poisson stimulation is that, especially for low rates, subjects seem able to perceive the average rate of the Poisson process, almost as if the rate of stimulation has a tone-like quality to it (i.e., it is perceived separately from place

white noise, one would also need to split the process randomly across all the electrodes (i.e., tonotopically), thus increasing the perceptual spectrum. This is equivalent to saying that one needs to present a Poisson process on each of the electrodes. However, adding this extra spatial dimension to the equation would complicate matters for within-channel investigations, and for that reason the Poisson process was presented only to a single channel for the bulk of this study.

The visual interface that was displayed for gap-threshold detection experiments is shown in fig. 4.4. The numbered circles at the top represent the two signaling lights for the 2AFC

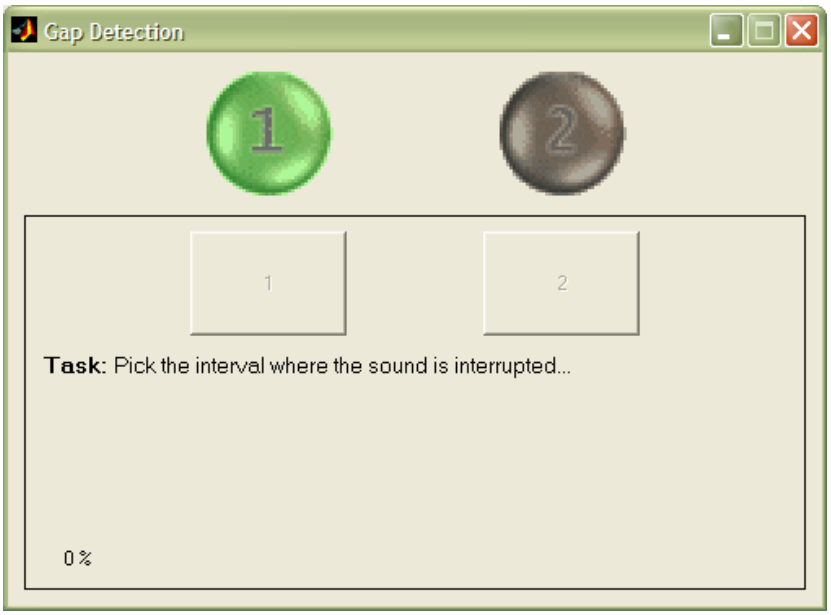

Figure 4.4: The graphical user interface of a gap-detection experiment is shown for a moment at which the first interval's stimulation sequence is presented, as implemented using the PSYCHOACOUSTICS TOOLBOX.

experiment, which were animated while stimulus intervals were presented. The description of the task is shown in the center; the participants were asked to "pick the interval where the sound is interrupted".

A 1-up 3-down 2AFC adaptive procedure (Levitt 1971) was used for all gap-detection measurements, with each interval's duration at least 400 ms (plus the gap duration, for the interval with the gap) and a 200 ms silence between the two intervals. Apart from the few exceptions noted hereafter, the starting values of the staircase procedure for the gap-threshold

pitch). Rate pitch is a well-known property of periodic stimuli, but noticing a similar rate-related perception when it comes to Poisson stimuli is fascinating; the pulse instants are random, yet the rate intensity has a pitch-like quality.

detection experiments were always 20 ms and 50 ms for the periodic and Poisson stimuli, respectively. These starting values were selected early during the initial experiments with subject S3b. (During the early experiments, starting values for bipolar stimulation varied between 10 ms and 100 ms, and for some loudness-balanced stimuli the starting values were in a range of 10 ms to 50 ms. However, different starting values should not adversely affect results, since calculated averages for threshold estimates only take the last segment of each staircase into account.) The termination condition for each run, the step-factor values and method for averaging of final estimates were the same as for the duration-discrimination experiments discussed in § 4.4.

This structure of experiment was decided upon because the 2AFC 1-up 3-down procedure settles for a 79.37% correct-response probability, in contrast with the 70.71% mark for 2AFC 1-up 2-down procedures, and the former was also found to result in smaller standard deviations in previous experiments. Furthermore, when considering the d' (d-prime) parameter of Green and Swets (1966), i.e., the index of sensitivity used in physiologic experiments that is defined as the ratio of the size of the response to the signal to the size of the standard deviation in response to noise (Hartmann 2000, p. 541), a 2AFC 1-up 3-down procedure has $d' = 1.159$, while the equivalent 1-up 2-down procedure corresponds with $d' = 0.7707$.[10] It can be argued that subjects should prefer experimental setups with $d' \geq 1$, since in this case the signal would more often be larger than the noise, which should result in a less frustrating experience for the participant, since the aspect to be measured would be perceived more often, which could result in positive psychological feedback (i.e., serve as a reward). In contrast, with small values of d' the experimental setup focuses more on subliminal measurements and less on conscious decisions, which could lead to a less interested subject who feels simply unable to perform the task at hand.

With the same experiment structure that has just been discussed, different gap-threshold experiments were performed, and these differences are discussed in the following subsections.

4.5.1 Monopolar versus Bipolar Modes

As part of an initial investigation into the stimulation parameters to be used for the main gap-detection experiments, a comparative pilot study was performed investigating the mode

[10] Note that the numerical values for d' shown here are the theoretical ones assuming a Gaussian probability distribution, and this is sufficient for the present argument to illustrate the point. However, the actual probability distributions would be used for modeling calculations presented later.

of stimulation. Like most of the other pilot studies, this one was done with subject S3b (see § D.4 for all the gap-detection experiments performed with this subject). Monopolar (MP1+2) and bipolar (BP+2) stimulation modes were used for these pilot experiments, and loudness-balanced current values were obtained at phase-widths of 100 μs for the bipolar case and 25 μs for the monopolar stimuli.[11] A two-track randomly-interleaved adaptive procedure (Jesteadt 1980) was used to measure the equal-loudness currents for the different modes and rates of stimulation. With the loudness-balanced current levels determined, gap-detection experiments were repeated at least six times for each of the different parameters. Results for the comparison between stimulation modes are reported in § 6.2.1.

4.5.2 Constant Current versus Equal Loudness

One would frequently find in literature that, for psychoacoustical experiments, loudness balancing is performed on different stimuli to eliminate any cues that might arise from the loudness percept. However, to be able to correlate experimental results with those from the model (see chapter 5) based on neural refractory behavior, it was decided that, for the main gap-detection experiments, loudness balancing would not be performed for stimuli at different rates. The reason for this is that the intended model could be verified in its simplest form when electrical current is taken as a constant. This might, however, have a negative impact on the performance of subjects for cases in which the stimuli are not loud enough. To ensure that the constant-current choice would make sense, a pilot study was done to determine how great the influence of loudness effects would be on the performance of a subject. For the comparison, two sets of gap-threshold results were needed: for the first set, while other parameters (such as stimulation rate and type) are varied, the electrical current levels would remain constant at each stimulation site[12], and, for the second set, different current levels are used that have all been loudness balanced for different parameter combinations.

Half of the results needed for this investigation can be drawn from the previous pilot study involving the mode of stimulation. The monopolar case (i.e., the MP1+2 stimulation mode) was chosen to be the reference for this comparison. As a result, the phase parameters for all these pilot experiments were 25 μs and 8 μs for the phase-width and phase-gap values,

[11] The phase-width of stimulation pulses could not be set to the same value for these two modes, since the implant device could not produce large enough electrical currents to evoke an equal-loudness perception for the bipolar stimulation mode.

[12] Note that the constant currents at different sites are initially loudness balanced for one set of parameters before being kept constant, as described in the next paragraph.

respectively. The electrical current levels for each of the stimulation channels were chosen as their 900 Hz loudness-balanced values. The reasoning behind this is as follows: it is expected that as the rate of stimulation decreases, the loudness of the sound would also decrease, and the reverse should in general also be true if the rate of stimulation is to be increased (van Wieringen et al. 2006). Choosing a value somewhere in the center of the stimulation-rate range should allow for an adequate range above and below this chosen rate without the stimulation becoming too loud to bear or too soft to hear. The measurements at all the data points were repeated at least six times; for the results of these experiments, refer to § 6.2.2.

4.5.3 Principal Experiments

The bulk of the experimental study focused on measurements of within-channel gap-detection thresholds using various stimuli, repeated with several participants. In the experiments, the following conditions were varied.

- Seven logarithmic equally spaced stimulation rates, from 100 Hz to 2700 Hz, were used.

- Two different kinds of stimulus sequences were used, i.e., a periodic sequence and a dead-time-modified Poisson sequence.

- Three spatial stimulation sites in each subject's cochlea were investigated, namely a basal, a central and an apical location.

Along with the detailed numerical results, specifics of the parameters for individual subjects are documented in appendix D. For example, the specific data include different stimulation modes (usually MP1+2, which could be used only for the Nucleus CI-24 implants), individual electrode numbers used for stimulation, and electrical current on the various electrodes. For these primary experiments, the phase-width for each phase of the charge-balanced biphasic stimulus pulses was always 25 μs, and the phase-gap value was always set at 8 μs. In some cases (applicable to one subject only) certain stimulation rates could not be presented to the subject, owing to discomfort experienced by the subject resulting from the combination of stimulation parameters; either the high end or low end of the rate spectrum was abandoned for different sets of experiments. All experiments, as measured through the outcomes of an adaptive-procedure sequence, were repeated at least four times, but in some

cases (e.g., where variations were initially larger) individual experiments were repeated up to 15 times for more accurate results, obtainable as a consequence of the lowering of statistical standard-deviations from more repeats. The results of the main gap-detection experiments are presented in § 6.2.3 and 6.2.4 for periodic and Poisson stimuli, respectively.

To conclude, this chapter presented the methods that were employed for the experimental component of the present study. Preceding the results of the experiments (which are presented in chapter 6), the next chapter provides details on the modeling aspects that augment the experimental research.

CHAPTER 5

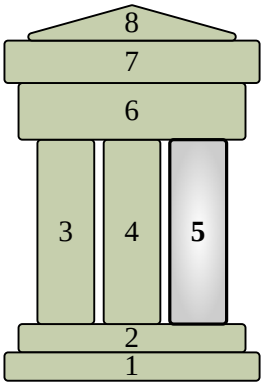

METHODS FOR MODELING OF GAP DETECTION

As mentioned in chapter 1, one of the factors contributing to the shortcomings of cochlear implants is the associated unnatural spatiotemporal firing patterns of neurons. From a bio-engineering perspective, it is necessary to find ways to improve the understanding of the underlying processes involved in the perception of electric hearing. The psycho-electrical experiments discussed in chapter 4 need to be understood using the tools of engineering, and an attempt to accomplish this can be made by studying the links between these psychophysical experiments, the underlying neurophysiology and engineering models. The last of these is the topic of this chapter, dealing with the assimilation of neurophysiological knowledge into a mathematical model that can be tied to perceptual measurements through model predictions. Having identified the unnatural firing patterns of neurons in electric hearing as one of the areas in need of better understanding, gap-detection experiments are used as an avenue to investigate the influence of temporal stimulation. The aim is to build a model that can take stimulation sequences as input and predict the psychophysically measured gap-detection thresholds. The model, therefore, predicts the temporal resolution

of perception, given different input stimulation sequences.

5.1 CONCEPTUAL MODELING FRAMEWORK

A block diagram is shown in fig. 5.1 that gives an overall view of the main steps involved in modeling the psychophysical gap-detection process. The model's design is based on the postulate that there is a direct correlation between the temporal resolution of perception (in this case gap detection) and the stochastic properties of neural firing patterns. That is, the model predicts psychophysical measurements for gap-detection thresholds based on the statistics (e.g., *probability density function*, or PDF) of the time-intervals between neural spikes that are caused by the electrical stimulation.

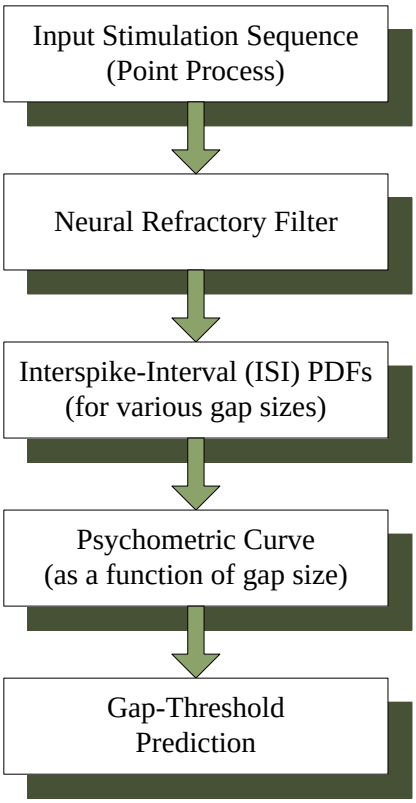

Figure 5.1: A flow-diagram is shown representing the overall structure of the model, from the point where a stimulation sequence is used to the final prediction of a psychophysical measurement (in this case, for gap-detection thresholds).

Looking at this diagram in more detail, it starts off with the electrical stimulation sequence that is viewed as a point process — in this initial formulation of the model all the stimulation pulses are, therefore, equal in strength (as measured, for example, by electrical charge) and

only the timing of the individual pulses is assumed to be of importance.[1] The stimulation pulses give rise to a neural firing pattern that is a filtered version of the stimulation sequence. The filter is primarily envisaged as a consequence of the refractory behavior of the neuron being stimulated (as will be discussed in § 5.3), but a more complex filtering process is not ruled out; for instance, one could incorporate other parameters, such as the strength of electrical pulses and the distance of a specific electrode from a neuron, into this filtering process. Details on specific model neurons are provided in § 5.4, and the process by which the filtering mechanism has been simulated is presented in § 5.5. Subsequently, ISI statistics can be drawn from the neural firing process.[2] In the case of gap detection, all these steps are repeated for several different gaps inserted into the input stimulation sequence. The intricacies pertaining to the precise selection of the intervals from which statistics are drawn are explained in § 5.6, and the influence of length-biased sampling on the interval statistics (mandated by the temporal nature of the ISIs) is discussed in § 5.7. Then, using the same principles as Green and Swets (1966), a *psychometric function* (also known as a *psychometric curve*) can be calculated from the probability functions, thus providing percentage-correct projections for a psychophysical experiment, given the nature of a single trial in the experiment (for the present study the 2AFC paradigm was used, which simplifies some of the calculations). Different gap lengths give rise to different interspike statistics, resulting in different percentage-correct values as a function of the gap threshold. Then, having chosen the staircase method used to link individual experiment trials into a complete run, it is possible to read the predicted gap-threshold from the psychometric function (for example, one needs to take the 79% correct value for a 2AFC 1-up 3-down experiment). These last steps of the overall model, pertaining to the psychometric curves and predicting gap-threshold measurements from these, are discussed at length in § 5.8, along with the approach to non-monotonic psychometric functions identified through modeling in § 5.9.

It is possible to execute the modeling process in a mechanical way by, for example, simply performing Monte Carlo simulations (Metropolis and Ulam 1949) to determine the probability distributions of the neural firing patterns. This avenue is used for some of the simulations performed in the present study. However, because it is a very computationally intensive way to run the simulations, one should also consider alternative ways to determine the probability distributions. It will be shown that for periodic stimuli it is possible to calculate the probability functions mathematically (e.g., using Markov-chain theory), saving

[1] Generation of the Poisson stimulation events is discussed in appendix C, in which periodic stimuli are treated as a logically degenerate case.

[2] The possibility that a gap detector for electric hearing would be based on ISIs is discussed in more detail in Hanekom (2001, chapter 4).

considerable time while providing greater accuracy than multitudes of brute-force simulation iterations. Though it could be possible to do the same for Poisson stimuli, the mathematical complexity of such a formulation should not be taken lightly.

The concept behind the forming of psychometric predictions is relatively simple. The procedural details become a bit more involved, but the effort is worth the trouble. In the end it is possible to relate stimulus to perception, traversing both the peripheral and central signal-processing steps in between.

In order to thoroughly understand the steps involved in the model, a common vocabulary for expressing the mathematical details is needed. In § 5.2 this underlying language is formalized, and thereafter the main concepts can be augmented with mathematical substance.

5.2 NOMENCLATURE AND NOTATION

The notation used for mathematical constructs is discussed at length in a much more formal style in appendix A, where the definitions are also presented to form a consistent set of mathematical formulae. However, a summary of the nomenclature and notations is listed in table 5.1. Note that the abbreviations used for the function names consistently use the C-*letter* prefix to represent *cumulative*, while the *letter*-C suffix is used to indicate *complementary*. While referring to appendix A, note that, for the sake of clarity, distinctions are made in the formalizations of the hazard functions, such as the HRF and DHF. Further details on the statistical relations among the functions can be found in appendix B.

Table 5.1: An overview of the mathematical notations is presented; statistical relations are discussed in appendix B. For details on the formal definitions, see appendix A.

$\mathcal{P}r(X)$	Probability of the *random variable*, or RV, X.
$\mathcal{P}r(A \mid B)$	Conditional probability of A given B.
$pdf_X(x)$	Probability density function of the RV X.
$pmf_X(x)$	Probability mass function of the discrete RV X.
$cdf_X(x)$	Cumulative distribution function of X.
$cdfc_X(x)$	Complementary cumulative distribution function of X.
$hrf_X(x)$	Hazard rate function of the RV X.
$chf_X(x)$	Cumulative hazard function of X.
$dhf_X(x)$	Discrete hazard function of the RV X.
$dhfc_X(x)$	Complementary discrete hazard function of X.
$E[X]$	Expected value, average or mean, of X.
$V[X]$	Variance of the RV X.

5.3 BACKGROUND FOR THE NEURON MODEL

The refractory behavior of neurons is described in literature in various and related ways, but when (as is too often the case) the formulations provided lack mathematical rigor, interpretive conclusions are fraught with peril. However, one may choose to formalize a neuron's recovery process using a statistical hazard function, such as the DHF, and with fidelity to the formal relationships between the various probability functions can remain true to a mathematically correct description in terms of probability theory. Such an approach should be preferred, and this is indeed the route taken for the present study. But before concrete descriptions of modeled neurons are presented (in § 5.4), it may be appropriate to reflect on probabilistic recovery functions and neural refractory effects. The latter are the topics of § 5.3.1 and 5.3.2.

5.3.1 Probabilistic Recovery Functions

In neurophysiology, often a hazard function is conceptually associated with the refractoriness of an excitable cell following the occurrence of a neural spike in that cell. Especially in the case of experimental research literature, one finds that authors tend to describe some probabilistic recovery function that is somehow related to the formal hazard functions, which the authors might then formulate in less exact mathematical terms. Because of the approximations made by the models that are used to describe the experimental measurements and the practical uncertainty related to precision of measurements, the exact correlation between these recovery functions and the formal mathematical hazard functions is sometimes not easily distilled. In such instances, it may be difficult to ascertain whether a function should be interpreted as the neuron's HRF or DHF, something proportional to one of these, or a filtered or normalized version thereof. From a practical perspective the distinctions may appear trivial, but in a mathematical sense the nuances are deserving of one's attention.

The hazard function concept is also referred to as a *recovery function* (Johnson and Swami 1983), *refractory function* (Irlicht and Clark 1996) or *fractionally recovered discharge probability* (Prijs et al. 1993). The recovery function is usually scaled (or normalized) by a rate constant in such a way that it can be interpreted as a probability function with a value from 0 to 1, or specified as a neural firing rate (e.g., spikes per second) that may be either spontaneous or excited through external stimuli. Such a recovery scaling constant is also referred to as the *recovered probability density* in Prijs et al. (1993), and the directly

proportional nature of such recovery functions in relation to the HRF is noted by Johnson and Swami (1983), with further reference to Snyder (1975). In the context of electrical stimulation of excitable cells, the scaling constant is sometimes set equal to the stimulation rate, so that the recovery function quantitatively corresponds with the probability of a stimulus pulse to evoke a spike. Similarly, in the case of spontaneous activity of a neuron, the constant might be taken to represent the spontaneous spike rate of that neuron. However, care should be taken not to oversimplify the relationship between the HRF and DHF (which is properly formulated in appendices A and B).

5.3.2 Perspectives on Refractory Effects

There are various ways in which one might think about the effects that are brought about by the refractory behavior of neurons, especially when one takes a simplified approach and assumes that the chance of a neural spike being evoked is influenced by the previous spike of that neuron but not by any spike before that. Although such an approximation is not true for all stimulation conditions, especially in extreme circumstances (such as very high rate stimulation for extended durations where adaptation could occur), one may judge this approach as reasonable in many cases. This leads to an interpretation of the refractory behavior that is governed by the hazard function of the neuron. When the applied stimuli are seen as a point process, the hazard function effectively filters out some of the stimulus events that do not generate spikes.

For the case where the input point-process is strictly a Poisson process, the statistics of the filtered point-process (i.e., the measured output point-process) would correspond exactly (as explained below) with the hazard function of the neuron. This property follows from the mathematics that governs the filtering process. It is also used in computer simulations as a technique to generate RVs that display more exotic distributions, yet allow the hazard function to be calculated.[3] The technique is then referred to as the *hazard rate method* (see Ross 1993). This property can also be used in a more practical way to measure an unknown hazard function of a specific neuron: simply apply a homogeneous Poisson stimulus sequence (approximated, because of practical limitations) and obtain a histogram of the output interspike intervals. The measured histogram can then be converted into a PDF, by normalizing the area underneath it to unity, and be used to calculate an estimate of the hazard function (applying eq. B.36). This procedure is also mentioned in Johnson and Swami (1983), and, although the present perspective is not used as a point of departure, the

[3] Even if the closed-form equation is unknown, this procedure can still be used numerically.

underlying principle is the same: the instantaneous rate of discharge must remain constant, which can be shown to be the case for a homogeneous Poisson process by calculating *its* hazard function. Prijs et al. (1993) also discuss this estimation procedure in some detail.[4]

Furthermore, when the input is strictly a Poisson point-process, one may interpret the resulting output point-process as one in which the interspike time-intervals are generated through a process of independent RV summation: one variable attributed to the input process (its forward-recurrence time) and another recognized as resulting from the dead-time that is modifying the Poisson process. The latter interpretation is explored in a very informative appendix to Young and Barta (1986). This perspective offers the added benefit that one can use *Laplace transform* theory to perform calculations involving these RVs. For example, the resulting PDF, which is the sum of independent RVs, is simply the inverse Laplace transform of the mathematical products of the Laplace transforms of the individual PDFs of the RVs. Despite its mathematical appeal, this interpretation does have some limitations, since it depends on a property of the pure Poisson process that cannot be extended to other input point-processes, namely, that the PDF of the forward-recurrence time is exactly that of the Poisson process itself. These formalizations are a result of the lack-of-memory property of a Poisson process;[5] emerging from the refractory period, the Poisson process behaves as if the dead-time never occurred. For other point processes one cannot divide the dead-time and input-process contributions in such a clear-cut way; the dead-time has an effect on the RV representing the forward-recurrence time of the input process, and the two RVs are, thus, not independent. Despite this limitation, the implications from such an interpretation can be used when appropriate. For example, if one were to generate a dead-time-modified Poisson process, it would be very convenient (as well as computationally efficient) to calculate the inter-event intervals as the sum of independent RVs. The Poisson stimuli used in some of the experiments performed as part of this study were constant dead-time-modified Poisson processes (i.e., the electrical stimuli had a constant waveform duration, and while generating one stimulus pulse the hardware could not generate another pulse — effectively being dead, as far as generation of further pulses is concerned — until the current stimulus had completed). Although the equation that was used for the stimulus-sequence generator

[4]Note that some intricacies are involved in the interpretation of sampled histograms (which are discrete because of the rounding mechanism of the bracketing interval bins) as estimates of corresponding (continuous) hazard functions. This was pointed out by Grimshaw et al. (2005), but perhaps has not yet received sufficient attention from the neural hazard-function research community.

[5]It is this property that gives rise to the exactly equal (and apparently paradoxical) results for the average inter-event interval and residual lifetime of the example involving the Poisson process given in § 5.7.

was initially derived[6] using the modified *inverse transformation method*[7], it turns out that the same equation results from the mathematics associated with the interpretation outlined above.

The branch of pure mathematics[8] applicable to neural refractory behavior can indeed be very intriguing by itself. However, the same theoretical mathematics is also fascinating from a more pragmatic approach, when it is applied to simulation of neural behavior: the refractory effects of neurons can be modeled with hazard functions that encapsulate the stochastic approach of describing when a neuron would fire in response to some stimulation sequence. The specifics of these model neurons are formulated next.

5.4 Choice of Modeled Neurons

For simulations and calculations that would illustrate the modeling of the gap-detection process, a set of neurons was chosen to be used throughout the quantitative models. With reference to fig. 5.1, these model neurons represent the neural refractory filters. Four specific neurons were modeled and are labeled A through D. The neurons are based on two different equations for the recovery function, and further differ in the actual assignment of numerical constants, such that each neuron exhibits unique characteristics.[9]

Neuron A was based on the following mathematical hazard function, $dhf_A(t)$, which lends itself better to analytical operations (e.g., the Laplace transform of this equation is quite elementary):

$$dhf_A(t) \;=\; \theta(t-t_0)\,.\,\left\{\frac{\frac{1}{(q-v).(q-w)}\,e^{-q.(t-t_0)}+\frac{1}{(v-w).(v-q)}\,e^{-v.(t-t_0)}+\frac{1}{(w-v).(w-q)}\,e^{-w.(t-t_0)}}{\frac{1}{(q-v).(q-w)}\,e^{-q.(t-t_0)}+\frac{q/v}{(v-w).(v-q)}\,e^{-v.(t-t_0)}+\frac{q/w}{(w-v).(w-q)}\,e^{-w.(t-t_0)}}\right\}\,, \quad (5.1)$$

where $\theta(t-t_0)$ represents the Heaviside function (i.e., unit step function) displaced by the dead-time period, t_0. The constant q represents the stimulation rate, while parameters v and w can be interpreted as two rate-constants characterizing the recovery behavior of the

[6] See appendix C for a description of the generator's equation, with specific reference to eq. C.2.

[7] See Ross (1993) and Devroye (1986) for details; or Huettel and Collins (2004), which contains a clear and concise description of using this method to generate a Poisson process.

[8] *Pure mathematics*, in this context, is contrasted with *applied mathematics*.

[9] This section provides a mathematical approach to the formulation of the model neurons, while a more practical perspective can be found in § 6.3 (e.g., fig. 6.10 graphically depicts numerical examples of the hazard equations).

specific neuron. The recovery function of eq. 5.1 expresses the absolute instantaneous spike probability of the neuron, which has a maximum value, $\mathcal{P}r_{\max A}$, given by

$$\mathcal{P}r_{\max A} = \min\left(1 , \frac{v}{q} , \frac{w}{q}\right) . \tag{5.2}$$

For numerical modeling purposes, values that may be biologically plausible[10] were selected for the constants of Neuron A, which are listed in table 5.2.

The equation that forms the basis for modeling the recovery behavior of Neurons B, C and D is one that is more commonly found in literature, such as in Prijs et al. (1993), where the recovery function is modeled with a simple exponential function using a single time-constant, τ, and an optional fixed dead-time period, t_0:

$$dhf_{B,C,D}(t) = \theta(t - t_0) \,.\, \mathcal{P}r_{\max B,C,D} \,.\, \left(1 - \mathrm{e}^{-(t-t_0)/\tau}\right) , \tag{5.3}$$

$$\text{where} \quad \mathcal{P}r_{\max B,C,D} = \min\left(1 , \frac{a}{q}\right) . \tag{5.4}$$

Above, symbols q and $\theta(t - t_0)$ have the same meanings as in eq. 5.1, whereas parameter a can be interpreted as a rate constant, which is discussed in more detail later in this section. In Prijs et al. (1993), parameter a is referred to as the *recovered probability density*, but it is there defined in the context of spontaneous neural activity, under the assumption that the fiber has fully recovered, in contrast with the neural stimulation context of the present study. That is, in Prijs et al. (1993) the notion of stimulation-rate parameter q is not present, such that their parameter a is perhaps more comparable to the entire quantity $\mathcal{P}r_{\max B,C,D}$ of eq. 5.4. Also, similar to eq. 5.1, the $dhf(t)$ from eq. 5.3 again represents instantaneous spike probabilities, with $\mathcal{P}r_{\max B,C,D}$ similarly representing the maximum possible DHF spike probabilities of Neurons B, C and D. The numerically modeled values that were selected for the variables of Neurons B through D are listed in table 5.2. Neuron B may be thought of as one that tracks the stimulation rate without a limit on its maximum spike rate. Although this neuron is arguably the least biologically plausible of all the simulated neurons, the present study's experimental results seem to indicate that the maximum firing rates of some electrically stimulated neurons (or, perhaps, the combined firing behavior of a group of neurons in a stimulus channel) may be much higher than normally expected. Neuron B provides for this possibility. Neuron C has a much longer dead-time refractory period than the other neurons,

[10] The chosen values for the parameters of Neuron A result in a hazard function that is comparable to the curves (in terms of refractory periods) of Neurons B, C and D (for a more practical visualization, see fig. 6.10). These last neurons' parameters are based more directly on literature, as will be discussed.

where, for t_0 that directly controls the ARP, a value of 1.7 ms was selected based on the maximum period recorded by Prijs et al. (1993) for the guinea pig cochlea. The values for Neuron D were mostly chosen in line with some of the experimental observations by Gaumond et al. (1982) for the cat cochlear nerve, where an ARP of 0.75 ms was recorded. Furthermore, the chosen value of τ leads to the noted approximately 60% complete recovery of the spike discharge probability after 4 ms, and to a fully recovered fiber after 20–25 ms, as reported by Gray (1967). ARP values of 0.7 ms (Neuron A) and 0.75 ms (Neurons B and D) are also consistent with the mean ARP values of between 0.56 ms and 0.86 ms for cat auditory nerve fibers reported by Li and Young (1993). Except for the differences already discussed, similar t_0 and τ values were also assigned to Neurons B and C, as shown in table 5.2.

Table 5.2: Listed in this table are the numerical values that were selected for the variables of the neurons, which were then modeled according to the spike probability expressions of eqs. 5.1 and 5.3. As before, parameter q represents the stimulation rate, which ranged between 100 Hz and 2700 Hz for the present study.

	v	w	a	τ	t_0
Neuron A	250 Hz	750 Hz	—	—	0.7 ms
Neuron B	—	—	q	1/280 Hz = 3.571 ms	0.75 ms
Neuron C	—	—	650 Hz	3.571 ms	1.7 ms
Neuron D	—	—	650 Hz	3.571 ms	0.75 ms

The choice of the numerical values for parameter a needs further clarification. Similar to parameters v and w in eq. 5.1, parameter a can be interpreted as a rate constant characterizing the recovery behavior of the specific neuron. These rate constants are closely related to the maximum firing rates of the specific neurons and the spontaneous firing rates of neurons[11] functioning under normal conditions, but should not necessarily be taken to correspond exactly with either of these two concepts, as explained below. For simulation purposes, the value of a was chosen as 650 Hz for Neurons C and D, and was left arbitrarily high for Neuron B by allowing it to match the stimulation rate exactly. These choices of values for a were based on the experimental results obtained from the present study, and were found to closely match patterns observed between simulated and experimental results. Steady-state spike rates of neurons are usually reported with a maximum in the range of 150 to

[11] A simple mathematical formulation of the strong relationship between parameter a and the spontaneous rate (SR, or r_s) of a neuron is given by Lütkenhöner's equation in Prijs et al. (1993): $r_s = 1/(t_0 + [2 - \exp(-a \,.\, \tau)]/a)$. Although extrapolated much further than the experimental data of that article, this equation predicts spontaneous spike rates of 216.2 Hz and 272.0 Hz for Neurons C and D, respectively, and a spontaneous spike rate of 670.8 Hz for Neuron B at the maximum stimulation rate of $q = 2700$ Hz (which goes up to a maximum spontaneous spike rate of 1.333 kHz in the limit).

300 spikes/s (Rattay 1990), while spontaneous spike rates are typically less than 150 spikes/s (Prijs et al. 1993). Given that the spike rate is the reciprocal of the ISI duration when interpreting hazard and recovery functions, it may be more appropriate to think of the parameter a as a rate above which the neuron's spike probability levels off at the peak asymptotic value. This probability plateau is reached at longer ISIs (considering the literature on neural refractory behavior referenced thus far) that would correspond (almost ironically) with lower instantaneous spike rates, but which would in practice seldom be observed if the long-term average spike rates were higher that what the instantaneous ISI would allow. In the chapter about auditory nerve stimulation in Rattay (1990, p. 207), the author states that the average auditory nerve fiber can attain relatively high firing rates of up to 2000 spikes/s within the first 10 ms after an "initial" spike.[12] If a spike that terminates a very long ISI is (by approximation) interpreted as a new "initial" spike, that would mean that the neuron can catch up with the higher average spike rate in the first 10 ms or so after that extended ISI. Since the present model is oblivious to preceding ISIs, this effect could manifest itself in the value of parameter a. Thus, it makes more sense to interpret parameter a as a parameter that strikes a balance between the sustainable maximum spike rate of a neuron (which tends to be lower) and the instantaneous spike rate of the neuron (which could be much higher, especially for neurons stimulated electrically at high rates) following longer ISIs where the spike probability reaches its peak. Seen in this light, the chosen value of 650 Hz for parameter a (or even a much higher value, as is the case for Neuron B) appears reasonable, as this value lies between the typical sustainable maximum spike rate and the higher instantaneous spike rates associated with the short intervals after the high spike probabilities for longer ISIs are encountered. The choice of a is also consistent with Bruce, Irlicht, White, O'Leary, Dynes, Javel and Clark (1999), in whose work even higher discharge rates of up to 800 spikes/s were shown for the auditory nerve stimulated with electrical pulse-trains, as well as with Javel and Shepherd (2000), who recorded discharge rates just short of 800 spikes/s.

5.5 Refractory Filter Mechanics

With proper hazard functions at hand to describe the model neurons mathematically (i.e., with the specific $dhf(t)$ formulations of § 5.4), a short description of how these equations may be used to calculate the neural behavior might be in order. The mechanism of the simulation process, as it pertains to the neural refractory filter depicted in fig. 5.1, can be understood using a description of the neural firing behavior that is formulated in terms of

[12] In this context, Rattay also refers to Javel (1986); however, a local copy of the latter could not be found for cross-checking.

renewal theory. As soon as a neuron spikes, the neuron is reset to an initial state without any knowledge of prior events — the only memory of the neuron is of the time period since the last spike, which is identified as parameter t. Normally, neurons of a deafened auditory system (unlike those of a normal-hearing system) exhibit little or no spontaneous activity (Shepherd and Javel 1997) and, thus, are excited primarily in response to electrical stimulation events. Therefore, testing for neural renewal is done only at the time instants when stimulus events occur. For each stimulation event since the previous spike, the neuron's hazard function is evaluated to determine the likelihood of the neuron to spike in response to the stimulus at that instant. With the probability for that moment taken into account, the neuron then randomly determines whether it should a.) "expire" (i.e., spike) and return to an initial state; or b.) ignore (i.e., filter) that stimulus and wait for the next one, at which instant the duration since the previous spike would have increased and the hazard function would be re-evaluated at the longer lifetime, $t + \Delta t$.[13] The procedure described above can be quantified mathematically so that the overall probability of finding a spike at instant t (i.e., the *probability mass function*, or PMF) can be expressed completely in terms of the neuron's hazard function (see eq. B.16):

$$pmf(t) \quad = \quad dhf(t) \,.\, \prod_{t_n<t} \Big(1 - dhf(t_n)\Big) \,, \tag{5.5}$$

where t_n represents all the prior instants (since the previous spike) at which stimuli failed to generate a spike; note that for the first stimulus after a spike, one needs to evaluate $dhf(t)$ for that given instant only.

As part of this study, Monte Carlo simulations were performed to determine the probability distributions of interspike intervals (refer to the center block in fig. 5.1) that can then be processed by subsequent phases of the proposed model. For these simulations, the following procedure was used to collect samples describing the neural-filtered intervals where gaps of various durations were (optionally) inserted in the center of a stimulus sequence:

- A sequence of stimulus events, which has the desired total duration (i.e., 400 ms for the present study), is generated.

- If required (i.e., for a nonzero gap duration), a gap period is added to the interstimulus interval that is located in the temporal center of the event sequence, effectively delaying

[13] For periodic stimuli, Δt is constant (except for any interval that also contains a gap), and the overall system's behavior can be simplified even further, with relative ease, by taking Markov-chain theory into account.

all stimulus events after that instant with the desired gap duration.

- The stimulus sequence is transformed consecutively (i.e., as eq. 5.5 dictates) into a spike sequence by filtering some stimulus events as determined probabilistically using the neuron's hazard function, given the time duration since the previous spike.

- The duration of the interspike interval, in the temporal center of the stimulation sequence in which the (optional) gap was inserted, is recorded.

- The process is reiterated with the same parameters to get a representation of the probability distribution that is sufficiently accurate, and the process is further repeated for different parameter values (such as various gap durations, neural filters, point-process intensities and interstimulus-interval distributions) to obtain probability distributions for all the parameter values under investigation.

For the present study, the simulations were performed for both types of stimuli (periodic and dead-time-modified Poisson, with the dead-time parameter identical to experimental stimuli, i.e., $\tau_d = 250\,\mu$s). All four model neurons were investigated, but at a much finer grain of stimulation rates than in the experiments: over the range from 100 Hz to 2700 Hz, a total of 61 data points were spaced with equal logarithmic distance and rounded to the nearest hertz (i.e., data points were placed at 100, 106, 112, 118, 125 Hz, and so on, up to 2419, 2556 and 2700 Hz). This allowed nine additional rate data-points to be simulated between each consecutive pair of experimental data-points. Furthermore, a total of 101 gap-duration data-points were evaluated, rounded to the nearest microsecond; these consisted of a set that is the union of the no-gap (i.e., 0 ms) interval and 100 logarithmic equally spaced data-points over the range from 0.1 ms to 125 μs. The simulation of each set of unique parameters was repeated between 34800 and 62800 times (with a rounded average of 45570 iterations). Results that are based on the Monte Carlo simulation are presented in § 6.3.1.

5.6 MIND THE GAP

Although eq. 5.5 describes the PMF of finding spikes at various instants of t, what it presents is the ISI distribution for *all* intervals that are part of the point process. Such a probability distribution is an appropriate description for simulating the successive behavior of the neuron as it proceeds through various stimulation instants until the neuron eventually spikes, but this PMF does *not* describe the distribution of the specific ISIs that would be found in the

temporal center of the stimulation sequences in which the additional gap period is inserted between two sequential stimuli. Thus, the PMF of eq. 5.5 does not describe the statistics that are recorded in the fourth step of the simulation procedure listed above. For the ISI distribution of the intervals in the center of the sequence, the PMF needs to be adjusted for length biasing, which is discussed in the next section, where it will become apparent that eq. 5.5 may be modified as follows to describe the ISI distribution of *specific* intervals such as the ones centered in the stimulation sequence where a gap could be inserted:

$$pmf(t) \quad = \quad \frac{t}{E\,[T]} \,.\, dhf(t) \,.\, \prod_{t_n<t} \Big(1 - dhf(t_n)\Big) \,. \tag{5.6}$$

The constant quantity $E\,[T]$ represents the expected value of this modified distribution and serves the purpose of renormalizing the new PMF. The appropriate mathematical description of the distribution of the collected gap-intervals for the procedure listed above is given by eq. 5.6.

Furthermore, as a matter of interest, the length-biased version of this PMF is numerically equal to the steady-state probability distribution under Markov-chain theory. The steady-state probabilities describe the likelihoods of finding the system in each of the specific states after sufficient time has passed since the onset of the process, such that any memory of its initial state has died out. With this in mind, there are even more ways in which the ISI PMF for the gap-containing interval can be calculated (typically involving matrix algebra), especially for the case in which a periodic stimulation pattern is used, such that the transition matrix of the Markov chain can easily be formulated with element values mapping directly to transition instants of the neuron's DHF and DHFC.

5.7 LENGTH-BIASED SAMPLING

Since ISI statistics, such as the PMFs of periodic stimuli, are key to the model that is being described for gap-detection perception, it is important to realize that these PMFs can be influenced by the way in which they are measured. Any time interval for which statistical samples are collected, such as the interspike intervals, could potentially be influenced by the way in which samples are collected over time (since the measurement process is also temporal in nature), which is something that may not be immediately obvious. For instance, the PMFs of all the inter-event-intervals of a point process have a characteristic form, but PMFs of specific intervals of that process take a different form, such as the PMF of the interstimulus interval to which a gap would be added for a gap-detection experiment. To

elaborate, for the gap-detection experiments discussed in chapter 4, two interval choices were presented to a subject during each step in the 2AFC adaptive procedure, and one of these signaling intervals was always modified to contain an additional gap of silence. The gap was always added to the specific interstimulus interval that occurred in the center of the 400 ms stimulus sequence, and when drawing the PMF statistics for all such intervals that are located in the center of a Poisson sequence, the PMF is different from that of all intervals belonging to that Poisson process. This interesting phenomenon is caused by *length-biased sampling* (Cox 1962, Cox and Isham 1980), which explains why, in the case of this example, shorter interstimulus intervals are less likely to be observed in the center of the stimulus sequence than longer ones. Length-biased sampling is clearly an integral part of gap-detection modeling, and its influence on the probability mathematics thereof is discussed further in this section.

To express length-biased sampling in mathematical terms, one takes the original RV's PDF, weights it by a factor that is proportional to the RV's magnitude, and then normalizes the value again so that the resulting probabilities would add up to one. Thus, the PDF of an RV, X, affected by length-biased sampling, can be described as follows, with k being an arbitrary proportionality constant:

$$\frac{(k.x) \times pdf_X(x)}{\int_{-\infty}^{+\infty} (k.u) \times pdf_X(u)\ du} = \frac{x\ .\ pdf_X(x)}{\int_{-\infty}^{+\infty} u\ .\ pdf_X(u)\ du} \tag{5.7}$$

$$= \frac{x\ .\ pdf_X(x)}{E\,[X]}\ . \tag{5.8}$$

As a matter of interest, as shown in Cox (1962, § 5.4) and Cox and Isham (1980, pp. 7–8), it is possible to derive an expression from eq. 5.8 for the limiting distribution of the recurrence times of any point process, which is the same for both the *residual lifetime* and *age* (i.e., for both the forward recurrence-time and backward recurrence-time), and this expression also applies exactly (i.e., in contrast to just the limiting case) to the recurrence times of an *equilibrium*[14] renewal process. For this calculation one needs to realize that, being arbitrarily chosen, the time instant has a uniform distribution over the entire duration of the interval, e.g., with length u, so that the probability of choosing an instant in this specific interval (knowing exactly which interval was chosen) is given by $1/u$. Cox then states the following

[14] A lucid explanation of the physical interpretation of an equilibrium renewal process is presented, along with the mathematical definition that matches eq. 5.9 (following shortly), in Cox (1962, § 2.2): "an equilibrium renewal process can be regarded as an ordinary renewal process in which the system has been running a long time before it is first observed".

expression for the PDF of recurrence time:[15]

$$\int_x^{\infty} \frac{1}{u} \frac{u \,.\, pdf_X(u)}{E[X]}\, du \quad = \quad \frac{cdfc_X(x)}{E[X]} \,. \tag{5.9}$$

Thus, when the CDFC of an RV is scaled by the reciprocal of the RV's average value, which is a constant for the specific RV (and is used to normalize the sum of all the resulting probability values), the result equals the limiting PDF of the *residual lifetime* and *age* of that same RV under equilibrium conditions. This means that if one were to look at a point process at any arbitrary instant, after a relatively long duration following the beginning of the stochastic process (so that the state in which the process was started no longer plays any significant role), the probability of the time duration since the previous event is given by eq. 5.9; note that this equation also describes the waiting time until the next event following the arbitrary instant. It is also worth noting that for a positive RV one can calculate this recurrence time PDF from knowledge of the normal RV's CDFC alone, since any of eqs. B.2, B.3 or B.4 can potentially be used in this case.

If length-biased sampling is not taken into account, one can easily encounter apparent paradoxes. For example, consider a periodic point-process with a constant duration between two events, represented by τ_λ. Given that it is constant, the average duration between two consecutive events of this periodic sequence is, therefore, also equal to τ_λ. If one were to draw statistics on the average waiting-time until the next event, randomly picking a time instant to start the measurement from,[16] then the expected value would be equal to $\tau_\lambda/2$. This makes sense, because on average a duration of $\tau_\lambda/2$ would elapse before starting the measurement, and the remaining time until the next event would, therefore, also have an average of $\tau_\lambda/2$. The scenario changes drastically when one considers a homogeneous Poisson process with an average duration between sequential events of τ_λ. It turns out that if one were to draw statistics on the average waiting time until a subsequent event, picking a time instant at random, then the expected value would also be equal to τ_λ, despite the time

[15] For alternative derivations of eq. 5.9, separately for the cases of forward and backward recurrence times, see Cox (1962, § 5.1–5.2). Also see p. 148, where this topic features in a different context.

[16] The average waiting-time (i.e., residual lifetime), $E[W_X]$, can be calculated from the following general equation:

$$E[W_X] \quad = \quad \frac{1}{2} \cdot \frac{E\left[X^2\right]}{E[X]} \tag{5.10}$$

$$= \quad \frac{1}{2} \cdot \left(E[X] + \frac{V[X]}{E[X]} \right) . \tag{5.11}$$

For more information on such calculations, refer to Gallager (1996, § 3.4) and Cox (1962, p. 64).

that has already elapsed since the previous event. Thus, irrespective of whether one were to know when an event took place and then wait until the next event, or were to start waiting at any random time after an event took place and again draw statistics on the time until the next event, one would get exactly the same answer for the two average values. If one were thinking about this intuitively, one might have expected an answer similar to that given for the periodic point-process, considering that (for the second averages) some time had already passed since the previous event. However, this nonintuitive result is a consequence of length-biased sampling that affects the average calculations in the second case but not in the first. Were the events those of a dead-time-modified Poisson process, or any point process different from the two just mentioned, the average waiting-time for the second case would turn out to be a value between these two extremes.

5.8 PSYCHOMETRIC FUNCTIONS

By definition, it is the *psychometric function* that describes the relationship between a parameter of a physical stimulus and the response of a subject who must judge a certain aspect of that stimulus. For the present gap-detection experiments, the subject needs to listen for (and then identify) the stimulus interval that contains a gap of silence. In this case, the psychometric curve is one that describes the relationship between the presented electro-acoustic stimulus and the number of correctly identified gap-containing intervals (or, stated differently, the probability of these correct responses). To predict the probability of correct responses obtained during a psychophysical experiment, *signal detection theory*[17] is used as a basis for the mathematical model. From the perspective of signal detection theory, it is assumed that the subject uses an internal parameter for the decision-making process. For the gap-detection experiments, the assumption is made that the listener uses the intervals between neural spikes, which are evoked as a result of the electrical stimuli, as a basis for the decision. As described below, it is then possible to devise a mechanism for the mathematical description of psychometric functions for gap-detection experiments that is based on PDFs of interspike intervals; the mechanism is formulated using signal detection theory and the fundamental principles of Green and Swets (1966).

Psychophysical experiments are frequently structured in such a way that multiple alternatives (a total of $M + 1$ intervals) are presented to the subject, who then chooses the one "correct" interval that contains the stimulus with the desired aspect. These kinds of experiments can be

[17] See Moore (2003, pp. 142–146) for a brief introduction to signal detection theory.

referred to as $(M+1)$-alternative forced-choice, or $(M+1)$AFC for short, and the probability of a correct response is then the probability that the excitation of the correct interval (i.e., the one that contains the so-called signal) exceeds the excitation of all of the M non-signal (i.e., "incorrect") intervals (Hartmann 2000, chapter 24).

For the simple 2AFC case, where there is only one non-signal interval, the percentage-correct probability can easily be calculated.[18] Let pdf_N and pdf_{SN} represent the probability densities of the noise-alone (i.e., non-signal) and signal-plus-noise (i.e., "correct") intervals, respectively, such that N represents a sample from pdf_N and SN represents a sample from pdf_{SN}. Then, let ΔS represent the difference between these two random variables (i.e., conceptually it can be interpreted as the abscissa of a particular probability distribution), such that

$$\Delta S \quad = \quad SN - N \; . \tag{5.12}$$

Assuming that the two random variables (SN and N) are independent, the difference distribution can be calculated using convolutions, which can be formulated for both continuous and discrete RVs:

$$\begin{aligned}
pdf_{\Delta S}(\delta s) &= pdf_{SN}(\delta s) \circledast pdf_{-N}(\delta s) && (5.13)\\
&= \int_{-\infty}^{+\infty} pdf_{SN}(u) \,.\, pdf_{-N}(\delta s - u)\; du && (5.14)\\
&= \int_{-\infty}^{+\infty} pdf_{-N}(u) \,.\, pdf_{SN}(\delta s - u)\; du \; , && (5.15)\\
\text{and} \quad pmf_{\Delta S}(\delta s) &= pmf_{SN}(\delta s) \circledast pmf_{-N}(\delta s) && (5.16)\\
&= \sum_u \Big(pmf_{SN}(u) \,.\, pmf_{-N}(\delta s - u) \Big) && (5.17)\\
&= \sum_u \Big(pmf_{-N}(u) \,.\, pmf_{SN}(\delta s - u) \Big) \; , && (5.18)
\end{aligned}$$

where $\circledast$ represents the convolution operator. Also, keep in mind that

$$\begin{aligned}
pdf_{-X}(x) &= pdf_X(-x) && (5.19)\\
\text{and} \quad pmf_{-X}(x) &= pmf_X(-x) \; . && (5.20)
\end{aligned}$$

The probability of a correct response is the same as the probability that ΔS is greater than zero, since this would imply that the excitation of the signal exceeds that of the noise.

[18] For the general $(M+1)$AFC case, the probabilities of all M non-signal intervals need to be incorporated, and the calculation becomes less trivial.

Therefore, one can formulate the probability of correct responses, $\mathcal{P}r(C)$, in terms of the complementary cumulative difference distribution:

$$\begin{aligned} \mathcal{P}r(C) &= \mathcal{P}r(\Delta S > 0) && (5.21)\\ &= \mathcal{P}r(\Delta S > \delta s)|_{\delta s=0} && (5.22)\\ &= cdfc_{\Delta S}(\delta s)\big|_{\delta s=0} && (5.23)\\ \therefore \quad \mathcal{P}r(C) &= cdfc_{\Delta S}(0)\ . && (5.24) \end{aligned}$$

The CDFC above can be substituted by pairs of eqs. A.15 & 5.13 and eqs. A.16 & 5.16 to calculate the probability of correct responses for continuous RVs (in the case of Poisson stimuli) and discrete RVs (e.g., periodic stimuli), respectively. The results are:

$$\begin{aligned} \mathcal{P}r(C) &= \int_0^{\infty} pdf_{\Delta S}(u)\ du && (5.25)\\ &= \int_0^{\infty} pdf_{SN}(u) \circledast pdf_{-N}(u)\ du\ , && (5.26)\\ \text{and} \quad \mathcal{P}r(C) &= \sum_{u>0} pmf_{\Delta S}(u) && (5.27)\\ &= \sum_{u>0}\Big(pmf_{SN}(u) \circledast pmf_{-N}(u)\Big)\ . && (5.28) \end{aligned}$$

Combing eqs. 5.14 & 5.26 and eqs. 5.17 & 5.28 leads to a practical mechanism for calculating the probability of correct responses for experiments having a 2AFC structure:[19]

$$\begin{aligned} \mathcal{P}r(C) &= \int_0^{\infty}\int_{-\infty}^{+\infty} pdf_{SN}(v)\ .\ pdf_{-N}(u-v)\ dv\ du\ , && (5.29)\\ \text{and} \quad \mathcal{P}r(C) &= \sum_{u>0}\left(\sum_{v}\Big(pmf_{SN}(v)\ .\ pmf_{-N}(u-v)\Big)\right)\ . && (5.30) \end{aligned}$$

In the context of psychometric functions, the equations above calculate a single point on the psychometric curve for the stimulus signal presented to the subject. In the case of gap-detection experiments, this would give the percentage of correct responses for a stimulus with a specific gap-duration, and one would repeat these calculations for all the gap durations to obtain a complete psychometric function for all possible gaps. To clarify further, eqs. 5.29 and 5.30 represent the mathematical essence of the calculations without the clutter of additional parameters that are specific to the problem to which they are applied, which in the present case is gap-threshold modeling involving a specific neuron. From a practical

[19] Note that in eqs. 5.29 and 5.30 the symbol v represents an iterator variable, and this should not be confused with the model parameter v of Neuron A presented earlier.

perspective, it is easier to conceptualize eqs. 5.29 and 5.30 as describing the calculation for a given set of model-specific parameters. For a complete mathematical description, one would need to expand all probability-distribution expressions to include all the specific model parameters that can be varied; for example, instead of simply writing $pmf_{SN}(v)$ in terms of the iterator variable v, one should (for example) expand this term to $pmf_{SN}(v, T, q, a, \tau, t_0)$, where T represents the gap duration, q again represents stimulation rate, and parameters a, τ and t_0 are model parameters of Neuron C. For periodic stimulation of this specific model neuron, eq. 5.30 could be expanded to:[20]

$$\mathcal{P}r(C)\Big|_{T,q,a,\tau,t_0} = \sum_{u>0}\left(\sum_{v}\left(pmf_{SN}(v, T, q, a, \tau, t_0) \,.\, pmf_{-N}(u-v, q, a, \tau, t_0)\right)\right). \quad (5.31)$$

For a single psychometric-function calculation, applying eqs. 5.29 and 5.30 in a practical manner to the particular problem, the left-hand sides of the equations are perhaps more thoroughly represented by

$$\mathcal{P}r(C)\Big|_{T=1\text{ ms}, q=900\text{ Hz}, a=650\text{ Hz}, \tau=3.5\text{ ms}, t_0=1.7\text{ ms}}, \quad (5.32)$$

such that it becomes clear that the probability is given for a very specific set of parameter values. However, this quickly leads to unnecessarily complicating the mathematical constructs; it may be preferable simply to realize that eqs. 5.29 and 5.30 are to be applied to a specific set of parameters for the given problem context.

It may be useful at this point to refer to fig. 5.1 again and note that the fourth step in the modeling process is now complete. With the calculated psychometric function at hand, it is then possible to predict the gap-threshold duration that one would expect to measure with an experiment. However, to do so, one needs to know where on the psychometric curve the adaptive procedure used in the experiment would converge. If the experiment were to use a 1-up 2-down staircase combined with the 2AFC structure, the measurement should converge to the 70.71% correct mark, and it should stabilize at $\mathcal{P}r(C) = 0.7937$ if a 2AFC 1-up 3-down staircase were used (Levitt 1971). The converging value of $\mathcal{P}r(C)$, therefore, determines the expected experimental measurement that can be obtained from the psychometric function, which completes the final step shown in fig. 5.1.[21]

[20] Note that the "noise-alone" distribution is not a function of the gap duration, and, for that reason, parameter T does not feature in the term $pmf_{-N}(u-v, q, a, \tau, t_0)$.

[21] Although the present implementation of the model did not explore the following possibility, conceptually it seems plausible that an algorithm could be devised to traverse the space of model parameters (e.g., the gap duration) in a more effective way while searching for the desired percentage-correct mark. However, such an algorithm may not be a trivial one, considering the complications

Since it is now possible to predict the expected experimental outcomes for one set of experiment parameters (e.g., the gap-detection measurements for Poisson stimuli at a specific rate), one can repeat all these calculations for different sets of parameters (e.g., reproduce the calculations for any combination of Poisson or periodic stimuli at any given stimulus rate). This technique was used, for example, to obtain the modeling results later presented in fig. 6.14.

5.9 PSYCHOMETRIC SMOOTHING

Although the calculation of correct-response probabilities can be formulated exactly from a theoretical perspective (as given by eqs. 5.26 and 5.28 and the pair of equations following directly thereafter), it turns out that when the relevant equations are applied to the gap-detection model of the present study, the resulting psychometric functions are *not* monotonic. This was a rather surprising result, and its consequences may be far-reaching. One may dismiss it as merely an artifact of the model itself, but the possibility that non-monotonic psychometric curves may indeed be a fundamental property of gap-threshold detection should also seriously be considered. This possibility is discussed in the remaining chapters of this document. However, to ensure that the resulting gap-detection psychometric functions would be monotonic non-decreasing as gap durations become longer, a simple compensation mechanism was implemented in the model of the present study.

The non-monotonicity of psychometric functions is prominent for periodic stimuli, as depicted in fig. 5.2, in which the raw non-monotonic psychometric curves are shown in addition to ones that have been smoothed with a sinusoidal weighing function. The jagged edges of the raw psychometric curves can be attributed to the summation and integration operators of eqs. 5.26 and 5.28, where convolution terms are incorporated immediately as they transition into the positive domain (i.e., for $u > 0$). The resulting convolved function for periodic stimuli is a comb function, as illustrated in fig. 5.3, in which the values change slowly as the function slides smoothly over the origin while the gap durations increase, and, as each mass of an individual comb moves over to the positive side, a jump is observed in the psychometric function. The contribution of these convolution terms can be made less abrupt as they transition from the negative to the positive side by introducing a smoothing function that starts to add terms in a fractional capacity while they are still approaching the origin and only weighs the terms completely when they have transitioned well into the positive

presented in § 5.9.

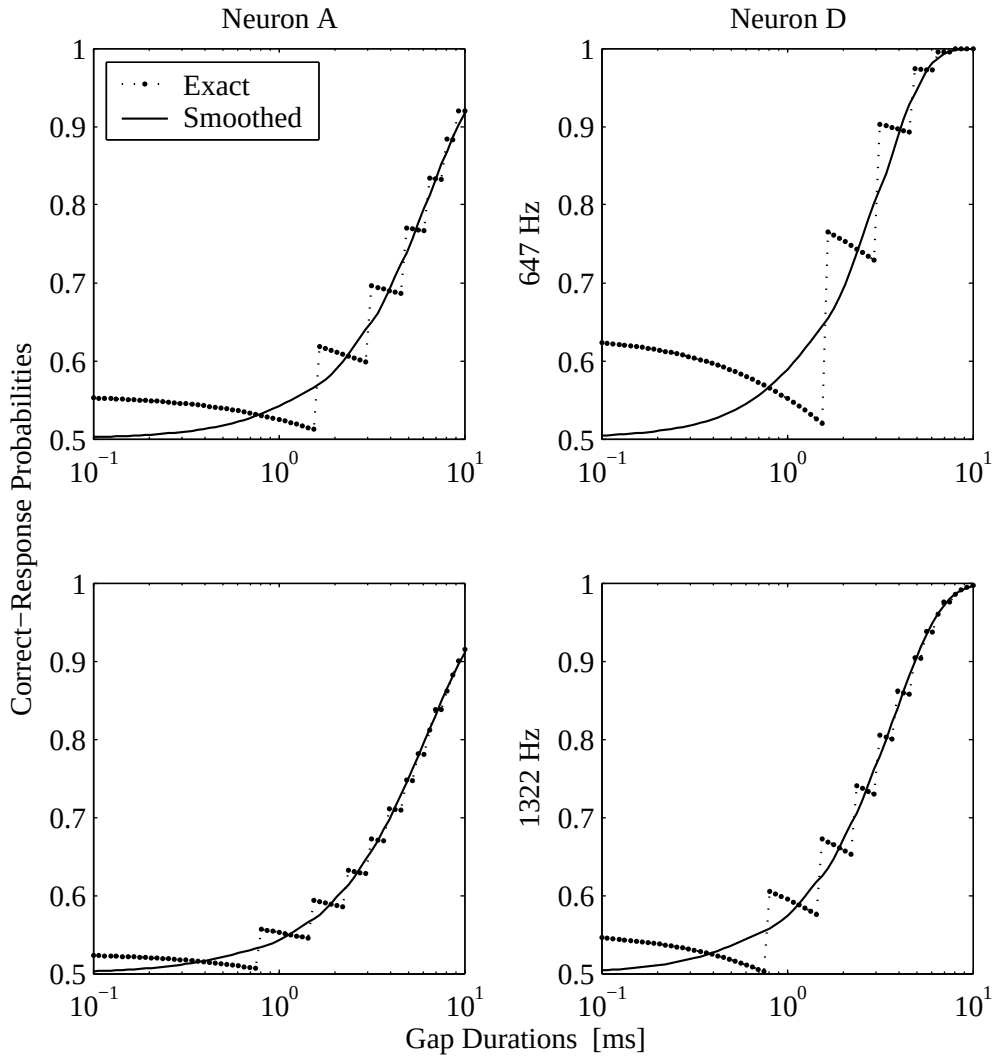

Figure 5.2: The calculated 2AFC psychometric functions are shown for two of the model neurons as they are subjected to periodic stimuli of two different rates. The jagged curves are for calculations corresponding with eq. 5.28, in which jumps are encountered at integral multiples of the stimulation periods. The non-monotonic psychometric curves are, therefore, much more prominent at lower stimulation rates. Also shown are the monotonic non-decreasing curves that have been smoothed using a sinusoidal weighing function with a total transition width of twice the stimulation period.

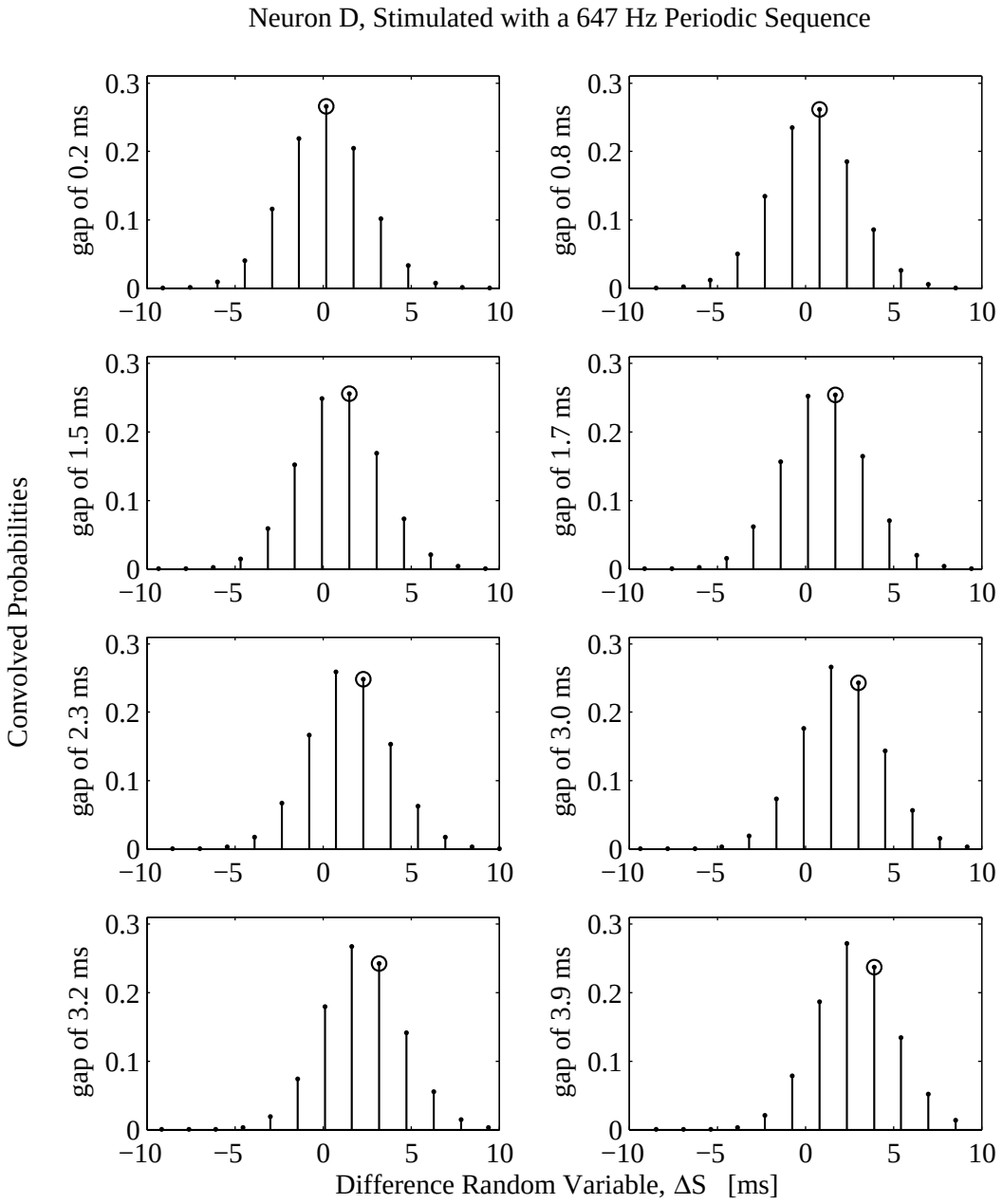

Figure 5.3: A sample is shown of difference distributions, $pmf_{\Delta S}(\delta s)$, for eight different gap durations. The fixed parameters correspond with the top-right graph in fig. 5.2, and the gap durations depicted here are of values surrounding and in between the non-monotonic jumps shown in that graph. Classically, only probability masses to the right of the origin are added to calculate the correct-response probabilities, $\mathcal{P}r(C)$ (see eq. 5.27); for smoothing of the non-monotonic psychometric curves, the masses are weighted before summation (see eq. 5.33). Although it is the cumulative effect of probability masses that should actually be considered for $\mathcal{P}r(C)$, the encircled mass serves as a conceptual example in which the probability mass reaches its maximum value close to the origin (as it classically starts to count), but diminishes as it moves away from the origin (thus, contributing less to $\mathcal{P}r(C)$ for longer gaps), until the next mass transitions the origin and another non-monotonic jump occurs. Furthermore, individual probability masses that do not contribute toward $\mathcal{P}r(C)$ in the classical sense (i.e., for $\Delta S < 0$), always become heavier as the gap lengthens.

domain. It was found that a simple sinusoidal weighing function can perform this filtering task quite well when terms are counted fractionally as they get within one stimulus period from the origin and counted completely only once the term's mass has moved one stimulus period into the positive domain. The mechanism can be illustrated mathematically through a modified version of eq. 5.26, in which one lets $\varsigma(u)$ represent a weighing function used for smoothing, and one can now integrate over the full domain, in contrast with adding only terms from the positive domain:

$$\mathcal{P}r(C) = \int_{-\infty}^{+\infty} \varsigma(u) \,.\, \left\{ pdf_{SN}(u) \circledast pdf_{-N}(u) \right\} du \tag{5.33}$$

$$\text{with} \quad 0 \leq \varsigma(u) \leq 1 \quad \forall \quad u \in \mathbb{R} \,. \tag{5.34}$$

The smoothing function described above can be formalized as follows, where τ represents the half-width of the transition interval that was set equal to either the stimulation period for periodic stimuli or the average period for Poisson stimuli:

$$\varsigma(u) = \begin{cases} 0 & \forall \quad u \leq -\tau \\ \left[1 + \sin\left(\frac{u.\pi}{2.\tau}\right)\right]/2 & \forall \quad -\tau < u < \tau \\ 1 & \forall \quad u \geq \tau \end{cases} \,. \tag{5.35}$$

It could also be argued that a sigmoidal weighing function similar to the one above may very well be a psychophysically plausible one, since it may be unlikely that the brain would make a sharp distinction between convolution terms as they contribute near the u-origin. The resulting smooth psychometric functions are not unlike the ones found in Florentine et al. (1999) for normal-hearing acoustic experiments, although a different experiment structure was used in that case, namely a Yes-No procedure, while the present study uses a 2AFC structure, which results in different ordinate ranges for the probabilities. However, the alternative of non-monotonic psychometric functions for gap-detection should not be ruled out altogether; for example, Shailer and Moore (1987) and Moore (2003, p. 158, fig. 4.6) seem to suggest that this possibility for electrical stimulation has a similar counterpart in acoustic hearing.

In summary, this chapter presented the method by which gap detection was modeled. The logical steps involved in the modeling process were depicted in fig. 5.1, which was followed in subsequent sections by detailed discussions of each aspect of the process. The model allows one to predict the thresholds of gap-detection experiments; it starts off with the temporal specification of the stimuli and includes an intermediate step that calculates

psychometric curves from ISI probability distribution statistics. Results of the modeling work are presented in the next chapter, along with those of the experimental work.

CHAPTER 6

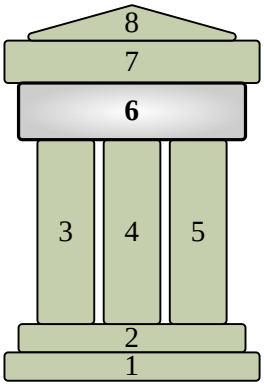

RESULTS

The results of experimental and simulation work performed as part of the present study (documented in chapters 4 and 5) are presented in this chapter.

6.1 RESULTS OF DURATION-DISCRIMINATION EXPERIMENTS

The results of the duration-discrimination experiments, discussed in § 4.4, are shown in table 6.1. The experiments for all three of the subjects were repeated three times for both kinds of stimuli. The last row in the table shows the averages and standard deviations for the nine combined experimental repeats of the two kinds of stimuli; the two standard deviations in this row are not just mathematically calculated from the standard deviations of the three subjects, but calculated from the outcomes of all nine experiments.

Table 6.1: Averages and standard deviations of measurements from duration-discrimination experiments, measured in units of ms for both periodic and dead-time-modified Poisson stimuli.

	Periodic		Poisson	
	Mean	S.D.	Mean	S.D.
Subject S5	102.7	47.0	80.7	9.2
Subject S10	116.8	15.3	108.8	28.8
Subject S3b	98.5	42.4	112.7	13.5
All Experiments	106.0	33.6	100.8	22.4

6.2 Results of Gap-Detection Experiments

For the full range of stimulation rates from 100 Hz to 2700 Hz, the range of repeat-averaged gap-detection results obtained from all subjects varied from 0.358 ms to 22.0 ms for periodic stimuli, with an average of 3.90 ms and a standard deviation of 4.09 ms; for the dead-time-modified Poisson stimuli, the range was from 2.51 ms to 76.1 ms, with an average of 18.6 ms and a standard deviation of 15.6 ms. The results from the initial pilot studies performed with subject S3b were also in these ranges. All these resulting gap-threshold ranges are smaller than those from the duration-discrimination experiments. The following paragraphs will discuss the results in more detail, focusing on a graphical representation. For a detailed numerical representation of all the results, refer to appendix D.[1]

6.2.1 Monopolar versus Bipolar Modes

Some of the initial pilot experiments with subject S3b can be used to compare the monopolar (MP1+2) and bipolar (BP+2) stimulation modes for both the periodic and dead-time-modified Poisson stimuli. The results for the periodic stimulation, detailed in tables D.9 and D.11, are shown in fig. 6.1. The Poisson results, detailed in tables D.10 and D.12, are shown in fig. 6.2. (Data for monopolar stimulation at 100 Hz are omitted. Those experiments were suspended because, in this parameter region, the subject experienced unpleasant sensations from facial nerve stimulation.)

[1] A graphical representation of the standard deviations have been omitted from figures 6.1–6.9 for the sake of clarity, but can be found in the tables referenced for each figure.

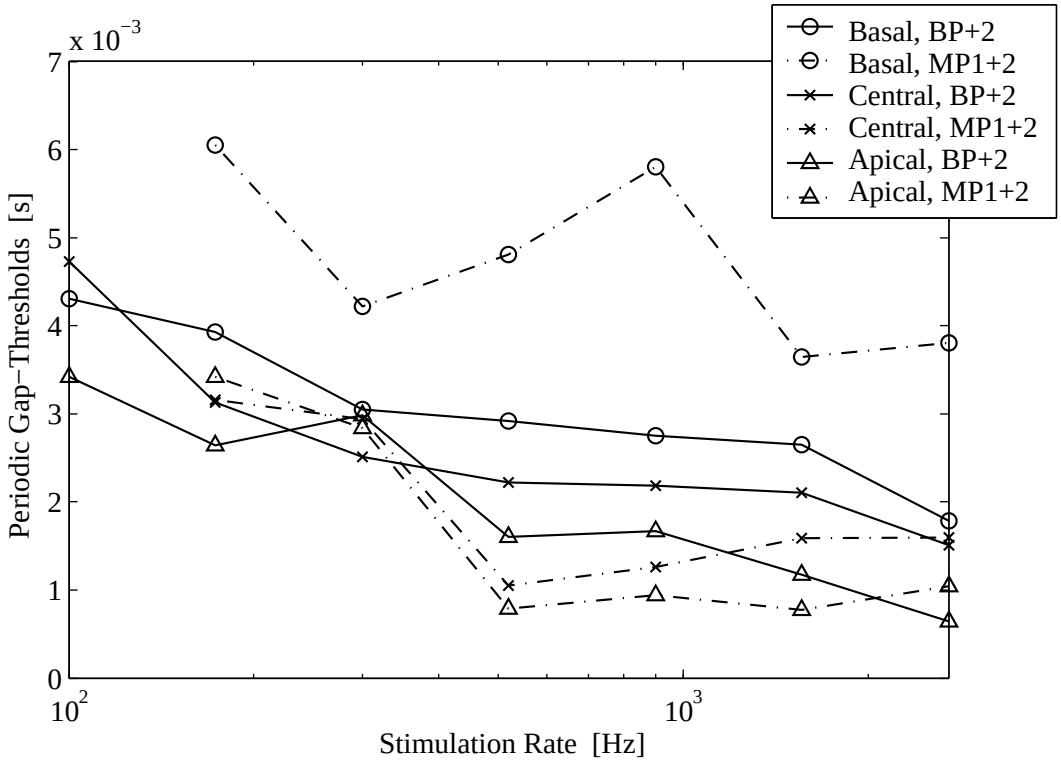

Figure 6.1: Results of gap-detection-threshold experiments with subject S3b, measured for loudness-balanced periodic stimuli, comparing different modes of stimulation.

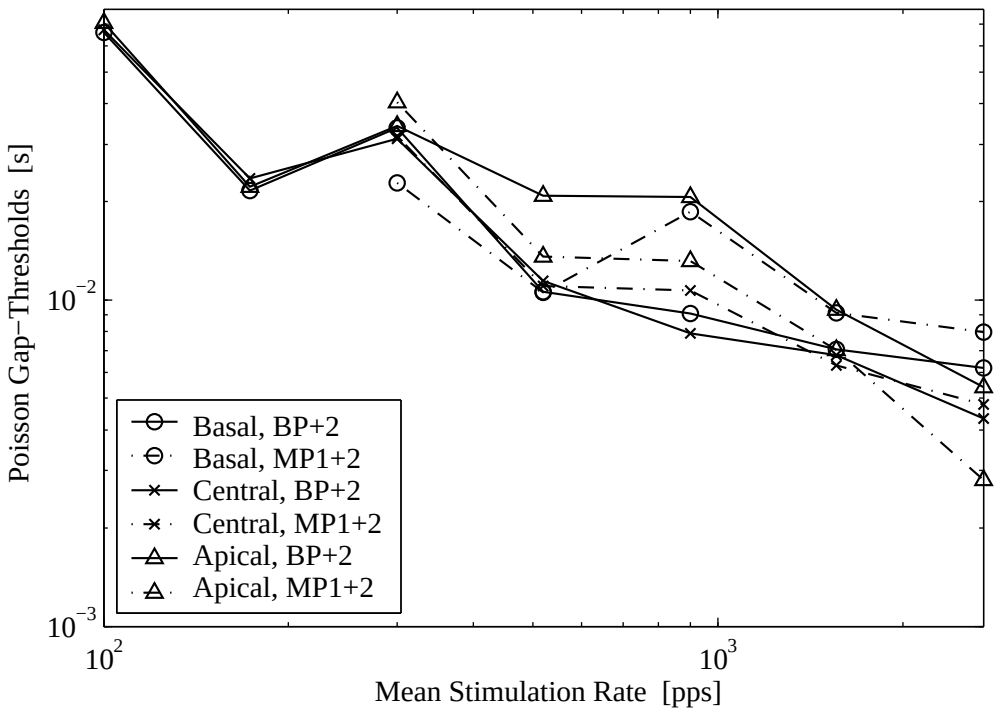

Figure 6.2: Results of gap-detection-threshold experiments with subject S3b, measured for loudness-balanced Poisson stimuli, comparing different modes of stimulation.

6.2.2 Constant Current versus Equal Loudness

For the purpose of determining the effect of loudness on the thresholds of detectable gaps, some additional pilot experiments were initially performed with subject S3b. For comparison purposes, half of the data were drawn from the previous section. The combined results are shown in figures 6.3 and 6.4 for the periodic and dead-time-modified Poisson stimulation sequences. As discussed in § 4.5.2, the electrical currents used in the constant-current experiments for the different stimulation locations were set to the loudness-balanced values of the 900 Hz stimulations from the reference set of experiments; as a result, these points coincide for the different kinds of experiments. The reason for the omitted data at the low-rate sides of these graphs is the same as noted for the previous monopolar experiments. The numerical data for these graphs can be found in tables D.7, D.8, D.9 and D.10.

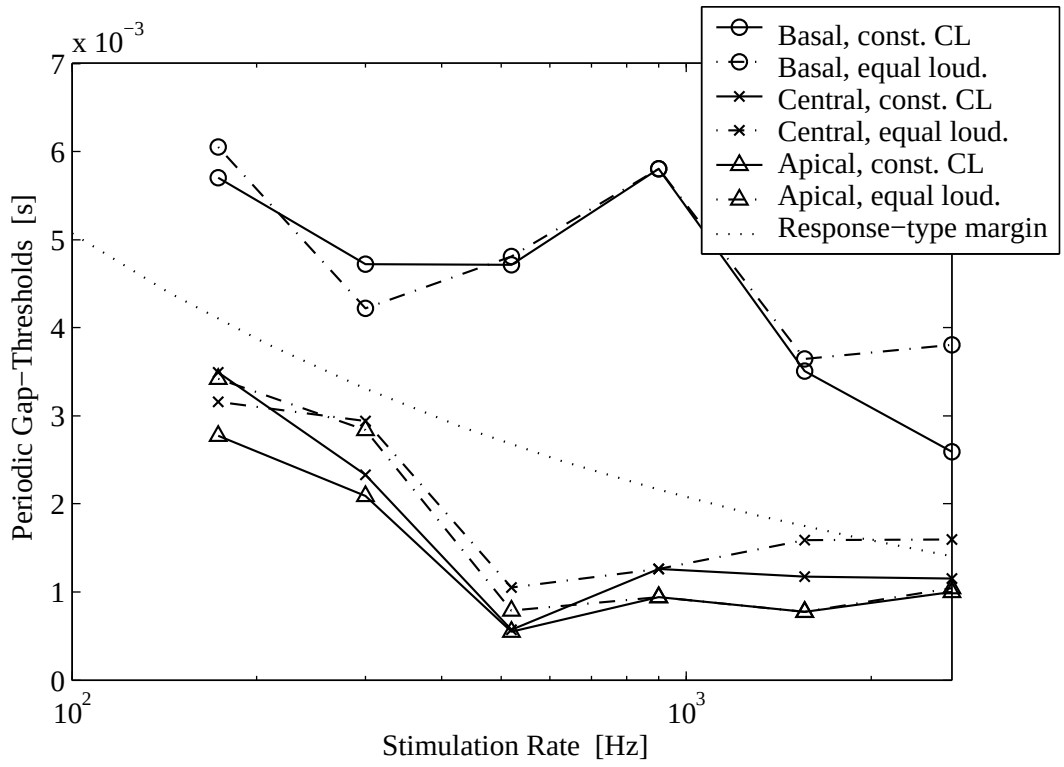

Figure 6.3: Results of gap-detection-threshold experiments with subject S3b, measured for monopolar periodic stimuli at three spatial sites, appear in this figure. For comparison purposes, results from equal-loudness stimuli and constant-current stimuli are shown. Two different types of response curves appear to be present.

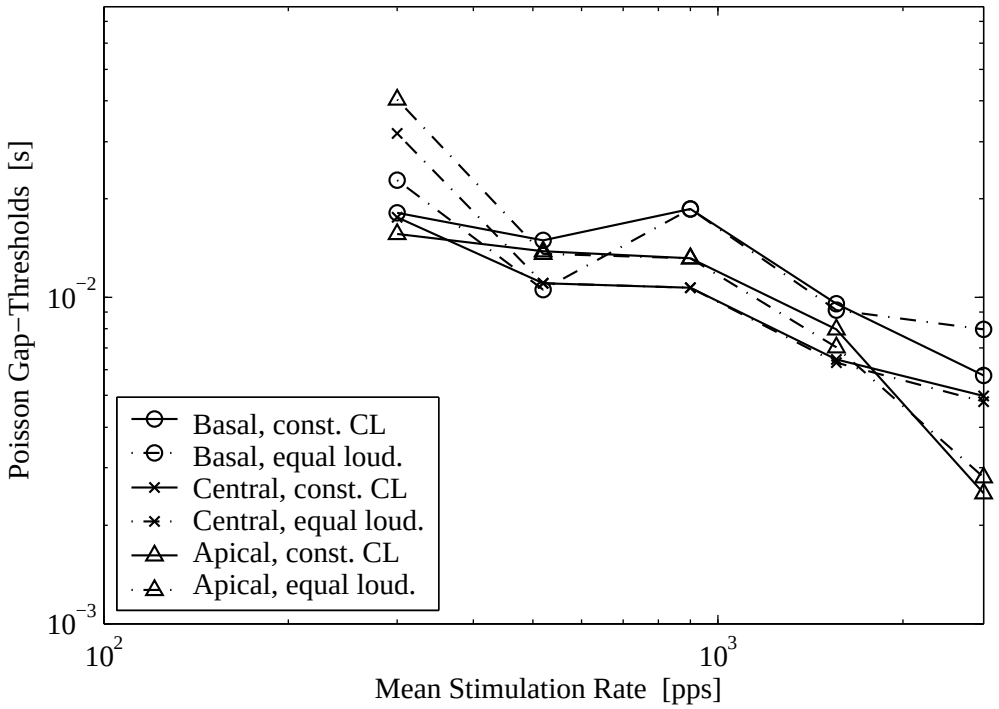

Figure 6.4: Results of gap-detection-threshold experiments with subject S3b, measured for monopolar Poisson stimuli at three spatial sites, appear in this figure. For comparison purposes, results from equal-loudness stimuli and constant-current stimuli are shown.

6.2.3 Periodic Stimuli

The results for the periodic stimuli from tables D.1, D.3, D.5 and D.7 are shown in fig. 6.5. With all the periodic stimuli results visible on a single figure, one can more easily identify the general trends for this kind of stimulus sequence. A comparison of the different stimulation sites is more clearly illustrated in figures 6.7, 6.8 and 6.9 (although these figures also incorporate the Poisson results).

6.2.4 Dead-Time-Modified Poisson Stimuli

The results for the dead-time-modified Poisson stimuli from tables D.2, D.4, D.6 and D.8 are shown in fig. 6.6. With all the Poisson data visible on a single graph, the general trend of the data becomes more clearly identifiable. As noted above (but in the context of periodic stimuli), figures 6.7, 6.8 and 6.9 also contain Poisson data from fig. 6.6, which might be less confusing for examining details.

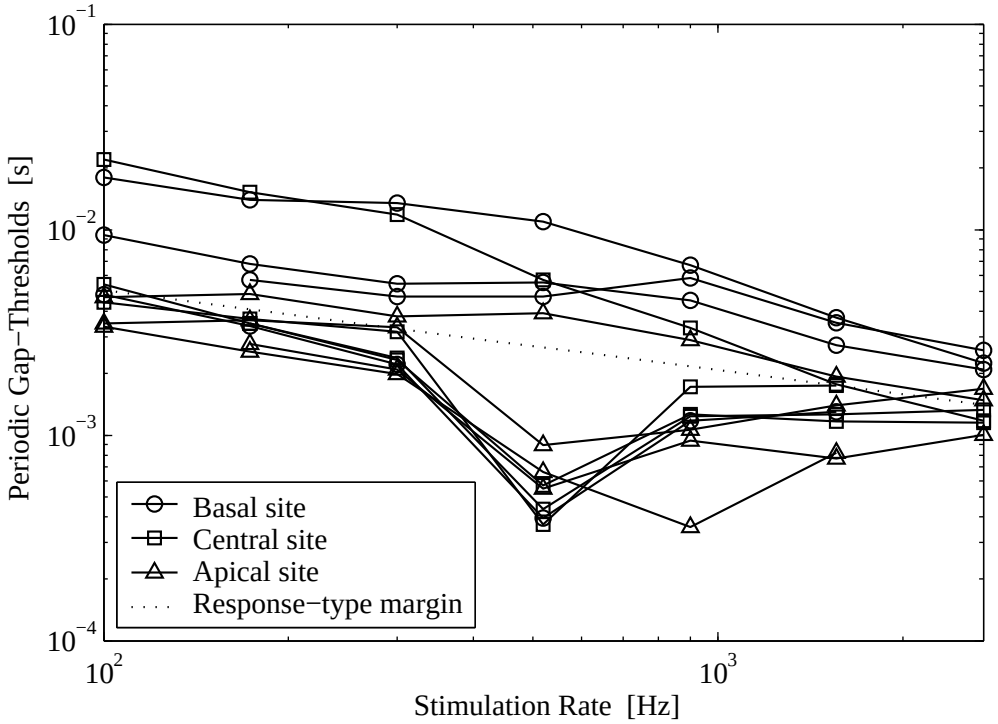

Figure 6.5: Results of gap-detection-threshold experiments with all subjects are shown, measured for periodic stimuli. The legend indicates specific types of cochlear stimulation sites. Two different types of response curves appear to be present.

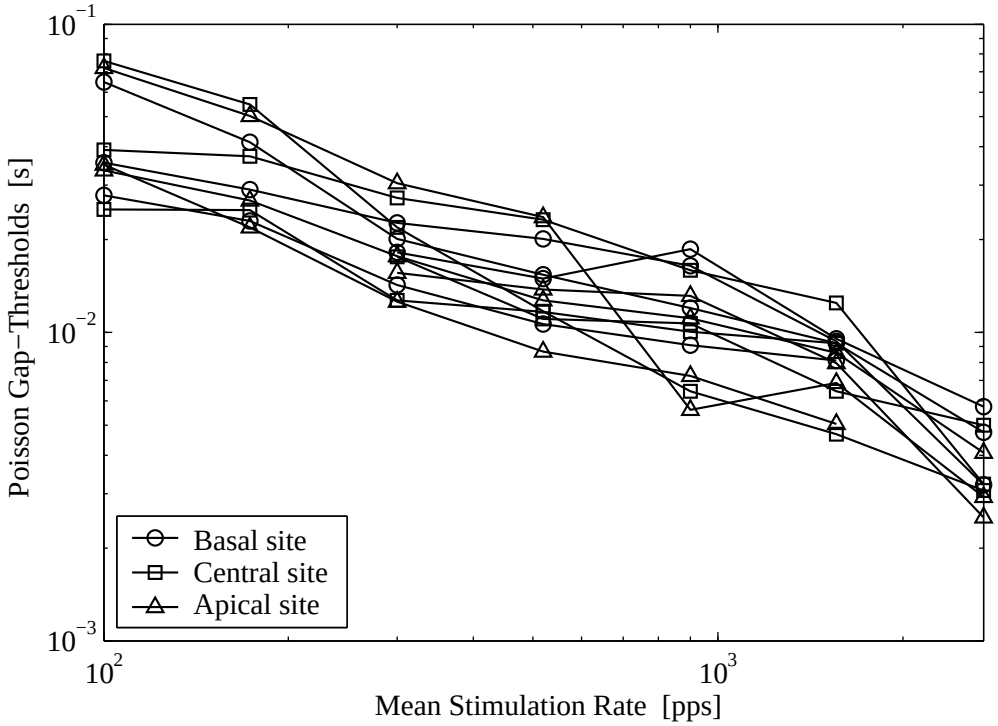

Figure 6.6: Results of gap-detection-threshold experiments with all subjects are shown, measured for Poisson stimuli. The legend indicates specific types of cochlear stimulation sites.

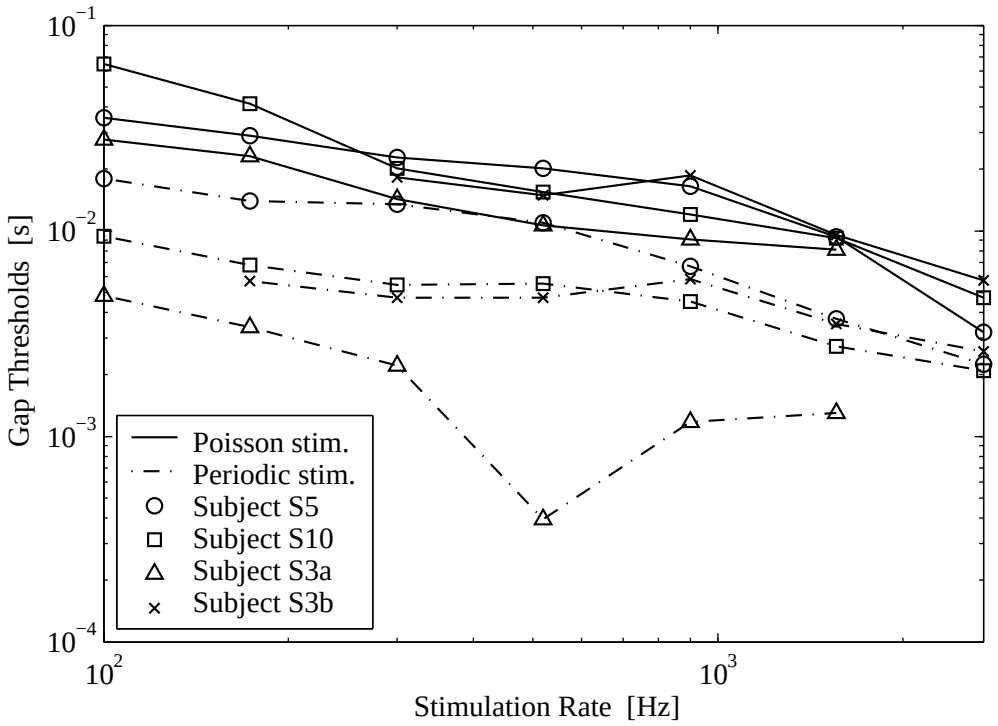

Figure 6.7: Results of gap-detection-threshold experiments with all subjects, measured for constant-current stimuli, with a basal stimulation site.

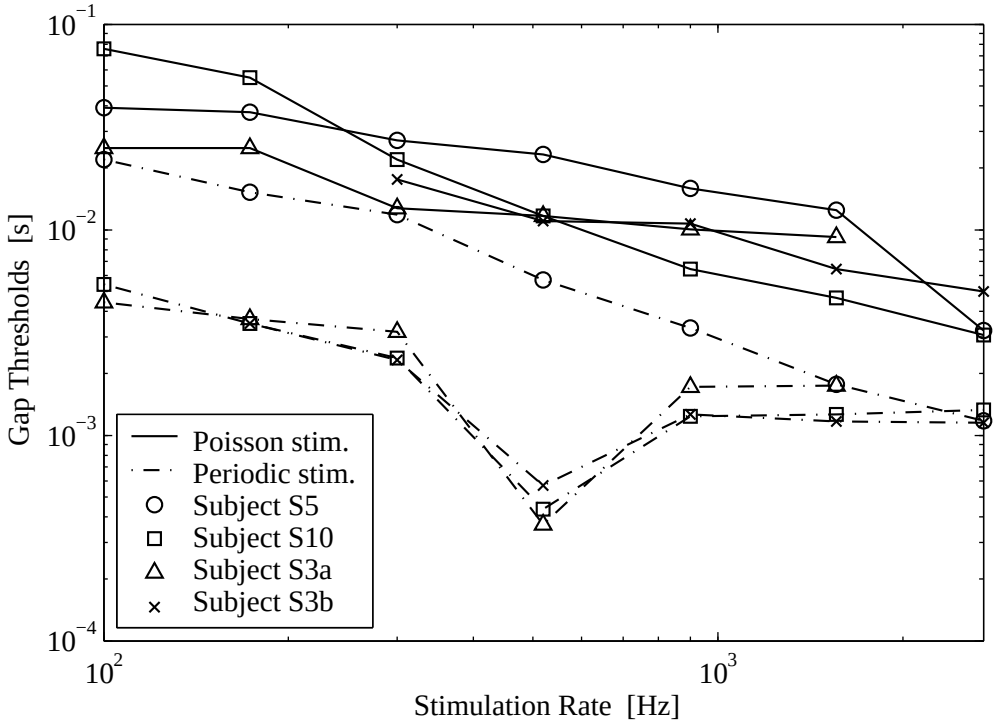

Figure 6.8: Results of gap-detection-threshold experiments with all subjects, measured for constant-current stimuli, with a central stimulation site.

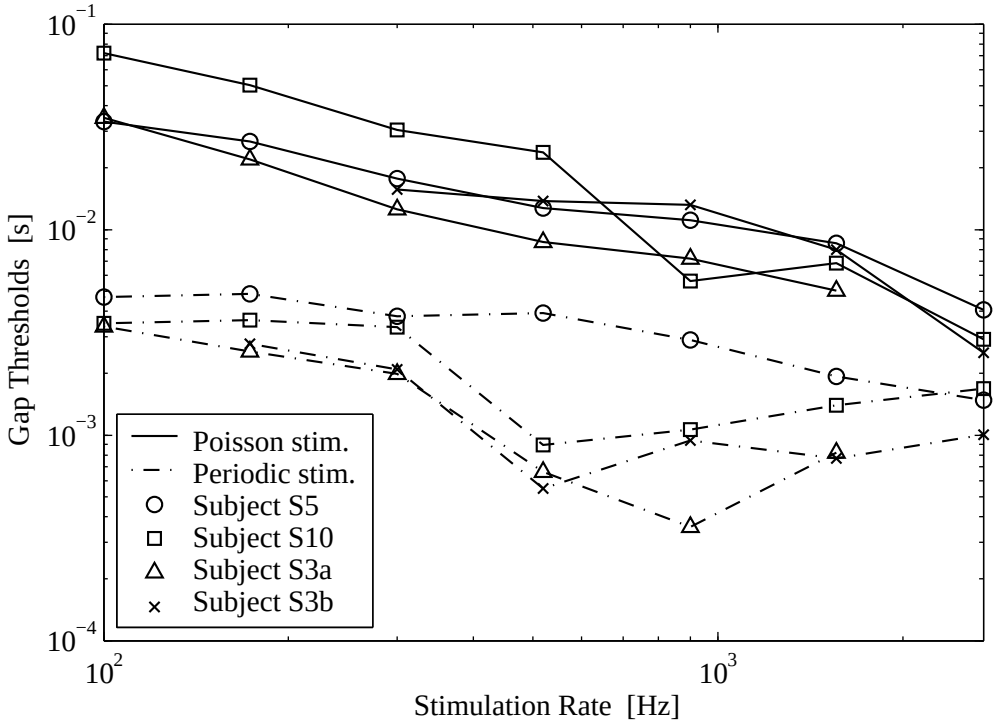

Figure 6.9: Results of gap-detection-threshold experiments with all subjects, measured for constant-current stimuli, with an apical stimulation site.

6.3 RESULTS OF GAP-DETECTION MODEL

The hazard functions of neurons that have been used throughout the model, representing the refractory behavior of neurons and envisaged as a neural filtering mechanism of stimuli, were formulated mathematically in § 5.4. These DHFs are depicted in fig. 6.10, which shows exactly how the spike probabilities increase for the different model neurons as the period since the previous spike becomes longer, making it more likely for a spike to be generated at the next stimulus instant. The initial paralysis period after a neuron has spiked can also clearly be seen as the zero probabilities for short ISIs. The spike probabilities for most model neurons are dependent on the rate of stimulation as well, which is also shown in this figure.

The model for gap detection that has been developed as part of this study allows for predictions through both simulations and, in the case of periodic stimuli, calculations. To demonstrate quantitative validity of calculations from theory, the results from the model will next be presented as a comparison of the two methods, followed by individual results for each method.

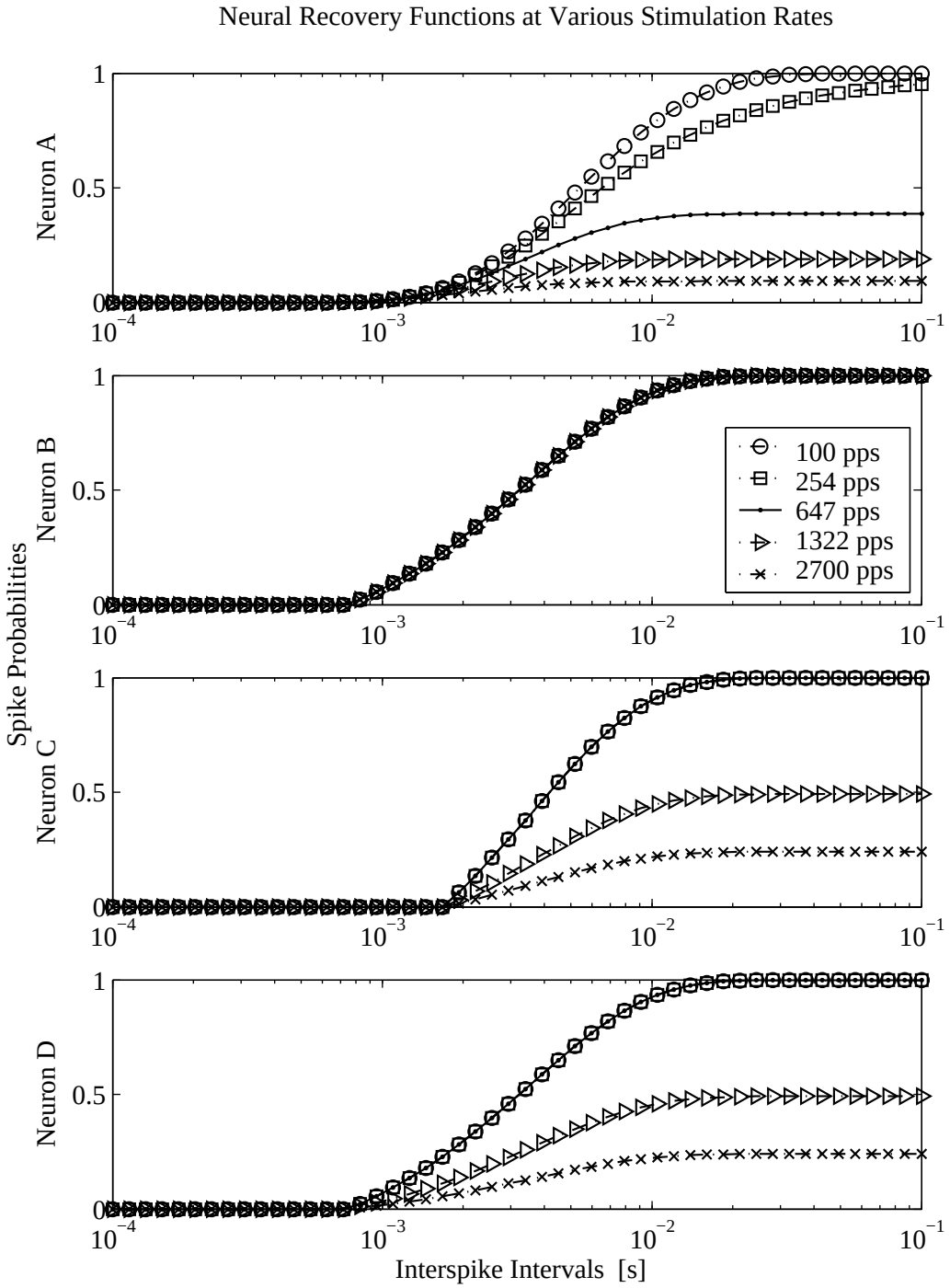

Figure 6.10: The recovery functions (DHFs) of the four simulated neurons show different refractory behavior at various stimulation rates.

Interspike-interval PMFs[2] are shown in figures 6.11 and 6.12, which make it clear that the calculated results track the results predicted by repeated simulations.[3] For illustrative purposes the gap was chosen as 3.924 ms, which is close to the average experimentally measured detectable gap of 3.90 ms. The PMFs are those of the spike probabilities for the ISIs that contain the specific gap, i.e., length-biased distributions. The centers of the circles represent the calculated values, while the bars are the normalized histograms of the simulated results. The illustrated widths of the bars also represent the actual widths of the bins used for the histogram calculations, which are so thin that they can easily appear to be lines only.

Since the simulated and calculated results for periodic stimuli appear to be identical (with the calculated results assumed to be more accurate), the simulated results are exchanged for their calculated counterparts when it could lead to more meaningful presentations of the results; for instance, this has been done for fig. 6.13 (discussed next) in which probabilities have been drawn on a logarithmic scale that accentuates the inaccuracies of simulations for very small probabilities.

6.3.1 Simulation Results

The comparison of results shown in fig. 6.13 highlights the differences between spike probabilities for periodic and dead-time-modified Poisson stimuli. These probability graphs are shown on a logarithmic scale due to the widely differing magnitudes of values in PMFs and PDFs. The PMFs are for periodic stimuli where probabilities are condensed into discrete points. "PDFs" (better described as normalized histograms that can be interpreted as PDFs), on the other hand, are for Poisson stimuli where the spike probabilities are theoretically defined continuously (though simulated discretely) over the ISI axis, resulting in much smaller magnitudes for individual points. Similar to figures 6.11 and 6.12, a gap period of 3.924 ms was used to obtain these PDFs and PMFs.

The graphs shown in fig. 6.14 present all the results from simulations for four different neurons — the outcome of several computer-processor months worth of calculations. The results have been separated into different graphs with individually scaled axes so that the unique shape of each curve can be discerned.

[2] Calculated PMFs follow from eq. 5.6, while the simulated results are for the Monte Carlo procedure described toward the end of § 5.5.

[3] As a matter of interest, the PMFs shown in figures 6.11 and 6.12 are qualitatively similar to ISI histograms from actual experimental data found in Gerstein and Kiang (1960, fig. 2b), although the context is somewhat different.

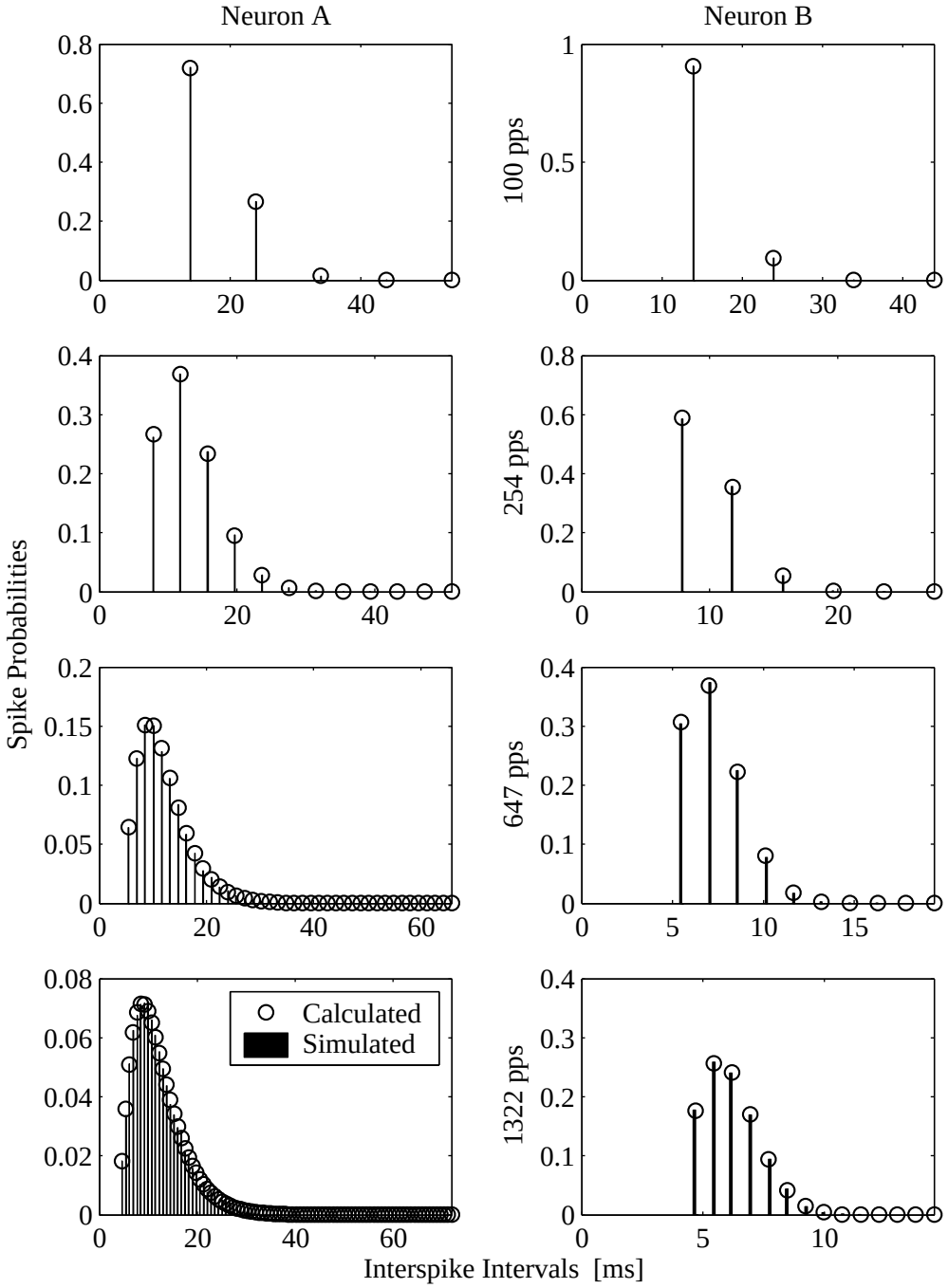

Figure 6.11: To illustrate the correspondence between simulated and calculated results, ISI-PMFs of the first two neurons are shown for a gap of 3.924 ms with different periodic stimulation rates. The dark lines represent the normalized histogram data from simulations (with 0.1 ms bins widths), while the circles identify the exact calculated values. Further evidence of the correspondence is provided in fig. 6.12.

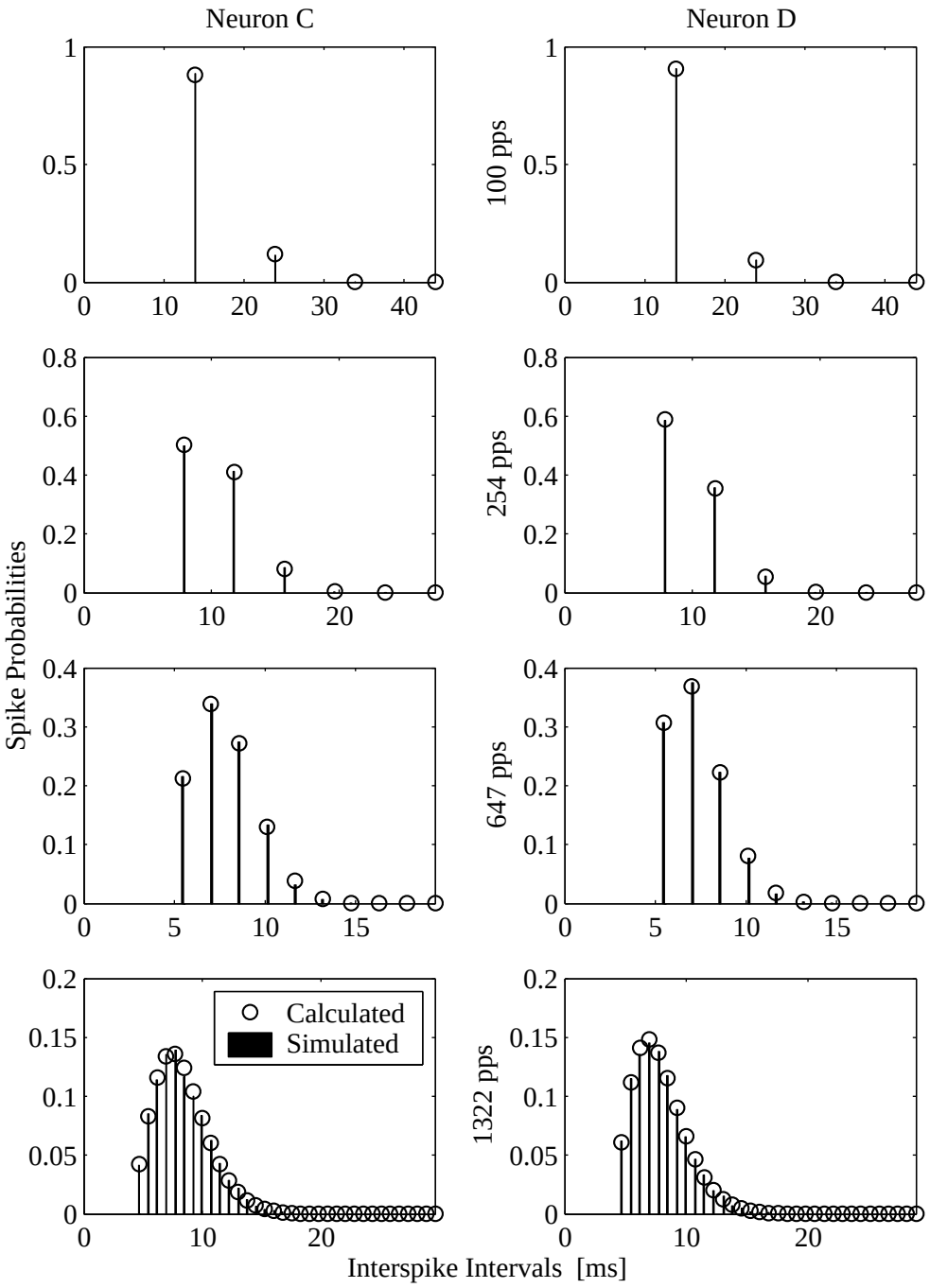

Figure 6.12: To further illustrate the correspondence between simulated and calculated results, similar to fig. 6.11, ISI-PMFs of another two neurons are shown, again for a gap of 3.924 ms and different periodic stimulation rates. The data points of the two methods clearly match up in both figures 6.11 and 6.12, indicating that the theoretical equations used for calculations are in line with the simulated models and the equations can be used as an efficient way for investigating neural responses to periodic stimuli.

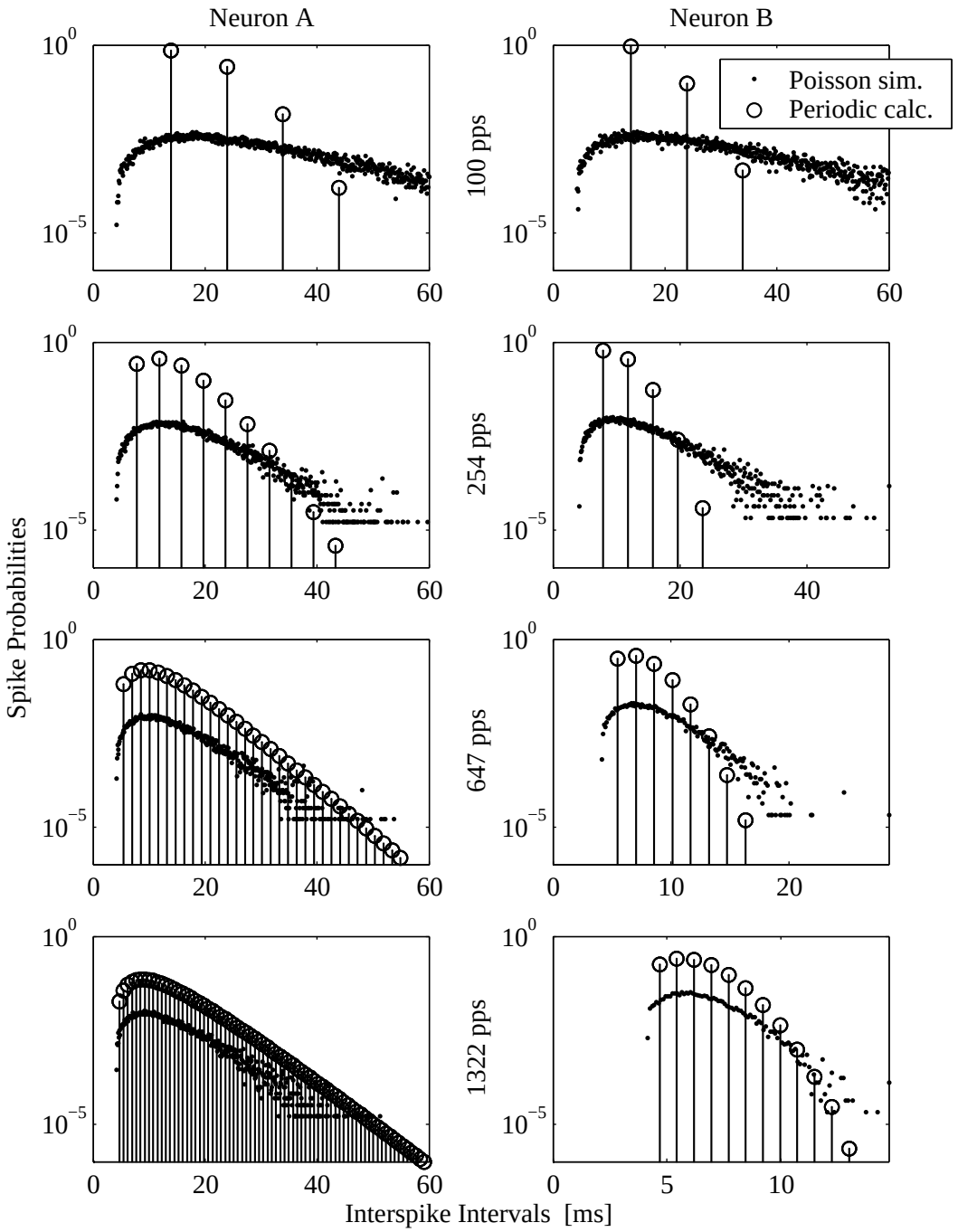

Figure 6.13: This figure compares the spike probabilities as a result of dead-time-modified Poisson stimuli to those of periodic stimuli. Two neurons are used for the comparison, and the effects of different stimulation rates are also shown. For better accuracy, the comparison shows calculated PMFs for periodic stimuli (instead of the simulation results). This is compared with the simulation PDF results of the Poisson stimuli (or more accurately, normalized histograms with 0.1 ms bins widths), where simulation accuracy issues present themselves at longer ISIs — issues similar to those encountered in the ISI histograms of Turcott et al. (1994) and in the hazard histograms of Prijs et al. (1993).

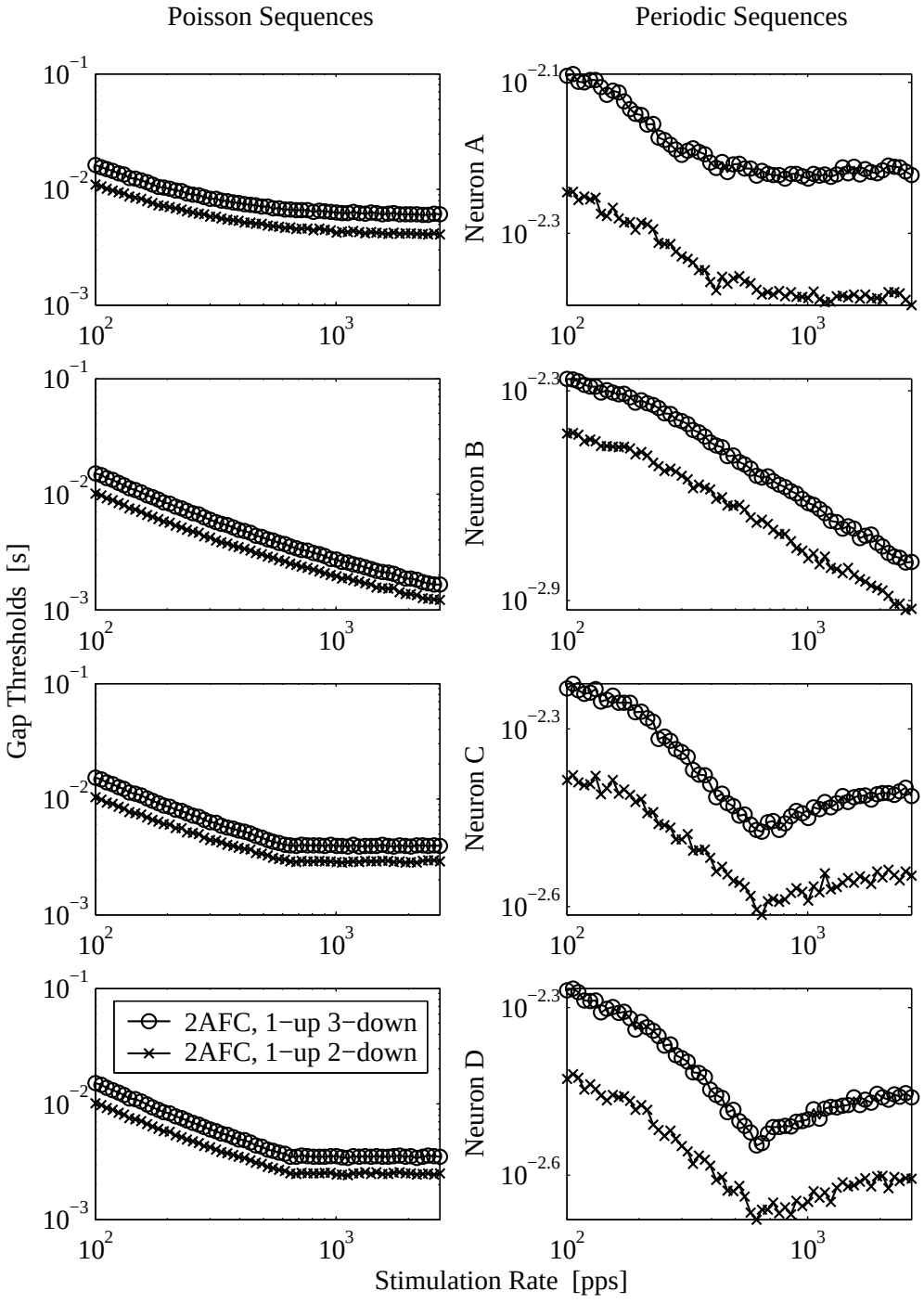

Figure 6.14: Consolidated results of gap-detection thresholds for four simulated neurons with different refractory behavior, showing the results for both dead-time-modified Poisson and periodic stimulation sequences, as well as two readings from each condition's psychometric function (at the 79.37 and 70.71 percentage-correct marks for "2AFC, 1-up 3-down" and "2AFC, 1-up 2-down" experiments, respectively).

Considering the dead-time-modified Poisson stimulation results, all simulated neurons show longer gap thresholds for lower stimulation rates. Although not clearly visible for neuron B, at high stimulation rates a lower limit seems to be reached for the gap threshold (varying from 1.6 ms to 6.1 ms at 2700 pps). The simulation results for periodic stimulation show more interesting gap-threshold curves, some of which exhibit a minimum value that is not located at the extremes of the stimulation-rate range.

6.3.2 Periodic Stimuli Calculations

As calculations for the model progress through the various steps in the process to ultimately predict gap thresholds, psychometric curves are calculated for each set of stimulation parameters right before a gap threshold is estimated from the curve. Examples of these intermediate psychometric-curve results have already been presented in fig. 5.2, which is accompanied by a description of the smoothing function that was used for all the gap-threshold results presented as part of this study (for both simulations and calculations, although the curves in fig. 5.2 are for periodic-stimulation calculations).

Results from numerical calculations (as opposed to simulated counterparts) can also be found in figures 6.11–6.13, in which ISI PMFs have been presented for model neurons in response to periodic stimuli.

Similar to the gap-detection results for periodic stimulation shown in fig. 6.14, the curves depicted in fig. 6.15 are for periodic-stimuli calculations. Whereas the simulation results took several computer-processing months to execute, the calculated results of fig. 6.15 were obtained in mere minutes with much greater accuracy.

With a much more efficient mechanism of predicting gap thresholds using numerical calculation instead of simulations, it is possible to investigate the influence of different model parameters on the threshold curves. For the next set of results, one model parameter value at a time was varied over a range of values that also brackets its default value, while all remaining parameters were kept constant at the values listed in table 5.2. Furthermore, whereas a number of the previous figures have shown gap-threshold results for both the 79.37 and 70.71 percentage-correct marks obtained from the psychometric curves, the remaining threshold results of numerical calculations only show the 79.37% values that correspond with a 2AFC, 1-up 3-down, procedure, in line with the adaptive procedure used for gap-detection experiments.

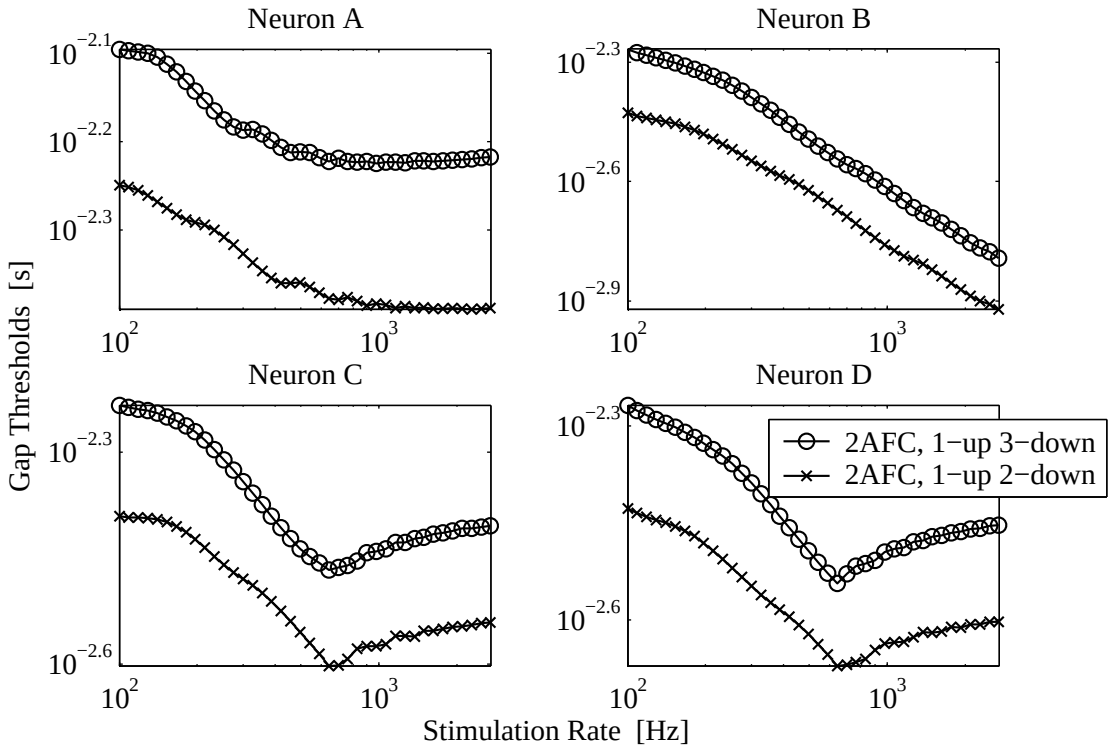

Figure 6.15: Numerical calculation results are shown that predict gap-detection thresholds involving the four model neurons subjected to periodic stimulation sequences. These curves correspond with the simulated results for the periodic stimuli shown in fig. 6.14, but the calculated results shown here exhibit better accuracy in comparison with the simulation results.

One parameter is common to all four modeled neurons (irrespective of whether they were based on eq. 5.1 or eqs. 5.3–5.4), namely the parameter that represents the inactivity period of the neuron shortly after it has spiked. The numerical-calculation results of varying this parameter, t_0, are shown in fig. 6.16 for all the model neurons. A general trend seems to be that longer dead-time periods result in longer gap-detection thresholds. Furthermore, the t_0 parameter seems to be able to change the shape of the threshold curves where sharper changes are observed for very short paralysis periods. For example, Neurons C and D with $t_0 = 0$ ms exhibit a distinct dip in the center region of stimulation rates, very similar to the shape of the experimentally measured curves shown in the lower part of fig. 6.5 (i.e., the curves found below the dotted "response-type margin" line). Threshold curves for larger values of parameter t_0 seem to be smoother and are located at greater gap-threshold values, not unlike the experimental curves found in fig. 6.5 for larger gap-threshold values above the "response-type margin" line.

In figures 6.17 and 6.18 the remaining two parameters of Neuron A, v and w (which are both rate parameters), are varied independently. The general effect of both parameters is that smaller values correspond with longer gap-detection thresholds. Furthermore, varying either of these parameters while keeping the other constant does not seem to make a big difference to the overall shape of the curve (except for moving it up or down); this is especially true for higher stimulation rates, where this model neuron tends to be approximately constant over a wide range of stimulation rates.

The effects of different values of parameter τ on the model neurons that are based on eq. 5.3, namely Neurons B, C and D, are shown in fig. 6.19. One obvious general trend is that smaller values of the time constant τ tend to result in shorter values for the detectable gap thresholds. Smaller values of τ also appear to alter the shape of the threshold curves more prominently, such that multiple local minima may be present (see Neuron C with $\tau = 0.52$ ms where local threshold minima occur around 300 Hz and again at 650 Hz).

Gap-threshold results from numerical calculations are also shown in fig. 6.20, where the influence of the rate-constant a was investigated. It is only parameter t_0 that is different between Neurons C and D (with values of $t_0 = 1.7$ ms and $t_0 = 0.75$ ms, respectively), which does not seem to make a meaningful difference to the resulting gap-threshold curves depicted here, except that slightly longer (on average by about 0.5 ms) thresholds are predicted for Neuron C with the larger t_0 value. Neuron B, which is also based on eqs. 5.3–5.4, is not shown in fig. 6.20, since parameter a for that model neuron is not a pre-set constant but is

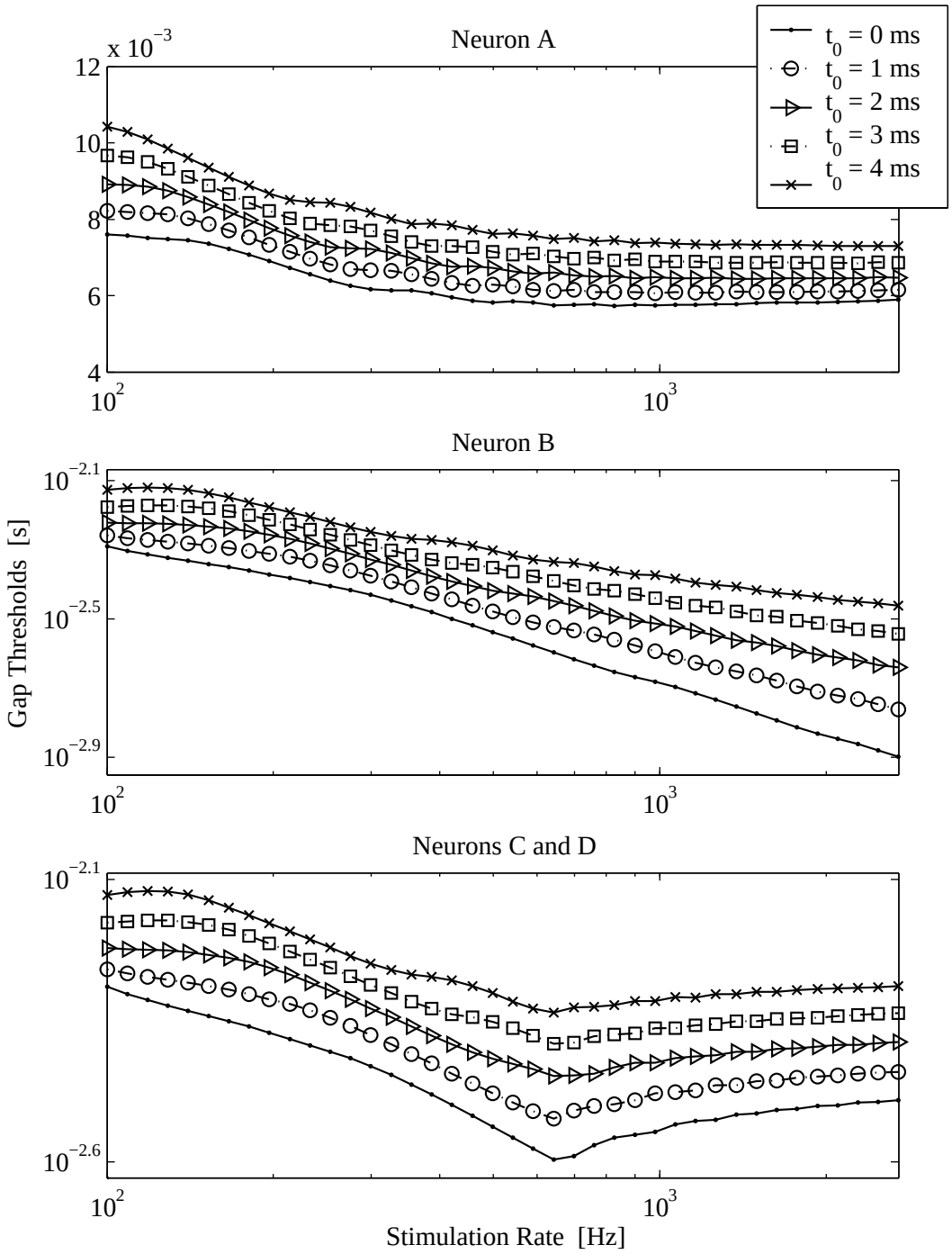

Figure 6.16: Results are shown for numerical calculations of gap-threshold curves (from the 79.37% correct mark on calculated psychometric functions) where the values of the neural-paralysis parameter t_0, which is common to all four model neurons, were varied. While the vertical axes of Neurons B, C and D are drawn on a logarithmic scale, this axis for Neuron A is drawn on a linear scale, since this configuration more clearly shows the range of values calculated for the different neurons. Varying parameter t_0 while keeping the other parameters of the model neurons constant at the values listed in table 5.2 gives identical curves for Neurons C and D, since all their other parameter values are the same except for their default values for t_0. For this reason the latter two neurons have been grouped together in this case.

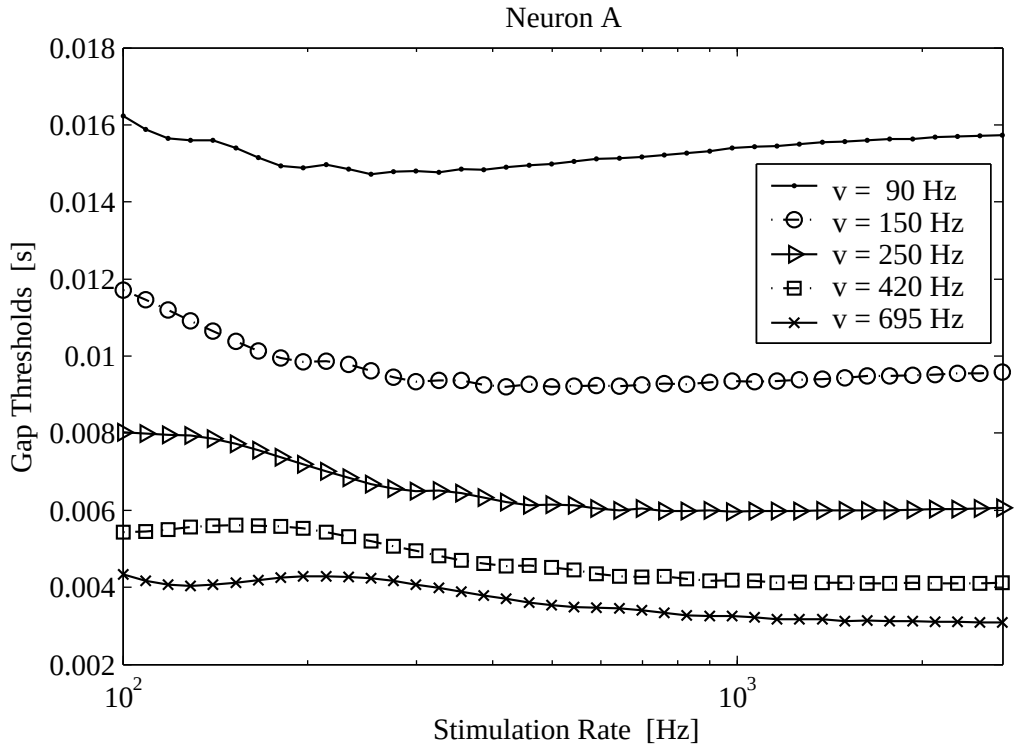

Figure 6.17: Gap-threshold curves are shown for numerical calculations in which parameter v of Neuron A was modified, while other parameter values remained constant at their respective default values ($t_0 = 0.7$ ms and $w = 750$ Hz).

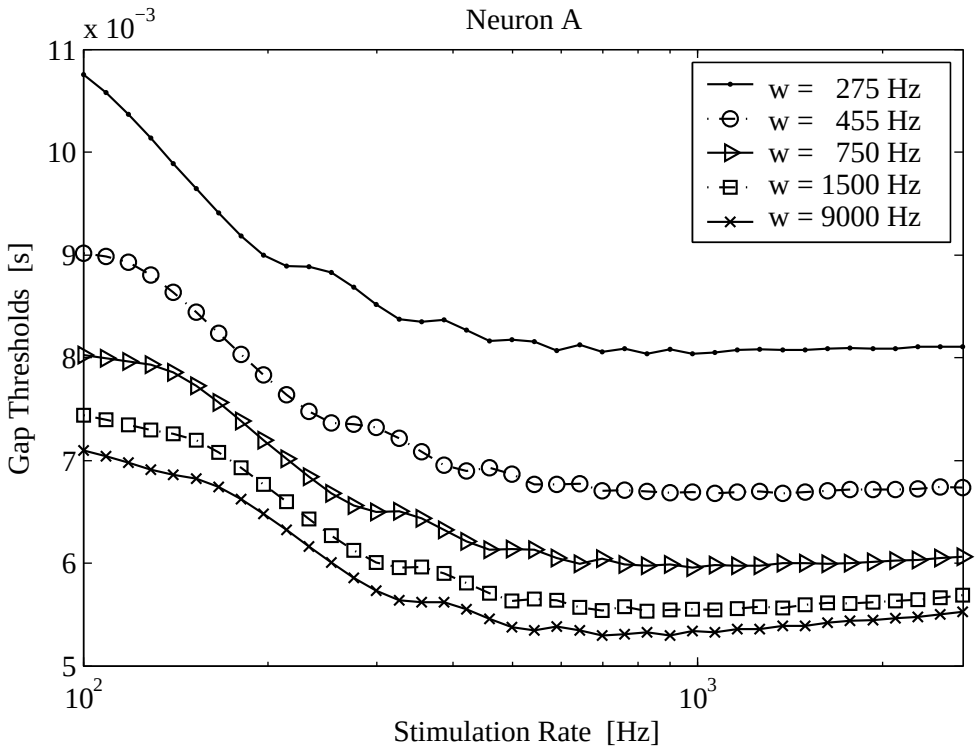

Figure 6.18: Similar to fig. 6.17, parameter w of Neuron A was changed over a range of values, while other parameter values remained constant at defaults $t_0 = 0.7$ ms and $v = 250$ Hz.

instead always set equal to the stimulation rate, q, which would have resulted in a fixed set of curves for Neuron B. This curve would be practically identical to the $\tau = 3.57$ ms curve shown for Neuron B in fig. 6.19. This curve would also overlap most of the way with the diagonal line shared between the different curves of Neuron D in fig. 6.20, but it would extend to even lower thresholds at the high end of stimulation rates.

This chapter communicated the results of the present study's experimental and simulation work. A discussion of the results is presented next.

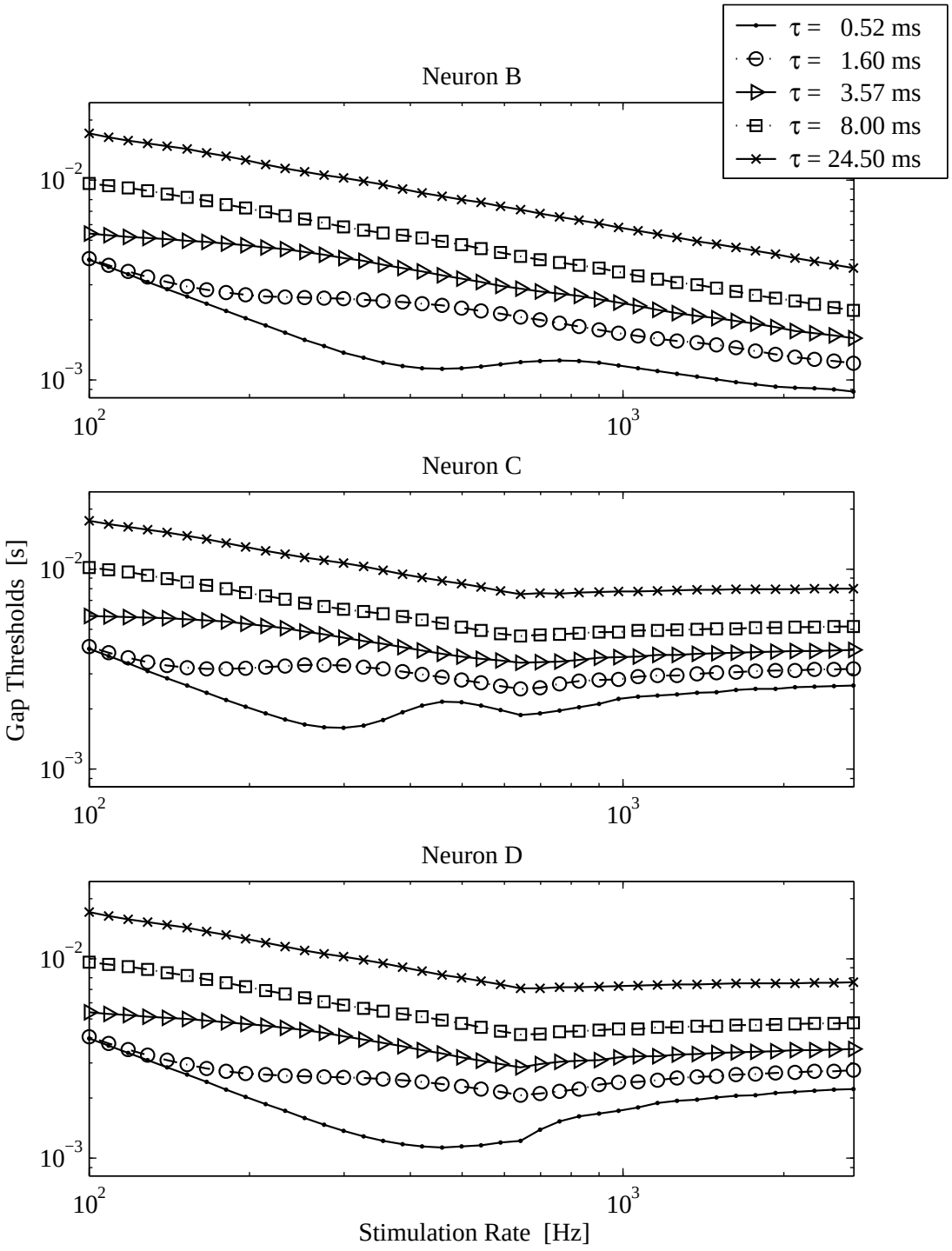

Figure 6.19: The value of parameter τ from eq. 5.3 was varied for Neurons B, C and D, which are all based on this neural-model equation. The predicted gap-threshold curves are for numerical calculations of a 2AFC, 1-up 3-down, adaptive procedure. See table 5.2 for the default values of other parameters that remained constant.

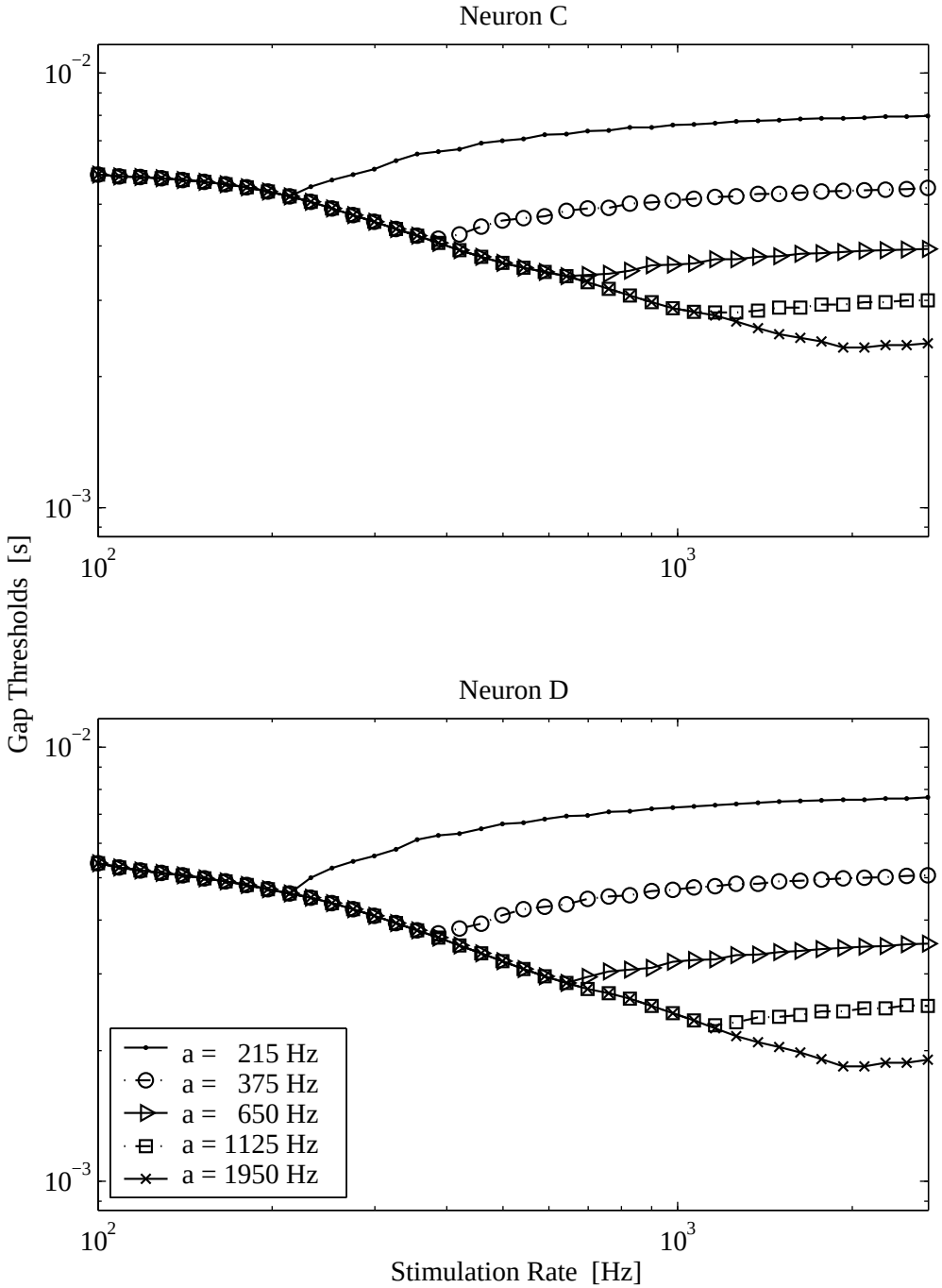

Figure 6.20: Shown in this figure, the rate-parameter *a* of eqs. 5.3–5.4 was varied over a wide range for Neurons C and D, which are based on this modeling equation. The percentage-correct mark used for the threshold readings from the psychometric curves is the same as before.

CHAPTER 7

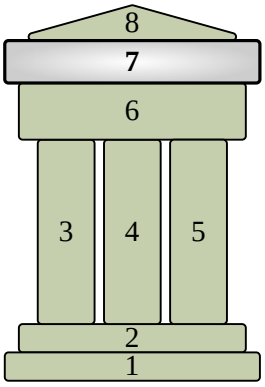

DISCUSSION

In earlier sections, the results of experiments and simulations were presented. The present chapter will discuss the results and integrate the experimental and simulation work. Where applicable, results from other researchers are also referred to and included in the discussions.

7.1 DURATION-DISCRIMINATION EXPERIMENTS

The data in table 6.1 suggest that duration discrimination is in the order of 100 ms for both periodic and Poisson stimuli. This result can be interpreted as a possible upper limit for gap-detection experiments, in which a subject may be able to use the duration of the stimulus as a cue instead of focusing on the perceptual aspects specifically related to the gap in a stimulus. The worst-case gap thresholds[1] are, on average, at least two standard deviations below the average duration-discrimination values. In the worst individualized case, as exhibited by an

[1] In each of tables D.1–D.12, the largest mean value is interpreted as a worst-case gap threshold.

averaged result for subject S10 involving lowest-rate Poisson stimuli, the gap-detection value is still 1.1 standard deviations below this subject's duration-discrimination value.

As a criticism, one could note that the pilot study for duration discrimination was performed with only one stimulation rate, namely 900 Hz, and discriminable durations might vary more substantially for different rates than assumed. As a counter argument it could be noted that the relatively high value of 100 ms for duration discrimination is in sharp contrast with the sub-millisecond gap-detection thresholds measured for quite a few of this study's periodic stimuli, providing substantial room for error. This large difference could also mean that duration discrimination is handled by a higher-level cognitive process in the brain that requires a decision involving conscious thought, while gap-detection tasks could perhaps be based on thought processes that are of a more subliminal nature.[2] From this perspective one would expect to notice changes in the shapes of gap-detection curves where a transition might occur between the two decision mechanisms. One would expect such an effect, if it is indeed an issue, to take place at the larger values of gap-threshold measurements. Thus, such an effect could have been expected for the larger measurements of low-rate Poisson stimuli. However, even under such stimulation conditions, the results shown in fig. 6.6 appear to continue the trend determined by the rest of this curve (which is qualified quantitatively in eq. 7.1), such that collision between the two decision mechanisms seems unlikely.

Seen as a whole, the duration-discrimination results lend support for the decision not to use stimulation-duration roving, as discussed in § 4.4. Since the measured gap-detection durations are generally so much shorter than the measured duration-discrimination values, it may be argued that duration discrimination and the absence of roving did not play a significant role in the outcome of gap-detection experiments.

7.2 COMMENTS ON GAP-DETECTION EXPERIMENTS

7.2.1 Monopolar versus Bipolar Modes

The results shown in fig. 6.1 seem to indicate that, for loudness-balanced periodic stimuli, the gap thresholds stay almost constant across modes of stimulation, although slightly shorter

[2] It may be noted that evidence has been offered (e.g., Wang et al. 2006) for the existence of duration-tuned neurons in the auditory mid-brain and higher auditory centers of several species. However, relatively few neurons are tuned to durations in the order of 100 ms and longer.

gaps can be detected at higher stimulation rates. Overall, the stimulation mode does not seem to make a significant difference, which is in line with the finding of Shannon (1989) that distance between stimulating electrodes (which effectively represents the stimulation mode) does not affect gap-detection performance. The largest difference between the two modes is observed with the basal electrode, where performance results are slightly worse with monopolar stimulation. However, considering the much wider range of gaps found with Poisson stimulation, the difference for this basal electrode does not seem particularly large.

Considering the results depicted in fig. 6.2, the mode of stimulation again does not seem to make a substantive difference. All of these gap-detection thresholds using Poissonian stimulation appear to inhabit a relatively narrow range of gap thresholds for each rate of stimulation, with the detectable gap decreasing generally as the rate of stimulation is increased.

7.2.2 Constant Current versus Equal Loudness

The results shown in fig. 6.3 suggest that loudness-balancing does not substantially influence the gap threshold for periodic stimulation sequences. Although not tested for statistical significance, there appears to be a trend for gap thresholds to be smaller for constant-current stimulation than for the same channel's loudness-balanced stimulation results, and this seems to hold on both the higher and lower stimulation rate sides of the common 900 Hz point. One would have expected that the constant-current gaps would be longer than their equal-loudness counterparts for lower rate stimulations, since here the constant-current stimulations should usually have a softer perceptual loudness, while the reverse is expected for higher stimulation rates (based on van Wieringen et al. 2006). These results for the lower stimulation rates suggest that loudness is not a major contributing factor to the detection of gaps when the evoked perception is still clearly audible (at comfortable listening levels), which, according to informal discussions with the subject, seems to be the case for the softer low-rate constant-current periodic stimuli.

Similarly, when considering results for Poissonian placement shown in fig. 6.4, the outcomes for the two different loudness levels are comparable for higher rates, although the difference becomes more pronounced at lower rates closer to 300 pps.

In summary, these results indicate no meaningful differences between gap thresholds for

equal-loudness stimuli and constant-current stimuli. The implication of such an observation is that, provided the perceived loudness is not too soft, loudness balancing is not required for gap-detection experiments at different rates of stimulation.

7.2.3 Dead-Time-Modified Poisson Stimuli

While perhaps less than ideal, a serviceable equation appears to match the experimental data quite well for the dead-time-modified Poisson stimuli:

$$gap_{threshold} = \frac{1}{rate^{0.68}} , \tag{7.1}$$

where $gap_{threshold}$ predicts the mean gap-threshold in *seconds*, and *rate* represents the average stimulation rate measured in pps (i.e., Hz). The predictions from this simple equation are shown in fig. 7.1 along with all of the actual constant-current Poisson stimuli results.

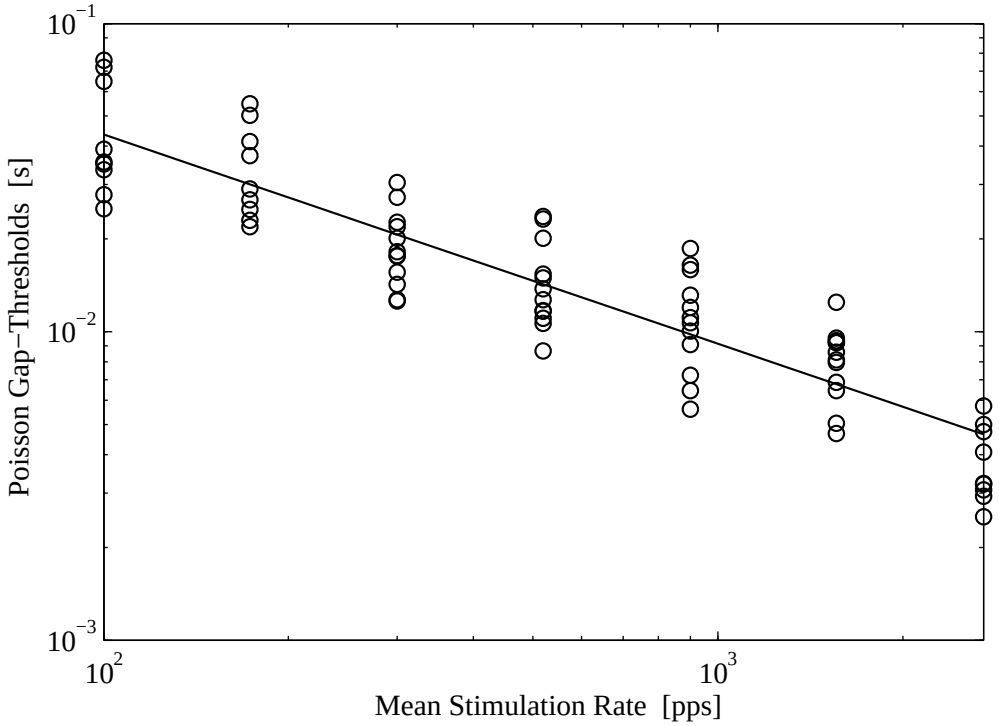

Figure 7.1: A rather simple equation predicts the results of the gap-detection-threshold experiments for constant-current Poisson stimuli.

To examine the origin of eq. 7.1, the best fit (in the least-squares sense) of a parametric-linear

equation[3] to the experiment data is given by:

$$\log(\,gap_{threshold}) \;=\; -0.68384 \times \log(rate) + 0.0090622\;. \tag{7.2}$$

This equation can then be approximated as follows:

$$\begin{aligned}
\log(\,gap_{threshold}) &= -0.68384 \times \log(rate) + 0.0090622 \times \log(10) && (7.3)\\
&= \log(rate^{\,-0.68384}) + \log(10^{\,0.0090622}) && (7.4)\\
&= \log(rate^{\,-0.68384} \times 10^{\,0.0090622}) && (7.5)\\
gap_{threshold} &= rate^{\,-0.68384} \times 10^{\,0.0090622} && (7.6)\\
&\approx rate^{\,-0.68384} \times 1.0211 && (7.7)\\
\therefore\quad gap_{threshold} &\approx 1/rate^{\,0.68}\;. && (7.8)
\end{aligned}$$

7.2.4 Periodic Stimuli

If one considers all the gap-threshold results in which periodic stimulus sequences were used (e.g., see fig. 6.5), it appears that all the rate curves can be classified into two main types.

Response-type 1 These curves show the smallest gap-threshold values. Sub-millisecond measurements are not uncommon. The curves tend to start off at higher thresholds for low stimulation rates, then decrease to a minimum as the stimulation rate increases, followed by an increase in the threshold value as the rate increases further above a critical value. The minimum gap-threshold was almost always observed at the 520 Hz mark, although one should realize that, in the rate domain, the resolution of the present experiments remains low; consequently, the minimum can only be said to usually reside somewhere in the 300 Hz to 900 Hz region (the two sampling points bracketing the 520 Hz point). However, in one case (see fig. 6.9) the minimum was observed at the 900 Hz point, indicating that the location of the real minimum might sometimes even be in a higher range between 520 Hz and 1559 Hz. The final increase of the thresholds at very high stimulation rates appears to level off, usually between 1 ms and 2 ms at a periodic rate of 2700 Hz.

Response-type 2 Where gap-threshold responses to periodic stimulus sequences have a

[3] An alternative fitting method of least squares, expressed using $Y = a\,(X/X_0)^b$, can be found in Abel (1972, table I), with additional detail apparently available in Guilford (1954).

tendency to be greater than a range between roughly 1.5 ms and 5 ms (respectively, for high and low rates at 2700 Hz and 100 Hz), the entire gap-detection-threshold curve tends to resemble a shape more typically found for the Poisson stimuli (refer to fig. 6.6). Although the measured gap-thresholds are usually still relatively small in comparison with those found for the Poisson stimuli, these curves generally tend to decrease monotonically as the stimulation rate increases, but the curve can also remain at a roughly constant value for a wide segment of values below 900 Hz. For higher stimulation rates, the thresholds tend to drop to the same values as for the type-1 responses; at a rate of 2700 Hz the measurements are typically between 1 ms and 2 ms.

The twelve[4] stimulus-site response-curves obtained for periodic stimuli were manually categorized: seven of type-1, and five of type-2. This outcome can clearly be seen in fig. 6.5, with a boundary that seems to separate the two types of responses. A parametric-linear equation was fitted to minimize the classification errors in a least-squares sense of all experimental data-points (with only incorrectly classified data-points contributing to the total error of the fit). This equation can be used as a rough guideline for the margin that separates the two types of periodic responses, as has been shown in figures 6.3, 6.5 and 7.2. In numerical form the equation is written as:

$$\log(gap_{threshold}) = -0.38821 \times \log(rate) - 1.5187 \tag{7.9}$$

$$gap_{threshold} = rate^{-0.38821} \times 10^{-1.5187} \tag{7.10}$$

$$\approx rate^{-0.38821}/33.015\ . \tag{7.11}$$

It is interesting to note that, using eq. 7.11 as a guideline along with the above descriptions of the two response types, the pulsatile gap-detection results of Dobie and Dillier (1985) also seem to contain both types of responses.[5] It appears that the results of their subject U.T. form a type-1 response curve with a minimum in the bracketing range between 250 Hz and 1000 Hz, while the pulsatile gap-threshold curve for subject E.P. is a type-2 response that decreases monotonically as the rate of stimulation is increased.

[4] One apical, central and basal stimulus site for each of subjects S5, S10, S3a and S3b.

[5] A close read suggests that table II (p. 48) of Dobie and Dillier (1985) may contain a misprint. For the current comparison, the classification would be more striking if one could assume that the measurement of 2.7 ms at 750 Hz is indeed for subject E.P., as discussed in the text on p. 49 of Dobie and Dillier (1985), and that the value has been incorrectly recorded in table II as belonging to subject U.T. But even if the reverse is true, the classification remains highly probable (considering the overall shapes of the curves).

There are also some striking similarities between the shape of the type-1 responses and the results from Abel (1972, second graph)[6], which are for acoustical gap-discrimination experiments. Despite very different experimental setups and procedures, similarities in results and their interpretation may indicate that a common underlying psychophysical process is involved, which may very well be captured by the temporal stochastic principles that underlie the model as it has been developed for the present study. When comparing the results, consider especially the common range of temporal stimulation: for electrical stimulation, rates from 100 Hz to 1558.8 Hz are considered and compared with the acoustical silence durations from 10 ms down to 0.63 ms. The assumed analogy is, therefore, that silence durations for the acoustical experiments correspond with the silent periods between electrical stimulation pulses (i.e., the reciprocal of the stimulation rates). Results from both sources show an asymptotic threshold in the order of 1–3 ms for short-period/high-rate stimulation. Both sources also show a minimum threshold in the center of the range of rates; for electrical stimulation this is typically around the 1.9 ms period (typically bracketed by sampling points at 1.1 ms and 3.3 ms), and for the acoustical results the minimum is observed around 2.5 ms (with neighboring sampling points at 1.25 ms and 5 ms). Furthermore, for long-period/low-rate stimulation (with 10 ms periods) the largest thresholds are measured (greater than 3 ms).

As in Abel (1972), with reference to Hirsh (1959) and Williams and Perrott (1972), threshold temporal separation for the report of two events is 2 ms. Similar to Abel's data-supported argument, it is at present argued that when the silence period (e.g., between successive stimulation pulses) plus the measured gap-threshold is greater than approximately 2 ms, the participant is likely to perceive two distinct sounds in the one signal-interval containing the extra gap. For stimulation with short periods between stimuli (high rate), the dominant factor would then no longer be the stimulation period itself, but instead the gap period (given that the gap period would be proportionally larger than the stimulation period). This would explain the asymptotic behavior for high-rate stimulation, even irrespective of the temporal fine-structure properties of the stimulation — thus explaining why similar thresholds are also measured for Poisson stimuli at high rates. Gap detection for high-rate electrical stimulation, therefore, corresponds with "Region 1" identified in Abel (1972). It is worth noting, though, that for electrical stimulation the duration of a detectable silence period (before or without the gap) is linked to the neural entrainment factor, such that several stimulation periods (in contrast to a single acoustical silence period) are likely to be combined at higher stimulation

[6]Note that the graphics of the two figures in this article should have been reversed. The second graph actually belongs with the caption of fig. 1. The plot referred to here is the one with axes $\Delta T_{0.75}$ versus T (not λ versus T).

rates (at which entrainment is lower due to more stimuli being filtered by neural refractory effects) to produce the total perceived silence period between the two events. Furthermore, the temporal separation for multi-event distinction (i.e., to hear two sounds, one before and one after the gap) might not necessarily be an absolute constant for the wide range of rates of these experiments.

This same argument about the identification of two events in a single interval might also explain the mechanism behind the two types of responses observed in electrical gap-detection experiments. When the sole criterion used to identify the interval containing the gap is whether a single sound or two distinct sounds can be identified in one of the intervals, it may be argued that the type-2 responses are worst-case measurements. Then, for type-1 responses to be possible, the participant must employ more cues to identify the gap-containing interval when all the choice alternatives contain a single perceptual sound. This possibility may also explain why type-2 responses are always found at higher thresholds in comparison with type-1 responses. However, one cannot rule out the possibility that the participant always tries to listen for an interval with two sounds, and the exact nature of the additional cues that play a role during type-1 responses is possibly simply a matter of finer intricacies of neural firing. Various interesting neural behaviors are discussed in Abel (1972) involving the topic of "Region 1", and similar neural properties could very well explain when firing presents these additional cues to hear two distinct sounds at lower gap thresholds. After all, a specific type of response curve is always identified for a specific site of stimulation, and different stimulation sites are likely to differ in the finer details of neural firing owing to slightly different physical properties surrounding those electrodes. This possibility is more in line with the assumptions of the model explored as part of this study: one that relies purely on the statistics reflecting the refractory behavior of neurons.

Finding a clear analogy to the discussion involving "Region 2" in Abel (1972), which corresponds with the low-rate periodic electrical stimulation for rates slower than where the minimum threshold is observed, could be somewhat more problematic. For the acoustic gap-discrimination experiments, it is assumed that two distinct sounds are always heard when the silence periods become long, and the decision criterion is based on perceptual loudness differences between the two first markers in each interval (i.e., the longer the silence period after the first marker, the more time for the exponentially decaying loudness perception following termination of the first marker and before the onset of the second marker). An analogy in the electrical-stimulation context would mean that each pulse in the stimulation sequence evokes a loudness perception which also dies out exponentially, and for rates

below approximately 500 Hz (i.e., matching the 2 ms two-event threshold) the subject can hear individual stimulation pulses. This concept might actually be plausible, since implant subjects describe these low-rate stimulation sequences as less smooth in comparison with high-rate sequences. The real question, then, is whether the subject actually listens for timing differences between individual spikes, or simply for a greater drop in loudness in each of the intervals. The distinction might be very subtle, and the answer might be difficult to determine. However, the model of the present study used interspike timing statistics as the common criteria, irrespective of the stimulation rate, and the outcome was quite successful (see § 7.3.3 for details).

As far as the use of an adaptive procedure for the periodic gap-detection experiments is concerned, one aspect could be discussed further. For adaptive procedures to work, the underlying psychometric functions need to be monotonic (either increasing or decreasing) as far as the one-dimensional parameter being measured is concerned. However, as discussed in § 5.9, the models of the psychometric functions have indicated that this might not actually be the case for periodic stimuli, and that phase effects may influence gap delectability. This may indicate that alternative experiment procedures would be better suited to these kinds of experiments. However, the experiment results measured with an adaptive procedure gave consistent results, and this may indicate that either the psychometric functions are monotonic after all and that the model is not completely accurate, or that the non-monotonic phase effects do not play such an important role. As previously discussed, to eliminate the non-monotonic behavior in the model, a smoothing function was applied, and it is possible that this weighing function also has an underlying biological counterpart (perhaps higher functions of the brain compensate for this), in which case the actual psychometric function would also turn out to be monotonic. The consistent experimental results from individual subjects seem to support this argument.

7.2.5 Stimulation Site

Comparing the results of figures 6.5 and 6.6 for any differences between apical, central and basal electrodes, it appears that, except for the differences noted below, moving the stimulation site does not make a huge difference for gap detection. Therefore, the results of the present study lend support, overall, to the findings of Shannon (1989), who also reported that gap-detection performance was not affected by electrode position in the cochlea. For high stimulus sensation levels, which could be comparable to the comfortably loud stimuli used in the present study, Preece and Tyler (1989) also reported no difference between apical

and basal electrodes, although the data in their figures 3 and 4[7] do show some differences (though not a consistent pattern).

Some differences may be noted, although, given the small number of curves available for comparison (only four per stimulation site), these are perhaps not indicative of a general trend. For the periodic stimulation results, most of the basal curves (i.e., three of the four) are type-2 responses, which may be more clearly visible from fig. 6.7. In contrast, most of the central and apical periodic responses (in both cases, again, three out of four) are type-1 responses (see figures 6.8 and 6.9). Thus, sub-millisecond responses are less abundant in the basal region than in the central and apical regions. However, one general trend appears to be evident, which is that the shortest periodic gap-threshold for any subject at any given rate is most often measured in the apical region, and all the mean apical responses for periodic stimuli are below 5 ms. In contrast, on the opposite tonotopic side, more than 40% of periodic basal mean gap-thresholds are above 5 ms, and most often the basal measurement is the longest of the three sites. Such a generalization also seems compatible with results from van Wieringen and Wouters (1999, experiments 1a and 4a), in which mean apical within-channel gap-threshold measurements are smaller than their basal counterparts for seven out of eight cases (see van Wieringen and Wouters 1999, fig. 8).

For Poisson stimuli, there does not appear to be any significant difference between the three stimulation sites. In summary, the electrode position in the cochlea may or may not make a difference for gap-detection performance, depending on the type of stimulation. But to know irrefutably whether a general difference is observable for periodic stimuli, more experimental data would need to be gathered.

7.2.6 Weber Fractions

The calculation of Weber fractions as it pertains to Weber's law for intensity discrimination, which is defined as the intensity discrimination threshold divided by the intensity of the stimulus itself (i.e., $\Delta I/I$), can also be applied to the gap-detection measurements for comparative purposes. Because Weber fractions relate the JND to the reference value, they are generally seen to be relevant only in the case of discrimination experiments. For

[7] The applicable graphs referred to here are specifically the bottom pairs shown in figures 3 and 4 of Preece and Tyler (1989), where the loudness of the present stimuli should be sufficient to obtain the smaller and more constant range of thresholds depicted in the graphs; these graphs of Preece and Tyler are similar to the results of periodic stimuli reported for the present study.

the present discussion, however, it is argued that gap detection involving pulsatile electric stimuli may also be interpreted as a gap discrimination task, since the participant needs to discriminate between an interstimulus interval containing an additional gap and a "standard" interstimulus interval. (The distinction between detection tasks and discrimination tasks becomes more prominent for normal hearing.) To get to an applicable equivalent of the Weber fraction in the context of gap detection, the gap duration is divided by the reciprocal of the average rate of stimulation (so that both the numerator and denominator are measured in units of time). Equivalently, the Weber fraction for gap detection can be calculated as the product of the measured gap-duration and the average rate of stimulation. The results of such calculations are shown in fig. 7.2 for all the constant-current experimental results.

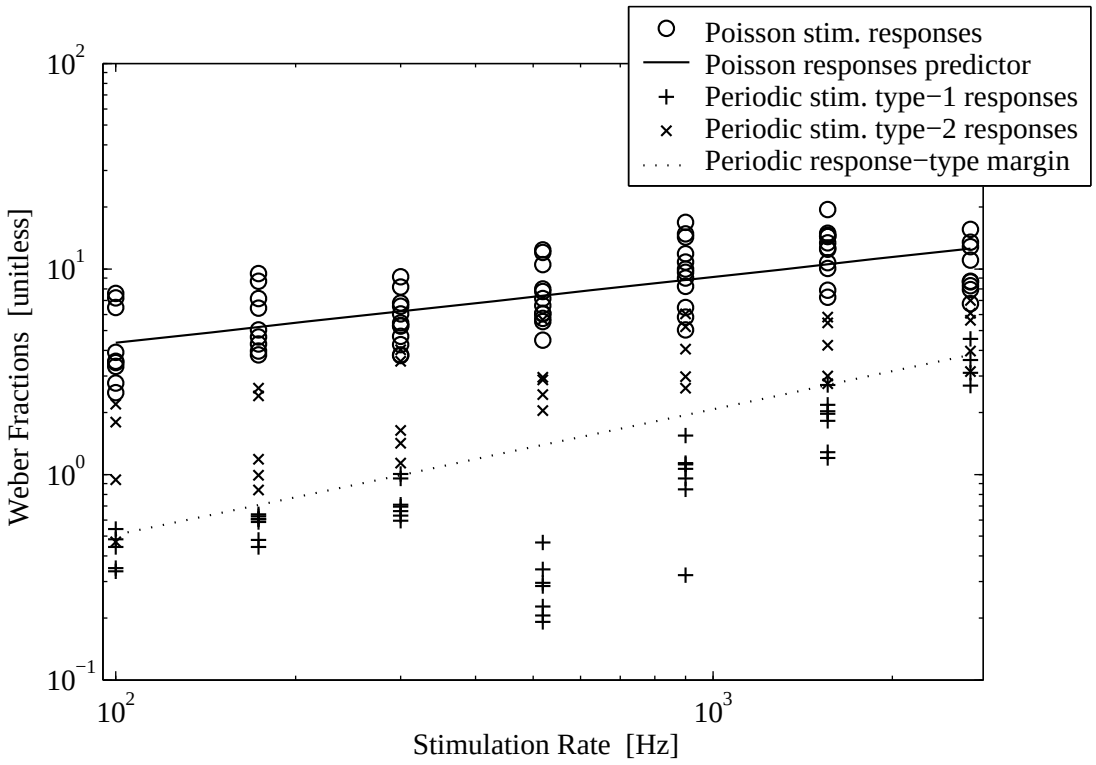

Figure 7.2: Calculated Weber fractions are shown for results of gap-detection-threshold experiments with all subjects, which were measured for constant-current stimuli. The Poisson response predictor corresponds with eq. 7.1, while the periodic response-type margin is that of eq. 7.11.

Weber's law of intensity discrimination states that the smallest perceivable loudness difference for a stimulus is proportional to the magnitude of that particular stimulus. For white noise, Weber's law is a relatively good approximation in the sense that the ratio of the smallest detectable intensity difference versus the intensity of the stimulus is approximately constant. A log-log plot of the difference-limen versus stimulus-intensity should give a slope of 1.0 for loudness perception if Weber's law were to hold. However, the *near miss* to

Weber's law reflects cases where the gradient is not unity, and this has been observed for narrow-band stimuli in loudness-discrimination experiments.

If an analogy to Weber's law were to hold for gap-detection experiments in electric hearing, it would state that the shortest detectable gap (i.e., change in the period) between successive stimulus pulses is inversely proportional to the rate of stimulation (i.e., directly proportional to the (average) period between successive pulses). For the "noisy" dead-time-modified Poisson stimuli, eq. 7.1 seems to approximate Weber's law as applied to gap detection. However, the slope of the line in fig. 7.1 is a bit further from unity than is the case for loudness experiments.

When it comes to periodic stimuli, Weber's law does not seem to apply for gap-detection experiments. In more than half of the periodic response-curves, the Weber fraction reaches a minimum somewhere around 520 Hz, which can clearly be seen in the bottom center of fig. 7.2. For higher stimulation rates around 2700 Hz, the Weber fractions become comparable for periodic and Poisson stimuli, and one can expect this tendency to continue at even higher rates.

The Weber fractions measured for the type-1 periodic responses correspond quite well with those by Abel (1972, table II), despite the fact that electrical constant-current gap-detection results are compared with acoustical equal-loudness gap-discrimination results and interpulse stimulation periods are traded for acoustic silence durations. For this comparison, consider electrical stimulation rates from 100 Hz to 1558.8 Hz and compare them with the range of silence durations from 10 ms down to 0.63 ms. In this range, the minimum and maximum Weber ratios from Abel (1972, table II) are 0.46 and 3.97, which were respectively located at 5 ms (i.e., a 200 Hz equivalent) and 0.63 ms (i.e., a 1600 Hz equivalent). Of the three acoustical marker conditions, all three maxima are found at the smallest silence duration, and two minima are found at 5 ms while the third one is located at 2.5 ms (i.e., a 400 Hz equivalent). The electrical stimulation type-1 responses for this range of rates have a minimum of 0.191 and maximum of 2.71 (at 519.6 Hz and 1558.8 Hz, respectively), which is very similar to the acoustical Weber-ratio range. Of these seven electrical response curves, all maxima are located at the highest rate of 1558.8 Hz. One curve has an absolute minimum at 900 Hz (only slightly lower than its factor at 100 Hz), five have absolute minima at 519.6 Hz, while the remaining curve has a local minimum at 519.6 Hz, although its absolute minimum is located at 100 Hz.

An interesting observation for the electrical stimulation is that the Weber fractions decrease again at very low rates (notice the lower left of fig. 7.2), though this trend is not seen in the acoustical results. This could possibly be related to differing loudness or spike entrainment for the various stimulation rates. With constant-current stimulation, the perceptual loudness tends to decrease as rate is decreased. Comparing the two acoustic marker conditions for 10 ms silence durations at different loudness (one at 85dB *sound pressure level* (SPL) and the other at 70dB), the softer marker always exhibits a larger Weber ratio for any of the silence durations. Logically, this is to be expected, since the psychophysical task is probably more difficult for softer sounds, and this should be reflected in larger Weber fractions. Since the Weber fractions for constant-current electrical type-1 responses always reach a local maximum around the 300 Hz mark, and then decreases again at lower rates, it is likely that the fading loudness-cue is more than compensated for by the increase in firing probability of neurons at these lower rates.

7.2.7 Comparing Notes

Overall, the gap-detection results from the present study indicate that longer thresholds are measured at lower stimulation rates, while smaller thresholds are measured at faster stimulation rates, though at very high rates the threshold may have an asymptote in the order of 2 ms. The threshold variations are much more pronounced when Poisson stimuli are used, and much less pronounced for periodic stimuli where gap thresholds are roughly of the same order of magnitude. However, in some cases for periodic stimuli, an absolute minimum (frequently below 1 ms) can be found in the region of 500 Hz.

This summary seems to contradict results for periodic stimulation from Busby and Clark (1999), who concluded that gap thresholds have no significant dependence on rate of stimulation. Unfortunately, the study by Busby and Clark only allowed integral multiples of the stimulation period to be presented to subjects, thus severely limiting exploration of the finer structure of the gap-threshold curves. Furthermore, these authors only sampled at three different stimulation rates, namely 200 Hz, 500 Hz and 1000 Hz, while the findings from the present study are based on more than double the number of sampled rates, spaced over a dynamic range also double that of this earlier study. The present study also averaged results over many repeats of the measurements, while Busby and Clark selected only one result per subject to reflect a specific stimulation rate. It further seems that most of the results of Busby and Clark are type-2 responses. Of the 15 subjects only subject S1 shows strong support for a type-1 response (subjects S2, S3 and S4 perhaps also fall into this category),

although the poor temporal resolution obscures the evidence. That is, based on their two-down one-up adaptive procedure and a step-size of 2 ms at 500 Hz, it would have been impossible to accurately measure the sub-millisecond gaps that have typically been found for type-1 responses in this region. Another interesting aspect of this comparison is that the measurements of Busby and Clark were for loudness-balanced bipolar stimulation, similar to the pilot study results shown in fig. 6.1, where the bipolar results show a rather constant trend over the center range of stimulation rates without the clear dip typically associated with type-1 responses (which have frequently been observed with monopolar stimuli).

7.3 GAP-DETECTION MODEL

7.3.1 Psychometric Curve Smoothness

As the theoretical principles of Green and Swets (1966) are applied to gap-detection experiments, the initial psychometric functions assembled for the model appear to be fundamentally non-monotonic, which was discussed at length in § 5.9. This attribute is a consequence of the very precise (perhaps overly theoretical) modeling of the PMF data that only looks at the statistics of the interval in the center of the stimulation sequence where the gap would be inserted; it might be more appropriate to incorporate statistics for multiple intervals near the center of the stimulation sequence to arrive at a model that could be more in line with the actual psychological decision-making process of the brain for this task. Nonetheless, a weighing function was then used to obtain psychometric curves that are smooth and would allow for simpler interpolation procedures to be used to estimate psychophysical gap-threshold measurements. The question remains whether the real psychometric functions are indeed jagged like the ones shown in fig. 5.2, or if the brain does, in effect, incorporate a smoothing function similar to the one incorporated into eq. 5.33. Even if a smoothing function should be used, the one suggested in eq. 5.35 may not be the most suitable or accurate function. A different weighing function might prove to be more appropriate, perhaps one modeled after the error function (i.e., the integral of the Gaussian distribution) or one involving the hyperbolic tangent, instead of a function having a sinusoidal transition phase. It may also be possible to leave the psychometric curves in the raw form (without smoothing) and use a smarter interpolation method to take the jumps in the psychometric functions into account when reading the threshold estimates from them. If one were to adopt the latter approach, it would also mean that standard 2AFC adaptive-staircase procedures cannot be used for experimental measurements (since

these rely on monotonic psychometric curves), but that one would need an appropriate measurement procedure that can take non-monotonic psychometric functions into account. The `ConstantStimuliExperiment` code class that has been implemented in the PSYCHOACOUSTICS TOOLBOX does allow for such an experiment configuration, but this is a much more inefficient mechanism for performing measurements. The results from the present study can be used as a baseline for comparisons of such further studies.

7.3.2 Simulations Discussed

The simulation curves shown in fig. 6.14 for the 1-up 3-down and 1-up 2-down staircase rules have almost identical shapes for the two staircase conditions and are almost just translated versions of each other with longer gaps found for the more difficult rule (i.e., for the 79.37% correct, 2AFC, 1-up 3-down rule). This seems to suggest that the structure of the gap-detection experiments is of less importance in determining the overall effect of the stimulus rate and kind of temporal structure on the gap thresholds. Whether one uses one staircase rule or another, or possibly introduces additional presentation-interval options (e.g., 3AFC), the overall shape of the results is not going to vary much. This is in line with Hartmann (2000, p. 556), who stated that for many studies "the thresholds *per se* are not particularly important" and that the "same information is learned about the effect of stimulus context", indicating that gap-detection experiments for electrical hearing might also fall into this category. A higher percentage-correct rule has been chosen for the present study, since this would also result in smaller variability in the measurements.

The high-rate (2700 pps) simulation results for the Poisson stimulation in fig. 6.14 range from 1.6 ms to 6.1 ms, similar to the range measured with experiments (between 2.5 ms and 5.8 ms, with the fitted value of 4.6 ms given by eq. 7.1). However, the experimental results provide no final answer to the question of whether a limiting value is reached at high frequencies, though such a limit may be expected, given that similar behavior is observed for the periodic experimental results, and also because dead-time-modified Poisson stimuli become similar to periodic stimuli as the rate increases.[8] Furthermore, the simulated results for the low-rate (100 pps) Poisson stimulation give somewhat smaller values that range from 15.1 ms to 16.2 ms, in contrast to the experiments' range of between 25.1 ms and 76.1 ms (and the fitted value of 43.7 ms from eq. 7.1). A remarkable similarity between the simulated and experimental results, however, is that the initial low-rate curve-shapes from the simulated results show straight lines that are highly consistent with the general trends of fig. 6.6.

[8] The two kinds of stimuli become indistinguishable at 4 kHz for the chosen dead-time period.

It may simply be that the turning point toward the asymptotic value for the experiments would be reached at a higher stimulation rate than the highest rate that has been measured, and that larger thresholds have been measured for Poisson stimuli below the rate at which the asymptotic trend would start. A possible explanation for this may be that "crackling sounding" Poisson stimuli and "smooth sounding" periodic stimuli are, in a perceptual sense, inherently different; if that is the case, the model would need to incorporate such a finding.

The model seems to predict periodic results better than Poisson results when comparing the absolute values (i.e., the magnitudes of the measured gap thresholds versus the magnitudes of the predicted gap thresholds) of the two different kinds of stimuli. This could be related to a concept discussed in § 7.3.1: in the model, PMFs are calculated only for the ISI in the center of the stimulation sequence. But the actual decision-making process of the brain might, in practice, be more complex, such that Poisson stimulation creates more confusion in higher functions of the brain than periodic stimulation does. It might be more difficult for the participant to focus on the center of the complete stimulation sequence in the case of Poisson stimuli. Periodic stimuli, by contrast, seems to elicit a smoother perception. Another plausible explanation for the longer experimental measurements of Poisson stimuli in comparison with simulated ones is that participants may be more easily confused by longer silence periods (sounding like gaps) that are located elsewhere in the Poisson sequence. A listener distracted by natural "gaps" located anywhere else in the interval sequence, characteristic of Poisson stimuli, may not locate the experimental gap in the center of that sequence. This may cause the subject to pick the wrong intervals more often, which would consequently increase the gap thresholds measured by the adaptive procedure.

When evaluating the simulation results for the periodic sequences, one notices that for individual neurons stimulated at a specific rate the periodic gap-thresholds are always[9] shorter than the Poisson thresholds. This is similar to what has been observed for results from experiments.

7.3.3 Periodic Stimuli Calculations

A number of insights may be gained from interpretations of the numerically calculated gap-detection-threshold results for periodic stimuli presented in § 6.3.2. ISI PMFs form a

[9] A very small number of data points on the high-rate side do not comply with this generalization, but this is likely to be a result of inaccuracies inherent to Monte Carlo simulations and should correct itself if the simulations were repeated over even more iterations.

foundation early in the sequence of phases of the developed gap-detection model; the good correspondence between simulation results and numerical calculations of model-neuron PMFs (shown in figures 6.11 and 6.12) suggests that the formulae used for numerical calculations of PMFs are indeed correct. The correlation between simulation and calculation results is further confirmed by a comparison between figures 6.14 and 6.15, which reflect the outcomes of the gap-detection model on the highest level. By using the much more efficient route of calculating the PMFs instead, it becomes easier to investigate the influence of various aspects on gap-detection-threshold perceptions involving periodic stimuli.

It was previously observed that in fig. 6.16, especially for Neurons C and D, the paralysis parameter describing the neural ARP is potentially linked to the response-type classification mechanism that has been formalized in eq. 7.11. The type-1 responses discussed in § 7.2.4 may correspond with neurons or neural regions that respond with high hazard probabilities to subsequent stimuli following a previous spike, mapping to a very small t_0 value in neuron models. Similarly, type-2 responses may correspond with larger values of t_0. Without regard to the specific shape of the threshold curves shown in fig. 6.16, a general observation about all model neurons is evident in that longer dead-time periods also correspond with longer gap-detection thresholds. This also makes intuitive sense; in general, where the brain should be able to detect temporal changes sooner if neurons respond more quickly and reliably to successive stimuli and do not filter out any event that could carry temporal information to the brain.

For the parameter values that were used to calculate its results, the gap-threshold curves of Neuron A, as shown in figures 6.16, 6.17 and 6.18, differ very little in shape. Given these various calculation results, this model neuron seems unlikely to be a good candidate to account for many of the variations observed in experimental results. Despite its initial promise as an analytically attractive formula, eq. 5.1, which underlies this neuron model, appears lacking in practical utility, even when biologically plausible values are assigned to its parameters.

As noted before, in fig. 6.19 the threshold curve for Neuron C with $\tau = 0.52\,\text{ms}$ presents two local minima around stimulation rates of 300 Hz and 650 Hz. The location of the latter minimum corresponds with Neuron C's rate-constant (i.e., with $a = 650\,\text{Hz}$), but the relatively small value of parameter τ appears to be the catalyst of the first minimum around 300 Hz. Neuron D (shown in this same figure) appears to exhibit two points of interest, the first around 450 Hz and the other near its $a = 650\,\text{Hz}$ stimulation-rate mark, although only

the first point is a clear local threshold minimum. For the very large values of τ shown in fig. 6.19, the threshold curves have a shape that reminds one distinctly of the simulation results obtained for Poisson stimuli, as shown in the left half of fig. 6.14, and similar to the experimental results for Poisson stimuli shown in fig. 6.5. The fuzziness of temporal resolution that is induced through Poisson stimuli may, therefore, have a psychophysical effect similar to that caused by large values for parameter τ, since gap thresholds for Poisson stimuli also tend to be much greater.

The dip in the threshold curves for Neurons C and D in fig. 6.16, becoming more prominent at smaller t_0 values, is located roughly between the 600 Hz and 700 Hz rates of stimulation. That is not a mere coincidence, probably, given that parameter $a = 650$ Hz. Furthermore, the curves for Neuron B do not exhibit this dip feature, which may again be related to the fact that parameter a is always set equal to the stimulation rate, q, for this neuron, such that the "dip" is always sliding along as the stimulation rate increases, leading to a new minimum value (i.e., a unique "dip") for each stimulation rate. This correlation between parameter a and the location of the dip (when evident) in the gap-threshold curve becomes even clearer when one looks at fig. 6.20. What is noteworthy about the curves shown in fig. 6.20 is that the separation point of each unique part of a threshold curve from the lower diagonal part that is shared between all curves, is always at the stimulation rate that equals the value of the rate-constant, a, for that specific curve. This is also the point at which the minimum gap-threshold occurs for each curve. The valuable consequence of this observation is that the rate parameter a can be obtained directly from gap-detection-threshold experiments using periodic stimuli when type-1 responses are evident. Another useful observation from fig. 6.20 is that, for small values of a, the asymptotic threshold values reached at high stimulation rates may be larger than the detectable gaps for the very low end of rates. Thus, higher stimulation rates do not necessarily imply relatively shorter gap thresholds for periodic stimuli.

Although the reasoning behind the specific choice of appropriate neuron models for the present study, including their parameter values, was examined in § 5.4, the study's focus has been the development of an overall statistical model for investigating a mathematical link between stimulus and perception. The determination of precisely which model neurons and what ranges of model parameter values would optimally describe experimental results is a matter for further investigation. However, even at this stage, it may be appropriate to contemplate the relevance of the chosen neuron models. As mentioned earlier in this section, Neuron A (based on eq. 5.1, using parameter values listed in table 5.2) does not appear to be a promising neuron model, although further investigations into appropriate

parameters for this neuron model may offer a different verdict. Neurons B, C and D (based on eq. 5.3, again using parameter values listed in table 5.2) show more promise in predicting the shapes of gap-detection curves for both periodic and Poisson experiments. The choice of model parameters for Neuron B appears to result in gap-threshold curves that match the shapes observed for Poisson and type-2 periodic responses, while Neurons C and D appear to be more suitable for predicting type-1 periodic responses. Despite the slightly differing shapes of response curves for Poisson stimuli predicted by Neurons C and D, the larger gap-thresholds measured through Poisson experiments may be masking the details of the curves at lower gap-thresholds predicted through modeling (a condition that perhaps also exists for Neuron B).[10] In summary, then, Neurons B, C and D may be appropriate models for both periodic and Poisson responses, and eq. 5.3 may be applicable to different stimuli in general. To match experimental results, the specific parameters to be selected for a model neuron can uniquely be determined for a particular implant user at each cochlear stimulation site. Such a custom set of optimal parameter values will then simply reflect the result of collective responses from surviving neurons in a region of a specific cochlea.

In closing, this chapter discussed the present study's experimental and simulation work, incorporating findings from others' research. Answers to the specific research questions of the present research can now be provided in the next chapter.

[10] The smaller gap-threshold predictions could perhaps be the lower envelope of responses that may be measured for a "star" subject (e.g., after much exposure and dedicated training with this specific kind of stimulus).

CHAPTER 8

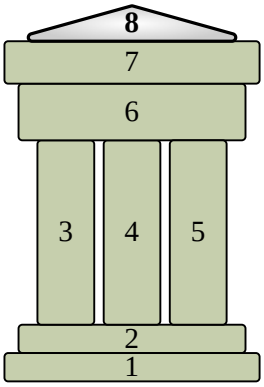

CONCLUSION

This last chapter reviews some of the key findings of the study and formalizes answers to the research questions identified in chapter 1. Directions for future research are also proposed.

8.1 IN REVIEW

The approach taken for the present study was largely an engineering one, incorporating practical aspects through experimentation and theoretical aspects through mathematics and modeling (the latter involving both simulations and numerical calculations). Psychoacoustics research software was also developed, and the combination of the software, experiments and modeling allowed for an investigation examining perception of temporal aspects in electric hearing through gap detection. Through this process, the objectives set out at the beginning of this document (see § 1.4) have been achieved.

8.1.1 Discussion of Research Questions

In response to the specific questions formulated at the end of § 1.2, it is now possible to provide definitive answers. This study provides substantive evidence to suggest that the link between stimulus and perception, as it pertains to temporal gap detection in electric hearing, is one that can be understood through statistics of ISI data as captured from auditory neurons. Using this argument as the basis for a theoretical model, it was possible to formulate each step in a psychophysical process, from the point of external stimulus presentation to the point of measured gap-thresholds as perceived internally by a participant, using sound mathematical constructs, as documented in chapter 5. As far as the degree to which mathematical predictions agree with experimental measurements is concerned, for both Poisson and periodic stimuli, the trends of gap-threshold predictions (as a function of stimulation rate) appear to be in good correlation with each other. The main features of experimental curves, which depend on the choice of assigned parameter values for the model, can be recognized in simulated and calculated modeling results. Although actual gap-threshold values measured experimentally for Poisson stimuli are typically all larger than the predicted values from the model, much stronger agreement is found between experimental values and modeled values for periodic stimuli. An explanation was also put forth in § 7.3.2 of how a participant might be distracted from the main task of the experiment for Poisson stimuli and why larger values are measured in experiments (based on the presence of more intervals elsewhere in the Poisson sequence that may sound like gaps). However, in the case of either larger experimental results or smaller simulation results, the shape of the gap-threshold curves will be much the same.

8.1.2 Summary of Main Findings

The primary findings of the present study are highlighted below.

- Based on duration-discrimination results, temporal roving may not be required for gap-detection experiments.

- Gap-detection thresholds appear to be insensitive to the mode of stimulation (at least in the case of the monopolar and bipolar modes that were investigated).

- For clearly audible stimuli, loudness balancing may not be required for gap-detection experiments. The added benefit of using constant current for stimulation at different

rates is that results from gap-detection modeling and experiments can be compared more directly without the need to incorporate the effects of loudness balancing.

- The place of stimulation (e.g., basal, central or apical) does not appear to significantly affect the types of gap-detection-threshold curves that present themselves.[1]

- As a function of rate, the gap thresholds for Poisson stimuli show a clear pattern that can be fitted with a linear curve (when both abscissa and ordinate are plotted on logarithmic scales). As the stimulation rate increases, gap thresholds decrease.

- Gap thresholds are larger for Poisson stimuli than for periodic stimuli.

- For gap thresholds that are measured in response to periodic stimuli, two different types of response curves appear to present themselves. Those of the first type (i.e., type-1 response curves) exhibit the smallest thresholds, which are typically measured for stimulation rates on the order of 520 Hz. Type-2 response curves have a shape similar to those of Poisson stimuli, although the actual measured thresholds are smaller.

- Generally, Weber fractions for gap detection increase as the stimulation rate is increased. They deviate from this general trend, however, for type-1 periodic responses in the central region of the range of stimulation rates explored in this study; there, the smallest Weber fractions are observed.

- Sub-millisecond gap thresholds are not uncommon for periodic stimuli and are typically observed in the center of the range of stimulation rates explored in this study.

- When different model parameters are varied for the neurons based on eq. 5.3, predicted gap-threshold response curves show shapes similar to those exhibited by experimental results.

- A formalist approach to the calculation of psychometric curves, based on ISI statistics of gap-containing intervals, results in psychometric functions that are not monotonic for periodic stimuli. This may indicate that psychometric curves for gap detection involving periodic stimuli are indeed non-monotonic or that the calculations need to

[1] This is the case for Poisson stimuli especially, although a similar observation may also apply to periodic stimuli (see § 7.2.5 for details).

be approached more broadly (e.g., through the use of psychometric-curve smoothing, as in the present study).

8.1.3 Gap Thresholds Compared

Gap thresholds are measurably dependent upon the rate of stimulation, results presented in this document suggest. That outcome appears to contradict Busby and Clark (1999), who found no significant dependency; but the resolution and range of their experiments may have led Busby and Clark to their conclusion, § 7.2.7 argues. Although the dependency between gap thresholds and stimulation rates might not be significant over a narrow range for some very specific stimuli, the thresholds can vary quite drastically for other kinds of stimuli, such as Poisson sequences, and even smaller variations for periodic stimuli can have a significant interpretation: for example, the dip of a type-1 response appears to correspond directly with one of the model parameters, which can consequently be obtained directly from experimental measurements. The finding that gap-threshold measurements do vary for different stimulation rates appears to be in line with experimental results of Dobie and Dillier (1985) and van Wieringen and Wouters (1999), as noted in § 2.2.

8.1.4 Contribution

In summary, the following aspects may be seen as the main contributions of the present study to the field of research:

- The PSYCHOACOUSTICS TOOLBOX was developed as a software suite for constructing psychophysical experiments in MATLAB. The software, by allowing the researcher to focus less on writing code and more on actual experiments and interpretation of results, can enhance research productivity.

- Extensive within-channel gap-detection experiments involving electric hearing were performed; numerous parameter combinations were investigated at high resolution.

- It was found that gap-detection thresholds are not constant as a function of stimulus rate, and that thresholds are also a function of stimulation pattern (e.g., when contrasting periodic and Poisson stimuli).

- A psychophysical model (in contrast with a phenomenological one), based on neural ISI statistics, was developed for investigating within-channel gap-detection by cochlear implant users.

- An apparent statistical link was found between stimulus and perception for temporal aspects of electric hearing, which may indicate that a similar link exists for normal hearing or temporal perception in general.

In the end, positive answers have been found for the specific questions addressed through this study. Encouraging progress has also been made toward addressing larger questions concerning the consequences of highly synchronized neural firing patterns. These patterns may be better understood if their temporal aspects can be grasped. The approach taken, in this case, was to explore the statistical properties of ISI data. The present study clearly highlights, through experiments and modeling, that the temporally synchronized nature of periodic stimuli gives rise to much better temporal resolution than if the same temporal data (in this case the presence of a gap) were encoded in a Poisson signal that is temporally less synchronous.

8.2 FUTURE WORK

The research reflected in this document may be expanded upon in various ways. The possibility that the psychometric function is not monotonic was discussed in § 5.8 and 7.3.1. A conclusive answer to this open question could be very informative, possibly leading to new ways of researching gap-detection phenomena. Also, as suggested in § 7.3.1, further research should address whether the smoothing of psychometric curves in modeling is necessary and, if it is, whether the weighing function should be revised.

A rather simplified approach was taken in § 5.4 to model the neuron behavior, though the approach resembles the hazard function of real neurons quite closely. The model does, however, allow for more complex neuron models to be incorporated, though one might then again have to resort to simulations and would perhaps not be able to use the more efficient numerical calculation approach.

Nonetheless, neuron models can then incorporate more advanced features, including: the possibility to model stimuli with varying electrical current or pulse width; additional paralyzation effects for high-rate stimuli; differences based on the spatial axis of the cochlea,

such as neural CF; or approaches based on a Hodgkin-Huxley neuron model, or even neuron models from Bruce, White, Irlicht, O'Leary, Dynes, Javel and Clark (1999) and Bruce, Irlicht, White, O'Leary, Dynes, Javel and Clark (1999). The overall structure of the gap-detection model would remain the same as described in chapter 5, even if more complex neural filtering mechanisms are used.

On the experimental front, the procedures performed by Busby and Clark (1999) could potentially be performed with the same subjects that took part in the present study to determine more precisely the effect of using a worse resolution (i.e., integer periods only) for changes in gap duration. A comparison between results would then be possible.

When investigating temporal aspects of hearing at relatively low frequencies, where perceptual cues can potentially be encoded by rate information of neural spikes (such as statistical ISI properties of the entrained fine temporal structure of spikes), it may be possible to draw comparisons between acoustic and electric hearing. This might be achieved by using acoustical click sounds that are band-pass filtered (in the higher audio frequency range) to resemble electrical stimulation pulses. Carlyon et al. (2002) found comparable results for electric and acoustic equivalents in pitch-matching experiments they performed. Thus, results from equivalent acoustical experiments can potentially be used to make comparisons with results obtained through the present study. For example, purely acoustical research results, such as those obtained by Pressnitzer et al. (2004) (who found that perceptual pitch-matching experiments cannot be explained using simple average-rate, power spectrum, or waveform autocorrelation mechanisms), can later be incorporated to enhance the models and to design future experiments that could use the present research as a basis.

As another avenue for exploration, it may be possible to derive the analytic equations needed for numerical calculations of Poisson-type stimuli (instead of needing to revert to simulations). However, judging from experimental results, the shapes of the Poisson curves are not likely to change very much for various parameter values. Thus, if the model is an accurate one, the value gained from such an exercise may be limited. On the other hand, with such analytic equations at one's disposal, it may be possible to devise an alternative processing strategy that would use Poisson-type stimuli instead of the synchronized patterns that are currently used in cochlear implants. It may also be possible for additional neural parameter data to be mined for a specific stimulation site if both the periodic and Poisson gap-detection thresholds are known, but further investigations would need to be performed to determine whether there would always be a deterministic relation between Poisson and

periodic responses. If it turns out that additional neural-parameter information is locked up in the gap-detection responses for Poisson stimuli, it may be possible to incorporate these parameters into the optimized processor strategies for individual stimulation sites.

Regarding the differences between stimulation sites, as observed in § 7.2.5, more experimental data should be gathered to determine with greater certainty whether the kind of stimulus, particularly in the case of periodic stimuli, could have an influence on gap-detection performance for various electrode positions. (This could resolve a question raised earlier: Would the apical region generally produce smaller gap thresholds, or are type-1 and sub-millisecond responses also abundant in the basal regions?)

Temporal experiments by Hant et al. (1997), which involved masked thresholds of voiceless plosive bursts in background noise, showed threshold-versus-duration results with shapes similar to those reported for temporal gap thresholds from the present study. In Hant et al.'s results, an optimal duration also seems to be present in some circumstances. It may be interesting to compare those experimental results with modeling results from an adaptation of the present gap-detection model. This may provide insights into understanding how the temporal gap-detection results presented here can be applied practically to the improvement of speech-processing algorithms, which can use the high temporal resolution observed for periodic stimuli to encode the short plosive sounds of speech more efficiently.

The model developed for this research could, with a few modifications, be applied to the setup of Chatterjee et al. (1998, experiment 3), in which different rates were used for bounding markers of within-channel gap-detection tasks. Such a modeling exercise may prove to be very informative, since it would show how accurately gap thresholds can be predicted using only stochastic timing information. The experimental results of Chatterjee et al. showed that threshold gaps are generally longer for larger differences in rate between the markers, although the minimum did not always correspond with the point of equal rates; the authors attributed the latter to poor pitch judgment among prosthesis users. Furthermore, van Wieringen and Wouters (1999) argued that this experimental data may "not reflect the temporal resolution of the auditory system, but rather serve as a measure of the perceived difference between the two markers". However, from an understanding of the ISI mechanisms of the present model, it is believed that the developed model should predict the general trends of Chatterjee et al.'s experimental results correctly and show that temporal aspects can account for the observations (at least to some extent). It is also plausible that the model would show curve minima at locations that would have a preference for higher-rate

rather than equal-rate markers, similar to the results of Chatterjee et al., because a higher-rate marker on either side of the gap would result in a higher probability (from a hazard-rate perspective) for either of the spikes that would enclose the gap. Thus, a smaller ISI would result than if equal-rate markers were to bind the gap. It would then also not be surprising that none[2] of the minima displayed in Chatterjee et al. (1998, fig. 3) showed up on the side of rates slower than the fixed-rate marker.

8.3 CONCLUDING STATEMENT

The exact way in which the brain combines temporal and place (i.e., stimulation site) information from the cochlea is not well understood. More research needs to be done with a fundamental psychoacoustics perspective in mind.

As mentioned in § 1.2, it is believed that performance in electric hearing can still be improved by personalizing processing strategies using algorithms that would take into account an individual's psychophysical parameters, to the extent that the generation of neural responses can be controlled with almost 100% statistical certainty with granularity of even individual spikes. To realize this feat, one would need to have (among other requirements) very accurate models of the behavior of individual stimulation sites for each specific subject. The model developed for the present study is based on statistical hazard functions that can incorporate neural parameters. The model was used to determine whether a logical connection can be made between such psychophysically plausible models and perceptions of subjects that can be measured with gap-detection thresholds. The approach used in this research has demonstrated that psychophysical measurements of experiments can be predicted using a statistical model. Indeed, a very simple (yet realistic) neuron model based on eq. 5.3, which describes a neural hazard function, can account for many features of gap-threshold curves.

This study has shed more light on some fascinating aspects of hearing perception. It is hoped that similar research will be conducted to allow for highly customized algorithms that utilize individual neural parameters, which can be measured accurately for specific stimulation models. Electric hearing and, specifically, its perceptual aspects, should now be taken to the next stage.

[2]Granted, one of the nine minima is an exception to this rule, if one accepts the mean measured values as absolutely correct. But if one takes the variances of the measurements into account, the sole exception can be eliminated.

References

Abel, S. M. (1972), 'Discrimination of temporal gaps', *Journal of the Acoustical Society of America* **52**(2), 519–524.

Adrian, E. D. (1926), 'The impulses produced by sensory nerve endings. Part I', *Journal of Physiology* **61**(1), 49–72.

Allen, J. B. and Sondhi, M. M. (1979), 'Cochlear macromechanics: Time domain solutions', *Journal of the Acoustical Society of America* **66**(1), 123–132.

Balkany, T., Hodges, A., Menapace, C., Hazard, L., Driscoll, C., Gantz, B., Kelsall, D., Luxford, W., McMenomy, S., Neely, J. G., Peters, B., Pillsbury, H., Roberson, J., Schramm, D., Telian, S., Waltzman, S., Westerberg, B., and Payne, S. (2007), 'Nucleus Freedom North American clinical trial', *Otolaryngology – Head and Neck Surgery* **136**(5), 757–762.

Barlow, H. B. (1995), The neuron doctrine in perception, *in* M. S. Gazzaniga, ed., 'The Cognitive Neurosciences', MIT Press, Cambridge, Massachusetts, chapter 26, pp. 415–435.

Barlow, R. E., Marshall, A. W. and Proschan, F. (1963), 'Properties of probability distributions with monotone hazard rate', *Annals of Mathematical Statistics* **34**(2), 375–389.

Blume, S. S. (1997), 'The rhetoric and counter-rhetoric of a "bionic" technology', *Science, Technology and Human Values* **22**(1), 31–56.

Box, D. (1997), *Essential COM*, Addison-Wesley, Upper Saddle River, New Jersey.

Bracquemond, C. and Gaudoin, O. (2003), 'A survey on discrete lifetime distributions', *International Journal of Reliability, Quality and Safety Engineering* **10**(1), 69–98.

Bruce, I. C. (1997), Spatiotemporal Coding of Sound in the Auditory Nerve for Cochlear Implants, PhD thesis, University of Melbourne, Melbourne, Australia.

Bruce, I. C., Irlicht, L. S., White, M. W., O'Leary, S. J., Dynes, S., Javel, E. and Clark, G. M. (1999), 'A stochastic model of the electrically stimulated auditory nerve: Pulse-train response', *IEEE Transactions on Biomedical Engineering* **46**(6), 630–637.

Bruce, I. C., White, M. W., Irlicht, L. S., O'Leary, S. J., Dynes, S., Javel, E. and Clark, G. M. (1999), 'A stochastic model of the electrically stimulated auditory nerve: Single-pulse response', *IEEE Transactions on Biomedical Engineering* **46**(6), 617–629.

Büchner, A., Frohne-Büchner, C., Battmer, R. D. and Lenarz, T. (2004), 'Two years of experience using stimulation rates between 800 and 5000 pps with the Clarion CII implant', *International Congress Series* **1273**, 48–51.

Busby, P. A. and Clark, G. M. (1999), 'Gap detection by early-deafened cochlear-implant subjects', *Journal of the Acoustical Society of America* **105**(3), 1841–1852.

Carlyon, R. P., van Wieringen, A., Long, C. J., Deeks, J. M. and Wouters, J. (2002), 'Temporal pitch mechanisms in acoustic and electric hearing', *Journal of the Acoustical Society of America* **112**(2), 621–633.

Chatterjee, M., Fu, Q.-J. and Shannon, R. V. (1998), 'Within-channel gap detection using dissimilar markers in cochlear implant listeners', *Journal of the Acoustical Society of America* **103**(5), 2515–2519.

Clark, G. M. (1996), 'Electrical stimulation of the auditory nerve: The coding of frequency, the perception of pitch and the development of cochlear implant speech processing strategies for profoundly deaf people', *Clinical and Experimental Pharmacology and Physiology* **23**(9), 766–776.

Clark, G. M., Cowan, R. S. C. and Dowell, R. C., eds (1997), *Cochlear Implantation for Infants and Children: Advances*, Singular Publishing Group, Inc., San Diego.

Colburn, H. S. (1973), 'Theory of binaural interaction based on auditory nerve data. I. General strategy and preliminary results on interaural discrimination', *Journal of the Acoustical Society of America* **54**(6), 1458–1470.

Collins, L. M., Miller, R. L. and Ferguson, W. D. (2000), On the relationship between noise and speech recognition in cochlear implant subjects: A theoretical and psychophysical study, *in* 'DSP for the Hearing Impaired', IEEE, Waldemar Ranch Resort, Hunt, Texas.

Collins, L. M., Zwolan, T. A. and Wakefield, G. H. (1997), 'Comparison of electrode discrimination, pitch ranking, and pitch scaling data in postlingually deafened adult cochlear implant subjects', *Journal of the Acoustical Society of America* **101**(1), 440–455.

Cox, D. R. (1962), *Renewal Theory*, Methuen, London.

Cox, D. R. and Isham, V. (1980), *Point Processes*, Chapman and Hall, London.

Czajko, J. (2004), 'On Cantorian spacetime over number systems with division by zero', *Chaos, Solitons and Fractals* **21**(2), 261–271.

Devroye, L. (1986), *Non-Uniform Random Variate Generation*, Springer-Verlag, New York.

Dingemanse, J. G., Frijns, J. H. M. and Briaire, J. J. (2006), 'Psychophysical assessment of spatial spread of excitation in electrical hearing with single and dual electrode contact maskers', *Ear and Hearing* **27**(6), 645–657.

Djourno, A., Eyries, C. and Vallancien, B. (1957), 'De l'excitation électrique du nerf cochléaire chez l'homme, par induction à distance, à l'aide d'un micro-bobinage inclus à demeure', *Presse Medicale* **65**(26), 612.

Dobie, R. A. and Dillier, N. (1985), 'Some aspects of temporal coding for single-channel electrical stimulation of the cochlea', *Hearing Research* **18**(1), 41–55.

Donaldson, G. S., Kreft, H. A. and Litvak, L. (2005), 'Place-pitch discrimination of single- versus dual-electrode stimuli by cochlear implant users (L)', *Journal of the Acoustical Society of America* **118**(2), 623–626.

Doob, J. L. (1948), 'Renewal theory from the point of view of the theory of probability', *Transactions of the American Mathematical Society* **63**(3), 422–438.

Eliasmith, C. and Anderson, C. H. (2003), *Neural Engineering*, The MIT Press, Cambridge, Massachusetts.

Florentine, M., Buus, S. and Geng, W. (1999), 'Psychometric functions for gap detection in a yes-no procedure', *Journal of the Acoustical Society of America* **106**(6), 3512–3520.

Florentine, M., Buus, S. and Robinson, M. (1998), 'Temporal integration of loudness under partial masking', *Journal of the Acoustical Society of America* **104**(2 I), 999–1007.

Frijns, J. H. M., Briaire, J. J., de Laat, J. A. P. M. and Grote, J. J. (2002), 'Initial evaluation of the Clarion CII cochlear implant: speech perception and neural response imaging', *Ear and Hearing* **23**(3), 184–197.

Gallager, R. G. (1996), *Discrete Stochastic Processes*, Kluwer Academic Publishers, Boston, Massachusetts.

Gaumond, R. P., Molnar, C. E. and Kim, D. O. (1982), 'Stimulus and recovery dependence of cat cochlear nerve fiber spike discharge probability', *Journal of Neurophysiology* **48**(3), 856–873.

Gerstein, G. L. and Kiang, N. Y. (1960), 'An approach to the quantitative analysis of electrophysiological data from single neurons', *Biophysical Journal* **1**, 15–28.

Geurts, L. and Wouters, J. (2000), 'A concept for a research tool for experiments with cochlear implant users', *Journal of the Acoustical Society of America* **108**(6), 2949–2956.

Gray, P. R. (1967), 'Conditional probability analyses of the spike activity of single neurons', *Biophysical Journal* **7**(6), 759–777.

Green, D. M. and Forrest, T. G. (1989), 'Temporal gaps in noise and sinusoids', *Journal of the Acoustical Society of America* **86**(3), 961–970.

Green, D. M. and Swets, J. A. (1966), *Signal Detection Theory and Psychophysics*, John Wiley and Sons, Inc., New York.

Grimshaw, S. D., McDonald, J., McQueen, G. R. and Thorley, S. (2005), 'Estimating hazard functions for discrete lifetimes', *Communications in Statistics: Simulation and Computation* **34**(2), 451–463.

Guilford, J. P. (1954), *Psychometric Methods*, McGraw-Hill, New York.

Han, S. K., Kim, W. S. and Kook, H. (2002), 'Synchronization and decoding interspike intervals', *International Journal of Bifurcation and Chaos in Applied Sciences and Engineering* **12**(5), 983–999.

Hanekom, J. J. (2001), Models and Psychophysics of Acoustic and Electric Hearing, PhD thesis, University of Pretoria, Pretoria, South Africa.

Hanekom, J. J. and Shannon, R. V. (1998), 'Gap detection as a measure of electrode interaction in cochlear implants', *Journal of the Acoustical Society of America* **104**(4), 2372–2384.

Hant, J. J., Strope, B. P. and Alwan, A. A. (1997), 'A psychoacoustic model for the noise masking of plosive bursts', *Journal of the Acoustical Society of America* **101**(5), 2789–2802.

Hart, J. M. (2004), *Windows System Programming*, third edn, Addison-Wesley, Upper Saddle River, New Jersey.

Hartmann, W. M. (2000), *Signals, Sound, and Sensation*, Springer, New York.

He, N.-J., Horwitz, A. R., Dubno, J. R., and Mills, J. H. (1999), 'Psychometric functions for gap detection in noise measured from young and aged subjects', *Journal of the Acoustical Society of America* **106**(2), 966–978.

Herz, A. V. M., Gollisch, T., Machens, C. K. and Jaeger, D. (2006), 'Modeling single-neuron dynamics and computations: A balance of detail and abstraction', *Science* **314**(5796), 80–85.

Hill, A. V. (1936), 'Excitation and accommodation in nerve', *Proceedings of the Royal Society of London. Series B, Biological Sciences* **119**(814), 305–355.

Hirsh, I. J. (1959), 'Auditory perception of temporal order', *Journal of the Acoustical Society of America* **31**, 759–767.

Hodgkin, A. L. and Huxley, A. F. (1952), 'A quantitative description of membrane current and its application to conduction and excitation in nerve', *Journal of Physiology* **117**(4), 500–544.

Hong, R. S. and Rubinstein, J. T. (2003), 'High-rate conditioning pulse trains in cochlear implants: dynamic range measures with sinusoidal stimuli', *Journal of the Acoustical Society of America* **114**(6), 3327–3342.

Hong, R. S. and Rubinstein, J. T. (2006), 'Conditioning pulse trains in cochlear implants: effects on loudness growth', *Otology and Neurotology* **27**(1), 50–56.

Huettel, L. G. and Collins, L. M. (2004), 'Predicting auditory tone-in-noise detection performance: The effects of neural variability', *IEEE Transactions on Biomedical Engineering* **51**(2), 282–293.

Irlicht, L. S. and Clark, G. M. (1996), 'Control strategies for neurons modeled by self-exciting point processes', *Journal of the Acoustical Society of America* **100**(5), 3237–3247.

Irwin, C. (about 2002*a*), *Nucleus Implant Communicator C-Interface Language Reference*, Cochlear Limited. Document number N94386F.

Irwin, C. (about 2002*b*), *Nucleus Implant Communicator Software User Manual*, Cochlear Limited. Document number N94462F.

Irwin, R. J. and Kemp, S. (1976), 'Temporal summation and decay in hearing', *Journal of*

the Acoustical Society of America **59**(4), 920–925.

Jansen, M. (2007), 'Multiscale change point analysis in Poisson count data', *Chemometrics and Intelligent Laboratory Systems* **85**(2), 159–169.

Javel, E. (1986), Basic response properties of auditory nerve fibers, *in* R. A. Altschuler, R. P. Bobbin and D. W. Hoffman, eds, 'Neurobiology of Hearing: The Cochlea', Raven Press, New York, pp. 213–245.

Javel, E. and Shepherd, R. K. (2000), 'Electrical stimulation of the auditory nerve: III. Response initiation sites and temporal fine structure', *Hearing Research* **140**(1-2), 45–76.

Jesteadt, W. (1980), 'An adaptive procedure for subjective judgments', *Perception and Psychophysics* **28**(1), 85–88.

Johnson, D. H. (1996), 'Point process models of single-neuron discharges', *Journal of Computational Neuroscience* **3**(4), 275–299.

Johnson, D. H. and Swami, A. (1983), 'The transmission of signals by auditory-nerve fiber discharge patterns', *Journal of the Acoustical Society of America* **74**(2), 493–501.

Kay, S. M. (1998), *Fundamentals of Statistical Signal Processing. Volume 2. Detection Theory*, Prentice Hall, Upper Saddle River, New Jersey.

Klein, S. A. (2001), 'Measuring, estimating, and understanding the psychometric function: A commentary', *Perception and Psychophysics* **63**(8), 1421–1455.

Laneau, J., Boets, B., Moonen, M., van Wieringen, A. and Wouters, J. (2005), 'A flexible auditory research platform using acoustic or electric stimuli for adults and young children', *Journal of Neuroscience Methods* **142**(1), 131–136.

Levitt, H. (1971), 'Transformed up-down methods in psychoacoustics', *Journal of the Acoustical Society of America* **49**(2), 467–477.

Li, J. and Young, E. D. (1993), 'Discharge-rate dependence of refractory behavior of cat auditory-nerve fibers', *Hearing Research* **69**(1-2), 151–162.

Litvak, L. M., Delgutte, B. and Eddington, D. K. (2001), 'Auditory nerve fiber responses to electric stimulation: Modulated and unmodulated pulse trains', *Journal of the Acoustical Society of America* **110**(1), 368–379.

Litvak, L. M., Smith, Z. M., Delgutte, B. and Eddington, D. K. (2003), 'Desynchronization

of electrically-evoked auditory-nerve activity by high-frequency pulse trains of long duration', *Journal of the Acoustical Society of America* **114**(4-1), 2066–2078.

Loizou, P. C. (1998), 'Mimicking the human ear', *IEEE Signal Processing Magazine* **15**(5), 101–130.

Loizou, P. C. (1999), 'Signal-processing techniques for cochlear implants', *IEEE Engineering In Medicine And Biology Magazine* **18**(3), 34–46.

Macherey, O., Carlyon, R. P., van Wieringen, A. and Wouters, J. (2007), 'A dual-process integrator-resonator model of the electrically stimulated human auditory nerve', *Journal of the Association for Research in Otolaryngology* **8**(1), 84–104.

Magrab, E. B., Azarm, S., Balachandran, B., Duncan, J., Herold, K. and Walsh, G. (2000), *An Engineer's Guide to MATLAB*, Prentice Hall, New York.

Marchal, B. (2001), *XML by Example*, second edn, Que Publishing, Indianapolis, Indiana.

McCulloch, W. S. and Pitts, W. (1943), 'A logical calculus of the ideas immanent in nervous activity', *Bulletin of Mathematical Biology* **5**(4), 115–133.

McKay, C. M., McDermott, H. J. and Carlyon, R. P. (2000), 'Place and temporal cues in pitch perception: Are they truly independent?', *Acoustics Research Letters Online* **1**(1), 25–30.

Merrill, D. R., Bikson, M. and Jefferys, J. G. R. (2005), 'Electrical stimulation of excitable tissue: design of efficacious and safe protocols', *Journal of Neuroscience Methods* **141**(2), 171–198.

Metropolis, N. and Ulam, S. (1949), 'The Monte Carlo method', *Journal of the American Statistical Association* **44**(247), 335–341.

Meyn, S. P. and Tweedie, R. L. (1993), *Markov Chains and Stochastic Stability*, Springer-Verlag, London.

Miller, T. (2003), *Managed DirectX 9: Graphics and Game Programming*, SAMS Publishing, Indianapolis, Indiana.

Molnar, C. E. and Pfeiffer, R. R. (1968), 'Interpretation of spontaneous spike discharge patterns of neurons in the cochlear nucleus', *Proceedings of the IEEE* **56**(6), 993–1004.

Moore, B. C. J. (2003), *An Introduction to the Psychology of Hearing*, fourth edn, Academic Press, London.

Moore, B. C. J., Glasberg, B. R., Donaldson, E., McPherson, T. and Plack, C. J. (1989), 'Detection of temporal gaps in sinusoids by normally hearing and hearing-impaired subjects', *Journal of the Acoustical Society of America* **85**(3), 1266–1275.

Moore, B. C. J., Glasberg, B. R., Flanagan, H. J. and Adams, J. (2006), 'Frequency discrimination of complex tones; assessing the role of component resolvability and temporal fine structure', *Journal of the Acoustical Society of America* **119**(1), 480–490.

Morse, R. P. and Evans, E. F. (1996), 'Enhancement of vowel coding for cochlear implants by addition of noise', *Nature Medicine* **2**(8), 928–932.

Morse, R. P. and Evans, E. F. (1999), 'Additive noise can enhance temporal coding in a computational model of analogue cochlear implant stimulation', *Hearing Research* **133**(1-2), 107–119.

Morse, R. P. and Meyer, G. F. (2000), 'The practical use of noise to improve speech coding by analogue cochlear implants', *Chaos, Solitons and Fractals* **11**(12), 1885–1894.

Morse, R. P., Morse, P. F., Nunn, T. B., Archer, K. A. M. and Boyle, P. (2007), 'The effect of Gaussian noise on the threshold, dynamic range, and loudness of analogue cochlear implant stimuli', *Journal of the Association for Research in Otolaryngology* **8**(1), 42–53.

Mudry, A. (2007), 'References in the history of otology: the importance of being earnest', *Ear and Hearing* **28**(1), 135–140.

Nathan, A. (2002), *.NET and COM: The Complete Interoperability Guide*, SAMS Publishing, Indianapolis, Indiana.

Neyman, J. and Pearson, E. S. (1933), 'On the problem of the most efficient tests of statistical hypotheses', *Philosophical Transactions of the Royal Society of London. Series A, Containing Papers of a Mathematical or Physical Character* **231**, 289–337.

Niparko, J. K. and Wilson, B. S. (2000), History of cochlear implants, *in* J. K. Niparko, K. I. Kirk, N. K. Mellon, A. McConkey Robbins, D. L. Tucci and B. S. Wilson, eds, 'Cochlear Implants: Principles and Practices', Lippincott Williams & Wilkins, Philadelphia, Pennsylvania, pp. 103–108.

Olkin, I., Gleser, L. J. and Derman, C. (1994), *Probability Models and Applications*, second edn, Prentice-Hall, Englewood Cliffs, New Jersey.

Papoulis, A. (1965), *Probability, Random Variables, and Stochastic Processes*, McGraw-Hill, New York.

Parker, A. J. and Newsome, W. T. (1998), 'Sense and the single neuron: Probing the physiology of perception', *Annual Review of Neuroscience* **21**, 227–277.

Perkel, D. H., Gerstein, G. L. and Moore, G. P. (1967), 'Neuronal spike trains and stochastic point processes. I. The single spike train', *Biophysical Journal* **7**(4), 391–418.

Plant, K., Holden, L., Skinner, M., Arcaroli, J., Whitford, L., Law, M.-A. and Nel, E. (2007), 'Clinical evaluation of higher stimulation rates in the Nucleus Research Platform 8 system', *Ear and Hearing* **28**(3), 381–393.

Plomp, R. and Bouman, M. A. (1959), 'Relation between hearing threshold and duration for tone pulses', *Journal of the Acoustical Society of America* **31**(6), 749–758.

Plonsey, R. and Barr, R. C. (2000), *Bioelectricity: A Quantitative Approach*, second edn, Kluwer Academic/Plenum Publishers, New York.

Preece, J. P. and Tyler, R. S. (1989), 'Temporal-gap detection by cochlear prosthesis users', *Journal of Speech and Hearing Research* **32**(4), 849–856.

Pressnitzer, D., de Cheveigné, A. and Winter, I. M. (2004), 'Physiological correlates of the perceptual pitch shift for sounds with similar waveform autocorrelation', *Acoustics Research Letters Online* **5**(1), 1–6.

Pretorius, L. L. and Hanekom, J. J. (2006), 'An accurate method for determining the conspicuity area associated with visual targets', *Human Factors* **48**(4), 774–784.

Prijs, V. F., Keijzer, J., Versnel, H. and Schoonhoven, R. (1993), 'Recovery characteristics of auditory nerve fibres in the normal and noise-damaged guinea pig cochlea', *Hearing Research* **71**(1-2), 190–201.

Rammer, I. and Szpuszta, M. (2005), *Advanced .NET Remoting*, second edn, Apress, Berkeley, California.

Rattay, F. (1986), 'Analysis of models for external stimulation of axons', *IEEE Transactions on Biomedical Engineering* **33**(10), 974–977.

Rattay, F. (1988), 'Modeling the excitation of fibers under surface electrodes', *IEEE Transactions on Biomedical Engineering* **35**(3), 199–202.

Rattay, F. (1989), 'Analysis of models for extracellular fiber stimulation', *IEEE Transactions on Biomedical Engineering* **36**(7), 676–682.

Rattay, F. (1990), *Electrical Nerve Stimulation: Theory, Experiments and Applications*, Springer-Verlag, Vienna, Austria.

Rattay, F. (1998), 'Analysis of the electrical excitation of CNS neurons', *IEEE Transactions on Biomedical Engineering* **45**(6), 766–772.

Rattay, F. (1999), 'The basic mechanism for the electrical stimulation of the nervous system', *Neuroscience* **89**(2), 335–346.

Rattay, F. (2000), 'Basics of hearing theory and noise in cochlear implants', *Chaos, Solitons and Fractals* **11**(12), 1875–1884.

Rector, B. E. and Newcomer, J. M. (1997), *Win32 Programming*, Addison-Wesley, Upper Saddle River, New Jersey.

Richardson, K. A., Imhoff, T. T., Grigg, P. and Collins, J. J. (1998), 'Encoding chaos in neural spike trains', *Physical Review Letters* **80**(11), 2485–2488.

Richter, J. (1996), *Advanced Windows*, third edn, Microsoft Press, Redmond, Washington.

Richter, J. (2002), *Applied Microsoft .NET Framework Programming*, Microsoft Press, Redmond, Washington.

Rieke, F., Warland, D., de Ruyter van Steveninck, R. and Bialek, W. (1999), *Spikes: Exploring the Neural Code*, The MIT Press, Cambridge, Massachusetts.

Rocha, A. F. (1997), 'The brain as a symbol-processing machine', *Progress in Neurobiology* **53**(2), 121–198.

Rogerson, D. (1997), *Inside COM*, Microsoft Press, Redmond, Washington.

Ross, S. M. (1993), *Introduction to Probability Models*, fifth edn, Academic Press, London.

Ross, S. M. (1996), *Stochastic Processes*, second edn, John Wiley and Sons, Inc., New York.

Rubinstein, J. T., Wilson, B. S., Finley, C. C. and Abbas, P. J. (1999), 'Pseudospontaneous activity: Stochastic independence of auditory nerve fibers with electrical stimulation', *Hearing Research* **127**(1-2), 108–118.

Sek, A. and Moore, B. C. J. (1995), 'Frequency discrimination as a function of frequency, measured in several ways', *Journal of the Acoustical Society of America* **97**(4), 2479–2486.

Shailer, M. J. and Moore, B. C. J. (1987), 'Gap detection and the auditory filter: Phase effects using sinusoidal stimuli', *Journal of the Acoustical Society of America* **81**(4), 1110–1117.

Shannon, R. V. (1989), 'Detection of gaps in sinusoids and pulse trains by patients with cochlear implants', *Journal of the Acoustical Society of America* **85**(6), 2587–2592.

Shannon, R. V. (1992), 'A model of safe levels for electrical stimulation', *IEEE Transactions on Biomedical Engineering* **39**(4), 424–426.

Shannon, R. V., Adams, D. D., Ferrel, R. L., Palumbo, R. L., and Grandgenett, M. (1990), 'A computer interface for psychophysical and speech research with the Nucleus cochlear implant', *Journal of the Acoustical Society of America* **87**(2), 905–907.

Shepherd, R. K. and Javel, E. (1997), 'Electrical stimulation of the auditory nerve: I. Correlation of physiological responses with cochlear status', *Hearing Research* **108**(1-2), 112–144.

Shepherd, R. K. and Javel, E. (1999), 'Electrical stimulation of the auditory nerve: II. Effect of stimulus waveshape on single fibre response properties', *Hearing Research* **130**(1-2), 171–188.

Siebert, W. M. (1968), Stimulus transformation in the peripheral auditory system, *in* P. A. Kolers and M. Eden, eds, 'Recognizing Patterns', MIT Press, Cambridge, Massachusetts, pp. 104–133.

Siebert, W. M. (1970), 'Frequency discrimination in the auditory system: Place or periodicity mechanisms?', *Proceedings of the IEEE* **58**(5), 723–730.

Snyder, D. L. (1975), *Random Point Processes*, John Wiley and Sons, Inc., New York.

So, P., Francis, J. T., Netoff, T. I., Gluckman, B. J. and Schiff, S. J. (1998), 'Periodic orbits: A new language for neuronal dynamics', *Biophysical Journal* **74**(6), 2776–2785.

Solomon, D. L. (1975), 'A note on the non-equivalence of the Neyman-Pearson and generalized likelihood ratio tests for testing a simple null versus a simple alternative hypothesis', *The American Statistician* **29**(2), 101–102.

Teich, M. C. and Khanna, S. M. (1985), 'Pulse-number distribution for the neural spike train in the cat's auditory nerve', *Journal of the Acoustical Society of America* **77**(3), 1110–1128.

Thompson, Jr., W. A. (1988), *Point Process Models with Applications to Safety and*

Reliability, Chapman and Hall, London.

Troelsen, A. (2001), *C# and the .NET Platform*, Apress, Berkeley, California.

Turcott, R. G., Lowen, S. B., Li, E., Johnson, D. H., Tsuchitani, C. and Teich, M. C. (1994), 'A nonstationary poisson point process describes the sequence of action potentials over long time scales in lateral-superior-olive auditory neurons', *Biological Cybernetics* **70**(3), 209–217.

van Wieringen, A., Carlyon, R. P., Macherey, O. and Wouters, J. (2006), 'Effects of pulse rate on thresholds and loudness of biphasic and alternating monophasic pulse trains in electrical hearing', *Hearing Research* **220**(1-2), 49–60.

van Wieringen, A. and Wouters, J. (1999), 'Gap detection in single- and multiple-channel stimuli by LAURA cochlear implantees', *Journal of the Acoustical Society of America* **106**(4), 1925–1939.

Wang, J., van Wijhe, R., Chen, Z. and Yin, S. (2006), 'Is duration tuning a transient process in the inferior colliculus of guinea pigs?', *Brain Research* **1114**(1), 63–74.

West, R. W. and Ogden, R. T. (1997), 'Continuous-time estimation of a change-point in a poisson process', *Journal of Statistical Computation and Simulation* **56**(4), 293–302.

Williams, K. N. and Perrott, D. R. (1972), 'Temporal resolution of tonal pulses', *Journal of the Acoustical Society of America* **51**, 644–647.

Xu, Y. and Collins, L. M. (2003), 'Predicting the threshold of single-pulse electrical stimuli using a stochastic auditory nerve model: The effects of noise', *IEEE Transactions on Biomedical Engineering* **50**(7), 825–835.

Xu, Y. and Collins, L. M. (2004), 'Predicting the threshold of pulse-train electrical stimuli using a stochastic auditory nerve model: The effects of stimulus noise', *IEEE Transactions on Biomedical Engineering* **51**(4), 590–603.

Xu, Y. and Collins, L. M. (2007), 'Predictions of psychophysical measurements for sinusoidal amplitude modulated (SAM) pulse-train stimuli from a stochastic model', *IEEE Transactions on Biomedical Engineering* **54**(8), 1389–1398.

Young, E. D. and Barta, P. E. (1986), 'Rate responses of auditory nerve fibers to tones in noise near masked threshold', *Journal of the Acoustical Society of America* **79**(2), 426–442.

Young, M. J. (2001), *XML Step by Step*, second edn, Microsoft Press, Redmond, Washington.

Zeng, F.-G. (2002), 'Temporal pitch in electric hearing', *Hearing Research* **174**(1-2), 101–106.

Zeng, F.-G., Chen, H. and Han, S. (2005), 'Temporal masking in electric hearing', *Journal of the Association for Research in Otolaryngology* **6**(4), 390–400.

Zeng, F.-G., Galvin, J. J. I. and Zhang, C. (1998), 'Encoding loudness by electric stimulation of the auditory nerve', *NeuroReport* **9**(8), 1845–1848.

APPENDIX A

NOTATION AND DEFINITIONS

This appendix presents the definitions and notations of the fundamental probabilistic concepts that are used in this document. Statistical relations between the quantities defined in this section, along with alternative ways for calculating these, are discussed in appendix B.

A.1 PROBABILITY AND CONDITIONAL PROBABILITY

The *probability* of the *random variable*, or RV, X is denoted by $\mathcal{P}r(X)$, with the understanding that the probability value is within the range $0 \leq \mathcal{P}r(X) \leq 1$. Similarly, the *conditional probability* of A given B is represented using the notation $\mathcal{P}r(A \mid B)$, which is defined by

$$\mathcal{P}r(A \mid B) \triangleq \frac{\mathcal{P}r(A \cap B)}{\mathcal{P}r(B)}, \tag{A.1}$$

where it is assumed that $\mathcal{P}r(B) \neq 0$, and $\mathcal{P}r(A \cap B)$ denotes the probability of the *intersection* of A and B, also called the *joint probability* (i.e., the probability that both A *and* B occur simultaneously). If A and B are two *independent* RVs, then $\mathcal{P}r(A \cap B) = \mathcal{P}r(A) \,.\, \mathcal{P}r(B)$, so that $\mathcal{P}r(A \mid B) = \mathcal{P}r(A)$, which asserts the notion that $\mathcal{P}r(A)$ is not conditional on $\mathcal{P}r(B)$ when A is determined independently from B.

In the context of neural activity, conditional probability is sometimes very useful in understanding relations between events preceding and following spikes. Gray (1967) has dealt with the application of conditional probability to this subject from a more practical perspective.

A.2 PROBABILITY DENSITY FUNCTION

The *probability density function*, or PDF, of an RV X is written as $pdf(x)$ when the RV is implied, or $pdf_X(x)$ where the RV is explicitly specified, and would generally be calculated as follows:[1]

$$pdf_X(x) \triangleq \lim_{\Delta x \to 0^+} \frac{\mathcal{P}r(x < X \leq x + \Delta x)}{\Delta x} \tag{A.2}$$

$$\text{with} \quad \int_{-\infty}^{+\infty} pdf_X(x)\, dx = 1\,. \tag{A.3}$$

It should be noted that this definition of the PDF is a probability *limit from above* where the probability involves the RV region (i.e., the collection of points) between the point x (but excluding itself) and a point $x + \Delta x$ (inclusive), and that this probability is expressed as a density because of the Δx denominator. Similarly, one may write an expression for the PDF that involves the *limit from below*, such that the probability would involve the region between $x - \Delta x$ (inclusive) and x (exclusive). For a *continuous* probability distribution, it follows from basic mathematical analysis of the limit of a continuous function that these two quantities (those in the limit) would numerically be exactly equivalent, and would also be equivalent to the probability expression evaluated directly at the point x. Thus, for any *continuous* distribution one would have:

$$\begin{aligned} pdf_X(x) &= \lim_{\Delta x \to 0^+} \frac{\mathcal{P}r(x < X \leq x + \Delta x)}{\Delta x} \\ &= \lim_{\Delta x \to 0^-} \frac{\mathcal{P}r(x > X \geq x + \Delta x)}{-\Delta x} \\ &= \lim_{\Delta x \to 0^-} \frac{\mathcal{P}r(x + \Delta x \leq X < x)}{-\Delta x} \end{aligned} \tag{A.4}$$

$$\therefore \quad pdf_X(x) = \lim_{\Delta x \to 0^+} \frac{\mathcal{P}r(x - \Delta x \leq X < x)}{\Delta x}\,, \tag{A.5}$$

$$\text{and} \quad pdf_X(x) = \lim_{\Delta x \to 0^+} \frac{\mathcal{P}r(X = x)}{\Delta x}\,. \tag{A.6}$$

[1] The notations k^+ and k^- should be interpreted as $k + \varepsilon$ and $k - \varepsilon$, respectively, while limiting $\varepsilon \to 0$ where $\varepsilon > 0$. (For the interested reader, note that 0^+ is then conceptually similar to the "real zero" that is symbolized by $0_{\bullet}$ in Czajko (2004).)

A.3 CUMULATIVE DISTRIBUTION FUNCTION

The corresponding *cumulative distribution function*, or CDF, of the RV X is denoted by $cdf_X(x)$, or simply $cdf(x)$ for short, and defined to be

$$cdf_X(x) \triangleq \mathcal{P}r(X \leq x) \tag{A.7}$$

$$= \int_{-\infty}^{x} pdf_X(u)\ du\ . \tag{A.8}$$

This definition of the CDF also implies that

$$\mathcal{P}r(a < X \leq b) = \int_{a}^{b} pdf_X(x)\ dx \quad \forall \quad a < b\ . \tag{A.9}$$

To arrive at eq. A.9, one can interpret the desired probability as that of two overlapping sets of events that need to be subtracted, so that

$$\begin{aligned} \mathcal{P}r(a < X \leq b) &= \mathcal{P}r(X \leq b) - \mathcal{P}r(X \leq a) \\ &= cdf_X(b) - cdf_X(a) \\ &= cdf_X(x)\Big|_{x=a}^{x=b} \\ &= \int_{a}^{b} pdf_X(x)\ dx\ . \end{aligned}$$

A.4 PROBABILITY MASS FUNCTION

In the case of discrete-valued RVs, such as *lattice* RVs (Ross 1996), it is sometimes more convenient to use the *probability mass function*, or PMF, which alleviates the need to use *Dirac delta*, $\delta(\cdot)$, functions if one were to use a PDF instead. This function will be represented by $pmf(x)$, or $pmf_X(x)$ when the RV X is explicitly specified, and is defined by

$$pmf_X(x) \triangleq \mathcal{P}r(X = x) \tag{A.10}$$

$$\text{with} \quad \sum_{x} pmf_X(x) = 1\ . \tag{A.11}$$

For discrete-valued RVs, the CDF can be expressed in terms of the PMF, so that the equivalent of eq. A.8 would be

$$cdf_X(x) = \sum_{u \leq x} pmf_X(u) \ . \tag{A.12}$$

It should be understood that PDFs can also be used for discrete-valued RVs, but such expressions would obviously consist of sums of Dirac delta functions. The use of PMFs for discrete RVs is simply an equivalent alternative to using PDFs.

A.5 COMPLEMENTARY CUMULATIVE DISTRIBUTION FUNCTION

In analogy with the *error function*[2] and *complementary error function* that are commonly represented by *erf* and *erfc*, respectively, the corresponding *complementary cumulative distribution function* (CDFC, also known as the *survivor function* (Cox 1962, Cox and Isham 1980), *survival function* (Thompson, Jr. 1988), *reliability* (Bracquemond and Gaudoin 2003), *tail probability function* (Olkin et al. 1994) or simply *tail distribution*) of the RV X will be denoted by $cdfc_X(x)$, or the terse alternative $cdfc(x)$, and is defined to represent

$$\begin{aligned} cdfc_X(x) &\triangleq \mathcal{P}r(X > x) && \text{(A.13)} \\ &= 1 - cdf_X(x) && \text{(A.14)} \\ &= \int_x^{\infty} pdf_X(u)\ du && \text{(A.15)} \\ &= \sum_{u > x} pmf_X(u) \ . && \text{(A.16)} \end{aligned}$$

In addition to providing a way to determine $\mathcal{P}r(X > x)$ of an RV, the CDFC actually has some very interesting alternative interpretations, such as being a scaled version (see eq. 5.9) of the PDF for both the *forward recurrence-time* and *backward recurrence-time* (also known as the *residual lifetime* and *age*, respectively) of an inter-event interval RV of a point process under equilibrium conditions (Cox 1962, § 5.1–5.2), which can also be derived from a slightly different perspective in the context of *length-biased sampling* (discussed on p. 71).

[2] Here, the *error function* refers to the integral of the Gaussian distribution in general, irrespective of its exact definition (of which there are many).

A.6 HAZARD RATE FUNCTION

The *hazard rate* (Thompson, Jr. 1988, Ross 1993) of an RV X is denoted by $hrf_X(x)$, or $hrf(x)$ for short. Alternative names for the hazard function include *age-specific failure rate* (Cox 1962), *failure rate* (Ross 1993, 1996), *conditional mortality rate*, *force of mortality* (Thompson, Jr. 1988), and *hazard function* (Young and Barta 1986). It is defined by

$$hrf_X(x) \triangleq \lim_{\Delta x \to 0^+} \frac{\mathcal{P}r(X \leq x + \Delta x \mid X > x)}{\Delta x} \tag{A.17}$$

$$= \frac{pdf_X(x)}{cdfc_X(x)} . \tag{A.18}$$

In the context of temporal RVs, the hazard function is a time-to-failure function that gives the instantaneous probability of the event (i.e., probability of *almost* immediate failure), given that failure has not occurred at the specific time (e.g., x, which is the independent variable of this hazard function), but is specified in rate units (e.g., hertz). That is, the value of a hazard function at time t, also written $hrf(t)$, conceptually corresponds with the probability that the event will occur *very* soon, given that the event has not occurred *up to and including* the specific moment t, but the probability is then concretely formulated as a *density* (e.g., *rate*) function, as opposed to a *dimensionless* probability function with the inclusion of the Δx denominator in the definition above.

Furthermore, note that eq. A.17 is equivalent to the more commonly found definition,

$$hrf_X(x) = \lim_{\Delta x \to 0^+} \mathcal{P}r(x < X \leq x + \Delta x \mid x < X) / \Delta x ,$$

since

$$\begin{aligned} \mathcal{P}r(X \leq x + \Delta x \mid X > x) &= \mathcal{P}r(X \leq x + \Delta x \cap X > x) / \mathcal{P}r(X > x) \\ &= \mathcal{P}r(x < X \leq x + \Delta x) / \mathcal{P}r(X > x) \\ &= \mathcal{P}r(x < X \leq x + \Delta x \mid X > x) . \end{aligned}$$

However, the definition given by eq. A.17 leads to a more intuitive interpretation of instantaneous risk, i.e., given the age, x, of a temporal RV, X, the hazard function expresses the probability that the RV will be terminated by an event in a very short interval, Δx, in the future.

A.7 DISCRETE HAZARD FUNCTION

The *discrete hazard function* (DHF), as defined by Barlow et al. (1963), has traditionally been interpreted as an equivalent of the hazard function in the discrete domain. The values of the function are dimensionless and represent simple probabilities. For example, in Markov chain theory, the DHF can be interpreted as the probability of a renewal process to return to its initial state.

Formally, the DHF of an RV X is written as $dhf_X(x)$, or simply $dhf(x)$, and it is defined as a conditional probability:

$$dhf_X(x) \triangleq \mathcal{P}r\,(X = x \mid X \geq x)\,. \tag{A.19}$$

A.8 COMPLEMENTARY DISCRETE HAZARD FUNCTION

The *complementary discrete hazard function*, DHFC, is defined simply as the complement of the DHF:

$$dhfc_X(x) \triangleq \mathcal{P}r\,(X > x \mid X \geq x) \tag{A.20}$$

$$= 1 - dhf_X(x)\,. \tag{A.21}$$

Similar to the DHF, the values of the DHFC are dimensionless and also represent simple probabilities. Continuing the Markov chain example from the previous section, the DHFC can be interpreted as the probability that a renewal process will move to its next state. Together, the DHF and DHFC probabilities can then be used to define a Markov chain transition matrix that can provide the solution for the overall state probabilities of a renewal process.

A.9 CUMULATIVE HAZARD FUNCTION

In § A.6 it was recognized that the HRF is a *density* function (as opposed to a dimensionless probability function). By integrating the HRF it is possible to derive a dimensionless function (though not a simple probabilistic one) that is best referred to as the *cumulative hazard*

function (CHF). The CHF of an RV X is denoted by $chf_X(x)$, or $chf(x)$ for short, and can be calculated as follows:

$$chf_X(x) = \int_{-\infty}^{x} \frac{pdf_X(u)}{cdfc_X(u)}\, du \tag{A.22}$$

$$= \int_{-\infty}^{x} hrf_X(u)\ du\ . \tag{A.23}$$

Conceptually the CHF is a rather basic construct, and can be interpreted as the sum total of all the hazard densities up to and including the point x. Also, Ross (1993, p. 439) calls the CHF simply the *hazard function* (and uses the contrasting term *failure/hazard rate function* when referring to the HRF).

A.10 MEAN AND VARIANCE

The *expected value*, *average* or *mean* of an RV X is indicated as $E[X]$ and defined by

$$E[X] \triangleq \int_{-\infty}^{+\infty} x\ .\ pdf_X(x)\ dx \tag{A.24}$$

$$= \sum_{x} x\ .\ pmf_X(x)\ . \tag{A.25}$$

Similarly, the *variance* of the RV X is written as $V[X]$ and defined as follows:

$$V[X] \triangleq E\left[(X - E[X])^2\right] \tag{A.26}$$

$$= \int_{-\infty}^{+\infty} (x - E[X])^2\ .\ pdf_X(x)\ dx \tag{A.27}$$

$$= \sum_{x} (x - E[X])^2\ .\ pmf_X(x)\ . \tag{A.28}$$

APPENDIX B

STATISTICAL RELATIONS

This appendix presents a cohesive set of relations between the statistical quantities as these have been defined for the purpose of this study. An overview of the notation and definitions related to this appendix can be found in appendix A.

B.1 MEAN AND VARIANCE

If an RV is continuous and its expected value is a finite number, the mean (as defined by eq. A.24) can also be calculated from[1]

$$E[X] = \int_0^\infty cdfc_X(x)\ dx - \int_{-\infty}^0 cdf_X(x)\ dx\,. \tag{B.1}$$

Note that the second integral in this equation, involving $cdf(x)$, evaluates to zero for nonnegative valued RVs (i.e., ones for which $cdf(x) = 0\ \forall\ x < 0$), so that eq. B.1 reduces to the following (Gallager 1996, p. 8, eq. 8) for continuous nonnegative RVs (e.g., when the RV describes time intervals that cannot be negative, as is the case for inter-event intervals of point processes):

$$E[X] = \int_0^\infty cdfc_X(x)\ dx\,. \tag{B.2}$$

[1] Olkin et al. (1994, p. 268) suggest that eq. B.1 applies to any continuous RV for which $E[\,|\,X\,|\,] < \infty$.

In the case of a nonnegative lattice RV with period T, a discrete version of eq. B.2 (interpreted graphically by Gallager 1996, fig. 1.3, p. 9) is given by

$$E[X] = T \cdot \sum_{n=0}^{\infty} cdfc_X(n.T) \ . \tag{B.3}$$

Furthermore, eq. B.3 applies as follows to positive lattice RVs, which are encountered in the periodic stimulus sequences used in the present study:

$$E[X] = T \cdot \left(1 + \sum_{n=1}^{\infty} cdfc_X(n.T)\right) \ . \tag{B.4}$$

Alternative ways of calculating the variance of an RV X (as defined by eq. A.26) are given below. These expressions are usually simpler to calculate than those of eqs. A.27 and A.28.

$$V[X] = E\left[X^2\right] - (E[X])^2 \tag{B.5}$$

$$= \int_{-\infty}^{+\infty} x^2 \cdot pdf_X(x)\ dx - E[X]^2 \tag{B.6}$$

$$= \left(\sum_{x} x^2 \cdot pmf_X(x)\right) - E[X]^2 \ . \tag{B.7}$$

B.2 Equivalent Random Variable Descriptions

An RV is uniquely defined by any one of the following functions: a probability density/mass function, hazard function (HRF or DHF), or any of their cumulative or complementary counterparts, if defined, such as the cumulative distribution function, cumulative hazard function, or survivor function (i.e., complementary cumulative distribution function). This can be illustrated through the statistical relations below. Expressions that are formulated in terms of x^- are often useful to calculate the desired function in a recursive or sequential manner, when a specific value of the function itself or a related function is known.

$$pdf(x) = \sum_{u} pmf(u) \cdot \delta(x-u) \tag{B.8}$$

$$= \frac{d}{dx}\{cdf(x)\} \tag{B.9}$$

$$= -\frac{d}{dx}\{cdfc(x)\} \tag{B.10}$$

$$= cdfc(x) \,.\, hrf(x) \tag{B.11}$$
$$= \frac{hrf(x)}{\exp\{chf(x)\}} \quad \text{(for continuous distributions only)} \tag{B.12}$$

$$pmf(x) = cdf(x) - cdf(x^-) \tag{B.13}$$
$$= cdfc(x^-) - cdfc(x) \tag{B.14}$$
$$= cdfc(x^-) \,.\, dhf(x) \tag{B.15}$$
$$= dhf(x) \,.\, \prod_{u<x} dhfc(u) \tag{B.16}$$

$$cdf(x) = \int_{-\infty}^{x} pdf(u)\ du \tag{B.17}$$
$$= \sum_{u\le x} pmf(u) \tag{B.18}$$
$$= cdf(x^-) + pmf(x) \tag{B.19}$$
$$= 1 - cdfc(x) \tag{B.20}$$
$$= 1 - \prod_{u\le x}\{1 - dhf(u)\} \tag{B.21}$$
$$= 1 - \prod_{u\le x} dhfc(u) \tag{B.22}$$
$$= 1 - cdfc(x^-) \,.\, dhfc(x) \tag{B.23}$$

$$cdfc(x) = \int_{x}^{\infty} pdf(u)\ du \tag{B.24}$$
$$= \sum_{u>x} pmf(u) \tag{B.25}$$
$$= cdfc(x^-) - pmf(x) \tag{B.26}$$
$$= \frac{pdf(x)}{hrf(x)} \tag{B.27}$$
$$= 1 - cdf(x) \tag{B.28}$$
$$= \prod_{u\le x}[1 - dhf(u)] \tag{B.29}$$
$$= \prod_{u\le x} dhfc(u) \tag{B.30}$$
$$= cdfc(x^-) \,.\, \{1 - dhf(x)\} \tag{B.31}$$
$$= cdfc(x^-) \,.\, dhfc(x) \tag{B.32}$$

$$hrf(x) = \frac{pdf(x)}{cdfc(x)} \tag{B.33}$$

$$= \frac{pdf(x)}{1 - cdf(x)} \tag{B.34}$$

$$= \frac{d}{dx}\Big\{chf(x)\Big\} \tag{B.35}$$

$$= \frac{pdf(x)}{\int_x^{\infty} pdf(u)\ du} \tag{B.36}$$

$$= -\frac{\frac{d}{dx}\Big\{cdfc(x)\Big\}}{cdfc(x)} \tag{B.37}$$

$$= -\frac{d}{dx}\Big\{\ln[cdfc(x)]\Big\} \tag{B.38}$$

$$= -\frac{d}{dx}\Big\{\ln[\prod_{u \le x} dhfc(u)]\Big\} \tag{B.39}$$

$$= -\frac{d}{dx}\Big\{\sum_{u \le x} \ln[dhfc(u)]\Big\} \tag{B.40}$$

$$= \sum_u \frac{pmf(u)}{cdfc(u)} \,.\, \delta(x - u) \tag{B.41}$$

$$chf(x) = \int_{-\infty}^{x} hrf(u)\ du \tag{B.42}$$

$$= \sum_{u \le x} \frac{pmf(u)}{cdfc(u)} \tag{B.43}$$

$$= \sum_{u \le x} \left\{ \frac{cdfc(u^-)}{cdfc(u)} - 1 \right\} \tag{B.44}$$

$$= chf(x^-) + \frac{cdfc(x^-)}{cdfc(x)} - 1 \tag{B.45}$$

$$dhf(x) = \frac{pmf(x)}{cdfc(x^-)} \tag{B.46}$$

$$= \frac{pmf(x)}{pmf(x) + cdfc(x)} \tag{B.47}$$

$$= 1 - dhfc(x) \tag{B.48}$$

$$dhfc(x) = \frac{cdfc(x)}{cdfc(x^-)} \tag{B.49}$$

$$= \frac{cdfc(x)}{cdfc(x) + pmf(x)} \tag{B.50}$$

$$= 1 - dhf(x) \tag{B.51}$$

B.3 EVALUATING PROBABILITIES

The following is a summarized list of equations that can be applied to probability calculations involving the specified sets of events.

Because the expressions for $\mathcal{P}r(X < x)$ and $\mathcal{P}r(X \geq x)$ do not themselves correspond directly with named probability functions (but, rather, with marginally shifted versions of the CDF and CDFC, respectively), they receive a bit more attention in this section. Included below are equivalent expressions in terms of other well known probability functions.

$$\begin{aligned}
\mathcal{P}r(X = x) &\triangleq pmf_X(x) && \text{(B.52)}\\
&= cdf_X(x) - cdf_X(x^-) \quad \text{(Papoulis 1965, eq. 4-12)} && \text{(B.53)}\\
&= cdfc_X(x^-) - cdfc_X(x) && \text{(B.54)}
\end{aligned}$$

$$\begin{aligned}
\mathcal{P}r(X \leq x) &\triangleq cdf_X(x) && \text{(B.55)}\\
&= 1 - cdfc_X(x) && \text{(B.56)}
\end{aligned}$$

$$\begin{aligned}
\mathcal{P}r(X < x) &= \mathcal{P}r(X \leq x) - \mathcal{P}r(X = x) && \text{(B.57)}\\
&= 1 - \mathcal{P}r(X \geq x) && \text{(B.58)}\\
&= \sum_{u<x} pmf_X(u) && \text{(B.59)}\\
&= cdf_X(x) - pmf_X(x) && \text{(B.60)}\\
&= cdf_X(x^-) && \text{(B.61)}\\
&= 1 - cdfc_X(x^-) && \text{(B.62)}\\
&= 1 - \prod_{u<x}\{1 - dhf_X(u)\} && \text{(B.63)}\\
&= 1 - \prod_{u<x} dhfc_X(u) && \text{(B.64)}
\end{aligned}$$

$$\begin{aligned}
\mathcal{P}r(X > x) &\triangleq cdfc_X(x) && \text{(B.65)}\\
&= 1 - cdf_X(x) && \text{(B.66)}
\end{aligned}$$

$$\begin{aligned}
\mathcal{P}r(X \geq x) &= \mathcal{P}r(X > x) + \mathcal{P}r(X = x) && \text{(B.67)}\\
&= 1 - \mathcal{P}r(X < x) && \text{(B.68)}\\
&= \sum_{u \geq x} pmf_X(u) && \text{(B.69)}\\
&= pmf_X(x) \,/ dhf_X(x) && \text{(B.70)}\\
&= 1 - cdf_X(x^-) && \text{(B.71)}\\
&= cdfc_X(x) + pmf_X(x) && \text{(B.72)}\\
&= cdfc_X(x^-) && \text{(B.73)}\\
&= \frac{cdfc_X(x)}{1 - dhf_X(x)} && \text{(B.74)}\\
&= cdfc_X(x) \,/ dhfc_X(x) && \text{(B.75)}\\
&= \prod_{u<x} \{1 - dhf_X(u)\} && \text{(B.76)}\\
&= \prod_{u<x} dhfc_X(u) && \text{(B.77)}
\end{aligned}$$

$$\begin{aligned}
\mathcal{P}r(a < X \leq b) &= \int_a^b pdf_X(x)\ dx \quad \text{(Equation discussed on p. 147)} && \text{(B.78)}\\
&= cdf_X(b) - cdf_X(a) && \text{(B.79)}\\
&= cdfc_X(a) - cdfc_X(b) && \text{(B.80)}
\end{aligned}$$

$$\mathcal{P}r(a < X < b) = \mathcal{P}r(a < X \leq b) - \mathcal{P}r(X = b) \quad \text{(B.81)}$$

$$\mathcal{P}r(a \leq X \leq b) = \mathcal{P}r(a < X \leq b) + \mathcal{P}r(X = a) \quad \text{(B.82)}$$

$$\mathcal{P}r(a \leq X < b) = \mathcal{P}r(a < X \leq b) + \mathcal{P}r(X = a) - \mathcal{P}r(X = b) \quad \text{(B.83)}$$

$$\begin{aligned}
\mathcal{P}r(X = x \mid X \geq x) &\triangleq dhf_X(x) && \text{(B.84)}\\
&= \mathcal{P}r(X = x) / \mathcal{P}r(X \geq x) && \text{(B.85)}
\end{aligned}$$

$$\begin{aligned}
\mathcal{P}r(X > x \mid X \geq x) &\triangleq dhfc_X(x) && \text{(B.86)}\\
&= 1 - dhf_X(x) && \text{(B.87)}\\
&= \mathcal{P}r(X > x) / \mathcal{P}r(X \geq x) && \text{(B.88)}
\end{aligned}$$

A summary of the probability expressions that correspond with each of the common

probability functions is given below.

$$pdf_X(x) \triangleq \lim_{\Delta x \to 0^+} \left\{ \frac{1}{\Delta x} . \mathcal{P}r\left(x < X \leq x + \Delta x\right) \right\} \tag{B.89}$$

$$= \lim_{\Delta x \to 0^+} \left\{ \frac{1}{\Delta x} . \mathcal{P}r\left(x - \Delta x \leq X < x\right) \right\} \tag{B.90}$$

$$pmf_X(x) \triangleq \mathcal{P}r\left(X = x\right) \tag{B.91}$$

$$cdf_X(x) \triangleq \mathcal{P}r\left(X \leq x\right) \tag{B.92}$$

$$cdfc_X(x) \triangleq \mathcal{P}r\left(X > x\right) \tag{B.93}$$

$$hrf_X(x) \triangleq \lim_{\Delta x \to 0^+} \left\{ \frac{1}{\Delta x} . \mathcal{P}r\left(X \leq x + \Delta x \mid X > x\right) \right\} \tag{B.94}$$

$$= \lim_{\Delta x \to 0^+} \left\{ \frac{1}{\Delta x} . \frac{\mathcal{P}r\left(x - \Delta x \leq X < x\right)}{\mathcal{P}r\left(X > x\right)} \right\} \tag{B.95}$$

$$chf_X(x) \triangleq \sum_{u \leq x} \frac{\mathcal{P}r\left(X = u\right)}{\mathcal{P}r\left(X > u\right)} \tag{B.96}$$

$$= \int_{-\infty}^{x} hrf_X(u)\ du \tag{B.97}$$

$$dhf_X(x) \triangleq \mathcal{P}r\left(X = x \mid X \geq x\right) \tag{B.98}$$

$$dhfc_X(x) \triangleq \mathcal{P}r\left(X > x \mid X \geq x\right) \tag{B.99}$$

It is worth noting that the expressions given by eqs. B.89 and B.90 are indeed equivalent when evaluated for continuous probability distributions, i.e., ones without any probability masses. In addition, the expressions of eqs. B.94 & B.95 and eqs. B.96 & B.97 are equivalent for continuous RVs, such that either eqs. B.94 or B.95 can then be used for the HRF expression in eq. B.97. This follows from basic continuous functional analysis, which requires that, for any function to be continuous, the two limits (the limit from above and below, respectively represented by $x + \Delta x$ and $x - \Delta x$) equate to exactly the same quantity as would result when evaluating the function itself at the point x. In this case, one is just further expressing this value as a density by dividing with Δx in the limit, so that both PDF expressions from eqs. B.89 and B.90 conceptually represent

$$pdf_X(x) \simeq \lim_{\Delta x \to 0^+} \frac{1}{\Delta x} . \mathcal{P}r\left(X = x\right) \tag{B.100}$$

$$= pmf_X(x) . \lim_{\Delta x \to 0^+} \frac{1}{\Delta x} . \tag{B.101}$$

The correlation that can be drawn between the PDF and PMF is reflected by eq. B.101, such that the PDF effectively represents the PMF expressed as a density at every point x.

The limiting Δx term that remains in this equation then, in effect, represents a Dirac delta function located at point x, which gives rise to eq. B.8.

APPENDIX C

POISSON-PROCESS GENERATOR

The Poisson point-process, and dead-time-modified versions of it, has played an important role in the investigation of temporal aspects of perception in the present study. Generating these stimulation sequences with computational efficiency while staying true to mathematical accuracy posed a challenge of its own. This appendix discusses the implementation of the Poisson-process generator in the PSYCHOACOUSTICS TOOLBOX[1], dealing with some of the particulars and mathematics related to the implementation.

The final implementation of the generator in MATLAB used a technique known as the *simplified inversion method* (also known as the *inverse distribution technique* or *inverse transformation method*) to calculate the inter-event periods of the required (dead-time-modified) Poisson process. The technique is described using terse mathematical constructs in Devroye (1986), and in Ross (1993, § 11.2.1)[2] one finds a complementary explanation with an example involving an exponential random variable that forms the basis of the inter-event intervals for a Poisson process. Although Poisson processes have been generated for the purpose of stimulation sequences in the present study, Poisson processes (and point processes in general) have been applied to various other problems, including describing normal neural firing patterns themselves, as has been discussed in Johnson (1996)[3]. The inverse distribution

[1] Refer to § 3.2 for more information on the PSYCHOACOUSTICS TOOLBOX.

[2] This book is a good introductory text on probability theory, including Markov-chain theory. It also contains a useful chapter dealing with the practical aspects of computer simulations involving numerous random-variable distributions, along with helpful comments on the generation of stochastic processes (which includes the use of the inverse transformation method as well as the hazard rate method that can be used to generate more eccentric RV distributions).

[3] The section titled "Generating Point Processes" is particularly applicable in the present context,

function technique has also been used by Huettel and Collins (2004) to generate spike trains for their auditory neuron model.

In general one does not need to enforce any additional rules when generating Poisson processes with the technique discussed, since the algorithm does generate processes with the correct statistics over the long run. However, for the experiments of the present investigation, relatively short sequences are generated with events numbering from only tens to a few hundred constituting a stimulation sequence. In this case, one needs to make sure that the short-term statistics are close enough to the long-term statistics so that individual trials in the experiment do not present vastly different stimulation sequences (which would otherwise result in large variations in perception). For this reason a tolerance criterion was introduced, which ensured that the average inter-event interval for a single sequence does not deviate by more than 0.3% of the desired rate for the homogeneous Poisson-process. The reasoning behind this specific value is simply that the number corresponds with 5 cents of a musical half-note, which is roughly the smallest difference limen that normal-hearing persons with musical training can perceive for pitch discrimination. Similar measurements for frequency difference limens can, for instance, be found in Sek and Moore (1995).

The mechanism of the inverse transformation method is based on the fact that, in general, it is possible to generate a variate with probability density function[4], $pdf_X(x)$, by using the inverse of the cumulative distribution function, $cdf_X(x)$. For the generation function one then needs a variate, U, with a uniform distribution over the range $(0, 1)$. The variate with the desired distribution can be obtained by applying the inverse distribution function to U:

$$X = cdf_U^{-1}(u) \ , \tag{C.1}$$

where $cdf_U^{-1}(u)$ is defined as the value of x for which $cdf_X(x) = u$.

In the PSYCHOACOUSTICS TOOLBOX, the main function of interest for the generation of Poisson sequences is called `GeneratePoissonInstants`, which, as the name suggests, generates a list of event instants such that the entire sequence of events can be classified as a Poisson process. The first two parameters for this function are required and specify the total duration of the sequence to be generated as well as the average period between events

where the author also discusses the use of the inverse transformation method in more detail, including its applicability to the Poisson processes with its exponentially distributed inter-event intervals.

[4]The notation and definition of the *probability density function* and *cumulative distribution function* are properly formulated in appendix A.

(i.e., the reciprocal of the rate of events). The third parameter is optional and specifies a dead-time period (which is zero by default), which allows for the generation of dead-time modified Poisson processes. The dead-time parameter is especially useful for a Poisson process that is constrained by cochlear implant hardware that, based on the stimulus-frame duration, imposes a limit on the closeness of sequential stimuli. As a matter of interest, the dead-time parameter also allows for the generation of different event sequences that can progressively transition from a strictly homogeneous[5] Poisson-process to a purely periodic sequence of events as the dead-time period is increased from zero to a value matching the average period between events. For additional documentation on this function, such as the optional tolerance criterion mentioned earlier, refer to its built-in help feature in MATLAB.

For the more general dead-time-modified Poisson process, the simplified equation to generate the point process, as implemented by the `GeneratePoissonInstants` utility function, can be written as

$$cdf_U^{-1}(u_s) \quad = \quad \tau_d - (\tau_\lambda - \tau_d) \,.\, \ln(u_s) \;, \tag{C.2}$$

where $u_s = 1 - u$ represents a sample of the simplified variate U_s, also with a uniform distribution over the range $(0, 1)$, while τ_d and τ_λ represent the dead-time period and average period of the process, respectively. The values generated with this equation represent the durations between successive event instants of the process. For the more specific homogeneous Poisson process, simply let $\tau_d = 0$. Furthermore, in the degenerate case when $\tau_d = \tau_\lambda$, a periodic sequence is generated. A direct implementation of eq. C.2 provided a highly computationally efficient mechanism for generating Poisson sequences, which could then be used for experimental stimulation as well as simulations.

[5] By definition, a *homogeneous* Poisson process is one in which the intensity (i.e., the rate of events) remains constant over time. Mathematically, one can write (see eq. B.12 for the specific relation) $pdf(t) = \lambda / \exp(t \,.\, \lambda)$ from $hrf(t) = \lambda$ and $chf(t) = t \,.\, \lambda$, where λ represents the constant hazard rate and t the inter-event interval.

APPENDIX D

DETAILED RESULTS FROM GAP-DETECTION EXPERIMENTS

This appendix presents the experimental results of the primary within-channel gap-detection-threshold experiments performed as part of this study, which are discussed in § 4.5.3. Data are provided in numerical form, and frequently tabulated, to the extent that graphical presentations of the data (found elsewhere in this document) can be reconstructed accurately.

The stimulus sequences used for the dead-time-modified Poisson experiments all had a dead-time period of 250 μs during which no further stimulus pulse would be generated. This limited the maximum instantaneous stimulation rate to 4 kHz, as discussed in more detail in § 4.1.

D.1 SUBJECT S5

The results of the gap-detection-threshold experiments with subject S5 are summarized in tables D.1 and D.2 for periodic and dead-time-modified Poisson stimuli, respectively. The experiments were repeated at least five times for each tabulated data point. The stimulation mode was MP1+2, and the current levels were kept constant on each channel while the stimulation rate and type (periodic or Poisson) were varied. For the three channels, numbered 4, 12 and 20, the current levels were, respectively, 192, 187 and 186 clinical units, which convert to 488.5 μA, 441.5 μA and 432.6 μA, respectively, for the Cochlear Nucleus CI-24 implant that was used. The phase-width was 25 μs for each phase of the charge-balanced biphasic stimulus pulses, and the phase-gap value was 8 μs.

Table D.1: Averaged results and standard deviations of gap-detection-threshold experiments with subject S5, measured for constant-current periodic stimuli.

Rate [Hz]	Channel 4 (basal)		Channel 12 (central)		Channel 20 (apical)	
	Mean [ms]	S.D. [ms]	Mean [ms]	S.D. [ms]	Mean [ms]	S.D. [ms]
100.0	17.89	1.12	21.95	2.69	4.69	0.22
173.2	13.91	1.23	15.21	3.38	4.85	0.58
300.0	13.49	3.09	11.85	2.51	3.77	1.21
519.6	10.91	1.80	5.69	0.42	3.92	0.41
900.0	6.69	2.65	3.31	0.54	2.91	0.38
1558.8	3.72	0.26	1.77	0.18	1.93	0.31
2700.0	2.25	0.36	1.17	0.15	1.48	0.31

Table D.2: Averaged results and standard deviations of gap-detection-threshold experiments with subject S5, measured for constant-current Poisson stimuli.

Avg. Rate [pps]	Channel 4 (basal)		Channel 12 (central)		Channel 20 (apical)	
	Mean [ms]	S.D. [ms]	Mean [ms]	S.D. [ms]	Mean [ms]	S.D. [ms]
100.0	35.54	7.08	39.11	7.45	33.51	6.13
173.2	29.02	3.49	37.22	10.83	26.80	5.02
300.0	22.68	2.90	27.24	7.39	17.66	1.81
519.6	20.11	5.01	23.17	6.02	12.72	1.27
900.0	16.43	2.52	15.90	2.55	11.10	2.04
1558.8	9.37	1.62	12.44	3.79	8.57	1.54
2700.0	3.20	0.79	3.23	0.63	4.08	0.76

D.2 SUBJECT S10

The results of the gap-detection-threshold experiments with subject S10 are summarized in tables D.3 and D.4 for periodic and dead-time-modified Poisson stimuli, respectively. The experiments were repeated at least four times for each tabulated data point. The stimulation mode was MP1+2, and the current levels were kept constant on each channel while the stimulation rate and type (periodic or Poisson) were varied. For the three channels, numbered 4, 12 and 20, the current levels were, respectively, 205, 220 and 220 clinical units, which convert to 635.7 μA, 861.3 μA and 861.3 μA, respectively, for the Cochlear Nucleus CI-24 implant that was used. The phase-width was 25 μs for each phase of the charge-balanced biphasic stimulus pulses, and the phase-gap value was 8 μs.

Table D.3: Averaged results and standard deviations of gap-detection-threshold experiments with subject S10, measured for constant-current periodic stimuli.

Rate [Hz]	Channel 4 (basal)		Channel 12 (central)		Channel 20 (apical)	
	Mean [ms]	S.D. [ms]	Mean [ms]	S.D. [ms]	Mean [ms]	S.D. [ms]
100.0	9.38	2.79	5.42	2.48	3.51	0.64
173.2	6.83	1.53	3.50	0.33	3.62	0.34
300.0	5.44	1.47	2.37	0.34	3.36	0.86
519.6	5.54	1.66	0.44	0.05	0.90	0.83
900.0	4.52	1.70	1.24	0.43	1.06	0.10
1558.8	2.73	0.83	1.26	0.24	1.40	0.29
2700.0	2.09	0.44	1.33	0.10	1.68	0.42

Table D.4: Averaged results and standard deviations of gap-detection-threshold experiments with subject S10, measured for constant-current Poisson stimuli.

Avg. Rate [pps]	Channel 4 (basal)		Channel 12 (central)		Channel 20 (apical)	
	Mean [ms]	S.D. [ms]	Mean [ms]	S.D. [ms]	Mean [ms]	S.D. [ms]
100.0	64.96	45.50	76.14	24.47	71.92	31.93
173.2	41.42	17.97	54.83	18.64	50.30	14.61
300.0	20.14	2.85	21.87	5.38	30.47	4.09
519.6	15.38	3.27	11.69	4.53	23.71	9.92
900.0	11.99	2.45	6.45	0.92	5.60	1.18
1558.8	9.22	1.60	4.67	1.31	6.87	3.47
2700.0	4.74	0.74	3.07	0.20	2.93	0.21

D.3 SUBJECT S3A

The results of the gap-detection-threshold experiments with subject S3a are summarized in tables D.5 and D.6 for periodic and dead-time-modified Poisson stimuli, respectively. The implant device is a Cochlear Nucleus CI-22, the first implant received by the subject, which is implanted in the left ear.[1] The experiments were repeated four times for each tabulated data point. Since this older device does not have any extracochlear electrodes, the stimulation modes were chosen such that the reference electrode was always number 22 (the most apical electrode of this implant), while the channel numbers refer to the electrode number used as the active electrode. This means that the stimulation modes for the three channels, numbered 2, 10 and 18, were in effect BP+19, BP+11 and BP+3, respectively. The current levels were kept constant on each channel while the stimulation rate and type (periodic or Poisson) were varied. For the three channels, numbered as before, the current levels were, respectively, 145, 153 and 187 clinical units, which convert to 283.3 μA, 328.3 μA and 613.9 μA, respectively, for this implant. The phase-width was 25 μs for each phase of the charge-balanced biphasic stimulus pulses, and the phase-gap value was 8 μs.

Table D.5: Averaged results and standard deviations of gap-detection-threshold experiments with subject S3a, measured for constant-current periodic stimuli.

Rate [Hz]	Channel 2 (basal)		Channel 10 (central)		Channel 18 (apical)	
	Mean [ms]	S.D. [ms]	Mean [ms]	S.D. [ms]	Mean [ms]	S.D. [ms]
100.0	4.83	0.74	4.43	0.40	3.37	0.37
173.2	3.39	0.26	3.67	0.84	2.55	0.11
300.0	2.21	0.25	3.18	0.62	1.98	0.32
519.6	0.40	0.06	0.37	0.03	0.66	0.12
900.0	1.18	0.19	1.72	0.57	0.36	0.13
1558.8	1.30	0.14	1.74	0.19	0.82	0.14

D.4 SUBJECT S3B

The implant device for subject S3b is a Cochlear Nucleus CI-24, the subject's second implant, which is implanted in the right ear. This subject was readily available during the time when this study was performed and participated in most of the pilot studies, of which

[1] The second of the subject's two implants was received several years later, is implanted in the right ear, is denoted as "subject S3b" and will be discussed separately in § D.4.

Table D.6: Averaged results and standard deviations of gap-detection-threshold experiments with subject S3a, measured for constant-current Poisson stimuli.

Avg. Rate [pps]	Channel 2 (basal)		Channel 10 (central)		Channel 18 (apical)	
	Mean [ms]	S.D. [ms]	Mean [ms]	S.D. [ms]	Mean [ms]	S.D. [ms]
100.0	27.78	4.61	25.03	15.11	35.09	8.82
173.2	23.02	6.80	24.90	11.01	21.95	5.79
300.0	14.23	2.20	12.68	0.79	12.57	1.77
519.6	10.66	2.22	11.63	1.64	8.67	1.30
900.0	9.11	1.24	10.05	2.28	7.21	1.10
1558.8	8.10	1.10	9.23	1.49	5.04	0.83

only some were repeated on other subjects. For this subject, the results that correspond with repeats on other subjects will first be presented, followed by data from other experiments.

The results of the constant-current set of gap-detection-threshold experiments with subject S3b are summarized in tables D.7 and D.8 for periodic and dead-time-modified Poisson stimuli, respectively. The experiments were usually repeated nine times for each tabulated data point, though the number of repeats varied from six to 15. The stimulation mode was MP1+2, and the current levels were kept constant on each channel for a specific stimulation type (periodic or Poisson) while the stimulation rate was varied. For the three channels, numbered 2, 10 and 18, the current levels were, respectively, 204, 206 and 204 clinical units for the periodic stimuli, which convert to 622.9 μA, 648.7 μA and 622.9 μA, respectively, for this implant. For the Poisson stimulus sequences, with the three channels numbered as before, the current levels were, respectively, 206, 207 and 205 clinical units (which convert to 648.7 μA, 661.9 μA and 635.7 μA, respectively). The phase-width was 25 μs for each phase of the charge-balanced biphasic stimulus pulses, and the phase-gap value was 8 μs.

As mentioned in the preceding paragraph, different current levels were used even on the same channels for the two types of stimuli; these were loudness-balanced values at a rate of 900 pulses per second, determined with a two-track, randomly interleaved adaptive procedure (Jesteadt 1980). However, for the experiment repeats with other subjects it was decided to use the same current levels for the two kinds of stimuli to make comparison with predictions from simulations easier (i.e., so that the models would initially not need to take effects of different current levels within a single channel into account). Despite this difference, these results should still be comparable with the constant-current results of other subjects, since the loudness-balanced values for the three channels do not differ substantially for the two

stimuli types.

Table D.7: Averaged results and standard deviations of gap-detection-threshold experiments with subject S3b, measured for constant-current monopolar periodic stimuli.

Rate [Hz]	Channel 2 (basal)		Channel 10 (central)		Channel 18 (apical)	
	Mean [ms]	S.D. [ms]	Mean [ms]	S.D. [ms]	Mean [ms]	S.D. [ms]
173.2	5.70	0.78	3.49	0.34	2.78	0.25
300.0	4.72	0.58	2.33	0.50	2.09	0.26
519.6	4.71	0.51	0.57	0.07	0.55	0.23
900.0	5.81	1.00	1.26	0.34	0.94	0.58
1558.8	3.51	0.49	1.17	0.10	0.77	0.06
2700.0	2.59	0.28	1.15	0.08	1.00	0.07

Table D.8: Averaged results and standard deviations of gap-detection-threshold experiments with subject S3b, measured for constant-current monopolar Poisson stimuli.

Avg. Rate [pps]	Channel 2 (basal)		Channel 10 (central)		Channel 18 (apical)	
	Mean [ms]	S.D. [ms]	Mean [ms]	S.D. [ms]	Mean [ms]	S.D. [ms]
300.0	18.14	5.39	17.58	2.87	15.61	2.12
519.6	14.93	2.47	11.04	1.42	13.81	2.44
900.0	18.65	5.68	10.69	2.98	13.14	4.92
1558.8	9.54	1.33	6.44	0.88	7.97	2.07
2700.0	5.75	0.38	4.99	0.62	2.51	0.32

In addition to the constant-current set of gap-detection-threshold experiments just discussed, pilot studies were run with subject S3b to investigate the effect of the stimulus mode (monopolar versus bipolar) as well as the effect of perceptual loudness on gap-detection thresholds. The next four tables contain data in which all the stimuli have been balanced for loudness, such that the current levels differ for most of the tabulated data points, even for different kinds of stimuli (i.e., periodic or Poisson) on the same channel.

Summarized in tables D.9 and D.10 are results for periodic and dead-time-modified Poisson stimuli, respectively, in which the stimulation mode was still MP1+2, but the electrical currents were adjusted to favor equal perceptual loudness. The experiments were repeated from six to 15 times for each repeat-averaged data-point. The phase-width was 25 μs for each phase of the charge-balanced biphasic stimulus pulses, and the phase-gap value was 8 μs.

For the purpose of comparing the previous monopolar results with a different mode of

Table D.9: Averaged results and standard deviations of gap-detection-threshold experiments with subject S3b, measured for loudness-balanced monopolar periodic stimuli.

Rate [Hz]	Channel 2 (basal)		Channel 10 (central)		Channel 18 (apical)	
	Mean [ms]	S.D. [ms]	Mean [ms]	S.D. [ms]	Mean [ms]	S.D. [ms]
173.2	6.05	1.00	3.16	0.15	3.42	0.67
300.0	4.22	0.73	2.94	0.27	2.84	0.71
519.6	4.81	0.55	1.05	0.50	0.79	0.47
900.0	5.81	1.00	1.26	0.34	0.94	0.58
1558.8	3.65	0.48	1.59	0.23	0.77	0.06
2700.0	3.80	0.53	1.59	0.23	1.05	0.11

Table D.10: Averaged results and standard deviations of gap-detection-threshold experiments with subject S3b, measured for loudness-balanced monopolar Poisson stimuli.

Avg. Rate [pps]	Channel 2 (basal)		Channel 10 (central)		Channel 18 (apical)	
	Mean [ms]	S.D. [ms]	Mean [ms]	S.D. [ms]	Mean [ms]	S.D. [ms]
300.0	22.89	9.21	31.72	9.54	40.30	14.11
519.6	10.53	1.79	11.04	1.42	13.56	4.12
900.0	18.65	5.68	10.69	2.98	13.14	4.92
1558.8	9.14	1.82	6.30	1.08	7.01	1.44
2700.0	7.98	3.47	4.78	0.86	2.81	0.78

stimulation, experiments were performed with this subject in BP+2 mode. However, the phase-width had to be increased to 100 μs to enable the loudness to be set at the same perceptual level as for the loudness-balanced measurements discussed above. The phase-gap value was unchanged at 8 μs. The combination of these phase-duration parameters resulted in a total pulse duration of 208 μs, which was used as a guide when the dead-time duration of the Poisson stimuli was chosen at 250 μs. The experiments were repeated from six to 15 times for each of the data points summarized in tables D.11 and D.12, which are the results for the periodic and dead-time-modified Poisson stimuli, respectively.

Table D.11: Averaged results and standard deviations of gap-detection-threshold experiments with subject S3b, measured for loudness-balanced bipolar periodic stimuli.

Rate [Hz]	Channel 2 (basal)		Channel 10 (central)		Channel 18 (apical)	
	Mean [ms]	S.D. [ms]	Mean [ms]	S.D. [ms]	Mean [ms]	S.D. [ms]
100.0	4.30	1.39	4.73	1.01	3.42	0.51
173.2	3.93	0.16	3.13	0.28	2.64	0.27
300.0	3.05	0.24	2.51	0.46	2.98	0.93
519.6	2.92	0.24	2.22	0.39	1.61	0.16
900.0	2.75	0.40	2.19	0.33	1.67	0.40
1558.8	2.65	0.15	2.10	0.17	1.18	0.10
2700.0	1.79	0.15	1.50	0.24	0.64	0.06

Table D.12: Averaged results and standard deviations of gap-detection-threshold experiments with subject S3b, measured for loudness-balanced bipolar Poisson stimuli.

Avg. Rate [pps]	Channel 2 (basal)		Channel 10 (central)		Channel 18 (apical)	
	Mean [ms]	S.D. [ms]	Mean [ms]	S.D. [ms]	Mean [ms]	S.D. [ms]
100.0	65.94	22.74	67.27	22.55	70.71	22.72
173.2	21.59	7.33	23.54	5.17	22.27	5.76
300.0	33.61	15.44	31.21	8.82	34.13	8.56
519.6	10.61	1.64	11.46	1.35	20.85	6.51
900.0	9.10	2.52	7.90	1.14	20.71	8.61
1558.8	7.05	2.49	6.76	1.12	9.35	2.03
2700.0	6.19	2.66	4.33	0.60	5.40	3.68

APPENDIX E

COCHLEAR PRODUCT TERMINOLOGY

This appendix provides a summary of the terminology related to the Cochlear product range. For a detailed introduction to the Nucleus hardware and speech-processing technologies, refer to Clark et al. (1997, chapters 8–9).

E.1 SPEECH CODING STRATEGIES

In the context of strategies for speech coding (i.e., algorithms), the following terms are frequently encountered.

ACE *Advanced Combinational Encoder*, which is an algorithm implemented in SPrint.

ADRO *Adaptive Dynamic Range Optimization*, an algorithm that works on the input signal of the speech processor, but is not a speech-coding strategy in itself.

CIS *Continuous Interleaved Sampling*.

SPEAK *Spectral Peak* is an interleaved pulsatile strategy.

E.2 HARDWARE COMPONENTS

Hardware components are listed next.

CPS *Clinical Programming (Interface) System*, which uses the IF5 card to interface with the PC.

ESPrit A speech processor that is compatible with WinDPS R126.

ESPrit 22 A speech processor that is compatible with WinDPS R125.

ESPrit 3G Third-generation, behind-the-ear (BTE) speech processor.

IF5 The interface card of the CPS, an ISA-slot card mounted inside a PC.

IF6 This is a PCI-slot card intended as a replacement for the IF5. Unfortunately (at the time of this research), this card was supported with WinDPS only, and not CPS or PPS, making it inaccessible for research purposes.

PCI *Programming (or Patient) Control Interface*. This is a (rather heavy) box, and is the portion of the CPS external to the PC; see Clark et al. (1997, fig. 8-13) for a photo.

PPS *Portable Programming (Interface) System*, which interfaces to the PC through a serial port (or a USB port, when a USB-serial converter box is used). The R125 or R126 version of the WinDPS software can be used with this hardware.

Spectra This is a speech processor that is compatible with WinDPS R125; see Clark et al. (1997, fig. 8-2) for a photo.

SPrint A body-worn speech processor that can also interface to both the CPS and PPS; see Clark et al. (1997, fig. 8-11) for a photo.

E.3 SOFTWARE COMPONENTS

Finally, a list of software components is provided.

NIC The *Nucleus Implant Communicator*, This is one of the older APIs that was generally available for research purposes, but it implements some features that are not available in newer APIs.

NICStream The *Nucleus Implant Communicator Streaming* API is a newer programming interface that eliminates some of the limitations of the older NIC interface, allowing for stimulation sequences of virtually unlimited duration (although it does not provide all the functions of the earlier version). It is exposed through both ANSI-C (stream.dll) and COM (xstream.dll) interfaces.

NMT The *Nucleus MATLAB Toolbox* builds on top of the NICstream interface and provides a modular framework for exploring speech-processing algorithms in MATLAB, but is limited to the CPS hardware. Many of the data structures used with NMT are compatible with the PSYCHOACOUSTICS TOOLBOX, thus making similar functions available to the PPS hardware.

NRT *Neural Response Telemetry* is a technology, available through newer implants (such as the CI-24), used to retrieve readings from neural activity around the implanted electrode array. It can be used with the PPS.

RxFrames This utility is a Win32 console application that records decoded RF frames via the CPS and stores the results in one of several file formats: words (RFW), bytes (RFB), or statistics (RFS).

Streaming Software (for SPrint) This software allows reading and writing of sequences with the SPrint speech processor.

WinDPS R110/R116 The *Windows-based Diagnostics & Programming Software, releases 110 and 116*, is an application used primarily in the clinical environment. It does not support the PPS, nor the ESPrit 22, but it does support the SPrint and ESPrit speech processors.

WinDPS R125 The *Windows-based Diagnostics & Programming Software, release 125*, is a version of this application that can be used with the PPS. It supports the Spectra and ESPrit 22 speech processors (but not the ESPrit).

Nucleus R126 The Windows-based diagnostics and programming software for the *Nucleus* implants, *release 126*, supports the PPS, as well as the SPrint, ESPrit and ESPrit 3G speech processors.

APPENDIX F

NUCLEUS CURRENT-LEVELS AND AMPERES

The NIC (version 1) API, provided by Cochlear, allows one to convert between clinical current levels and electrical current. The equations provided in this appendix match these operations with great accuracy for all the values that are allowed as parameters to the conversion functions. Having these equations in an analytical form allows for interpolation between the values that are physically possible with the hardware. This is useful when values from experiments are averaged and fractional clinical current-levels come into play.

For the Cochlear Nucleus CI-24 implant (a.k.a. CIC3), the electrical current, represented by μA (in *micro-amperes*), and clinical level, denoted by CL, are related as follows:

$$\begin{aligned} \mu\text{A} &= \exp(0.02025406264283728 \times \text{CL} \\ &\quad + 2.30258509299405) \quad \forall \quad 0 <= \text{CL} <= 255\,, \quad \text{and} \qquad \text{(F.1)} \\ \text{CL} &= 49.37281066194607 \times (\ln(\mu\text{A}) \\ &\quad - 2.30258509299405) \quad \forall \quad 10 <= \mu\text{A} <= 1750\,. \qquad \text{(F.2)} \end{aligned}$$

With the older Nucleus CI-22 implant (a.k.a. CIC1), the conversions can be done as follows:

$$\begin{aligned} \mu\text{A} &= \exp(0.01841035441232463 \times \text{CL} \\ &\quad + 2.977059008288367) \quad \forall \quad 0 <= \text{CL} <= 239\,, \quad \text{and} \qquad \text{(F.3)} \\ \text{CL} &= 54.31725960313723 \times (\ln(\mu\text{A}) \\ &\quad - 2.977059008288367) \quad \forall \quad 19.63 <= \mu\text{A} <= 1599\,. \qquad \text{(F.4)} \end{aligned}$$